Fluctuations and phase transitions in Larkin-Ovchinnikov liquid-crystal states of a population-imbalanced resonant Fermi gas

Leo Radzihovsky
Department of Physics, University of Colorado, Boulder, Colorado 80309, USA
(Received 2 March 2011; published 8 August 2011)

Motivated by a realization of imbalanced Feshbach-resonant atomic Fermi gases, we formulate a low-energy theory of the Fulde-Ferrell and the Larkin-Ovchinnikov (LO) states and use it to analyze fluctuations, stability, and phase transitions in these enigmatic finite momentum-paired superfluids. Focusing on the unidirectional LO pair-density-wave state, which spontaneously breaks the continuous rotational and translational symmetries, we show that it is characterized by two Goldstone modes, corresponding to a superfluid phase and a smectic phonon. Because of the liquid-crystalline "softness" of the latter, at finite temperature the three-dimensional state is characterized by a *vanishing* LO order parameter, quasi-Bragg peaks in the structure and momentum distribution functions, and a "charge"-4, paired-Cooper-pairs, off-diagonal long-range order, with a superfluid-stiffness anisotropy that diverges near a transition into a nonsuperfluid state. In addition to conventional integer vortices and dislocations, the LO superfluid smectic exhibits composite half-integer vortex-dislocation defects. A proliferation of defects leads to a rich variety of descendant states, such as the charge-4 superfluid and Fermi-liquid nematics and topologically ordered nonsuperfluid states, that generically intervene between the LO state and the conventional superfluid and the polarized Fermi liquid at low and high imbalance, respectively. The fermionic sector of the LO gapless superconductor is also quite unique, exhibiting a Fermi surface of Bogoliubov quasiparticles associated with the Andreev band of states, localized on the array of the LO domain walls.

DOI: 10.1103/PhysRevA.84.023611 PACS number(s): 67.85.−d, 74.20.Mn, 03.75.Ss

I. INTRODUCTION

A. Background

1. Imbalanced resonant atomic gases

Experimental progress in trapping, cooling, and coherently manipulating Feshbach-resonant atomic gases opened an unprecedented opportunity to study degenerate strongly interacting quantum many-body systems in a broad range of previously unexplored regimes [1–6]. These include paired fermionic superfluids (SFs) (with s-wave SFs now readily realized [7–11], and p-wave SFs under extensive current study [3,12–16]), the associated Bardeen-Cooper-Schrieffer (BCS) to Bose-Einstein condensation (BEC) crossover [3,17–25], Bose-Fermi mixtures [26], bosonic molecular superfluids [27–30], and many other states and regimes [31] under both equilibrium and nonequilibrium conditions [24,32,33]. In addition to the tunability of the Feshbach-resonant interaction strength (and its effective sign), temperature, and many types of external perturbation, a species number imbalance in, e.g., a two-atom hyperfine-state mixture turned out to be an extremely fruitful experimental knob [34–37].

A nonzero species imbalance frustrates conventional BCS pairing of a two-species Fermi gas [38–41] and the associated BCS-BEC crossover [42–46], driving quantum phase transitions out of a paired superfluid to a variety of interesting possible ground states and thermodynamic phases [44,46–51]. This rekindled considerable theoretical activity in the context of species-imbalanced resonant Fermi gases [4,52–72]. The identification of the number species imbalance with the magnetization of an electronic system, and the chemical potential difference with an effective Zeeman energy, connects these recent atomic gas studies with a large body of research on solid-state electronic superconductors under a Zeeman field [73–77], as well as extensively studied realizations in nuclear and particle physics [78–81]. The obvious advantage of the current atomic system is the aforementioned tunability, disorder-free "samples," and absence of the orbital part of the magnetic field, which always accompanies a solid-state charged superconductor in a magnetic field [82]. In these neutral paired superfluids the orbital field effects can be independently controlled by a rotation of the atomic cloud [83].

As illustrated in Fig. 1, among many interesting features, such as the gapless imbalanced superfluid (SF_M) [44–47], ubiquitous phase separation [4,40,44,47], tricritical point [69,72], etc., observed experimentally [34–37] and studied extensively theoretically [4,6], the interaction-imbalance BEC-BCS phase diagram is also predicted [4,44,46,52,70,71] to exhibit the enigmatic Fulde-Ferrell-Larkin-Ovchinnikov (FFLO) state [76,77]. First predicted in the context of solid-state superconductors over 45 years ago [76,77], the FFLO states has so far eluded a definitive observation, though some promising solid-state [84] and quasi-one-dimensional atomic [85] candidate systems have recently been realized.

At its most generic level the FFLO state [86] is a fermionic superfluid, paired at a finite center-of-mass momentum. Generically such a state spontaneously "breaks" gauge and translational symmetry, i.e., it is a periodically paired superfluid (superconductor), akin to a supersolid [87–90], and thus can appropriately be called a pair-density wave (PDW) [91,92]. Microscopically, it is driven by Fermi surface mismatch [76,77] due to an imposed pairing species number (and/or mass [93]) imbalance. As a compromise between the superfluid pairing and an imposed imbalance, at intermediate values of the latter, the superconducting order parameter condenses at a set of finite center-of-mass momenta determined by the details of the Fermi surface mismatch and interactions, thereby self-consistently leading to FFLO pairing between these imbalanced fermionic species. At sufficiently large

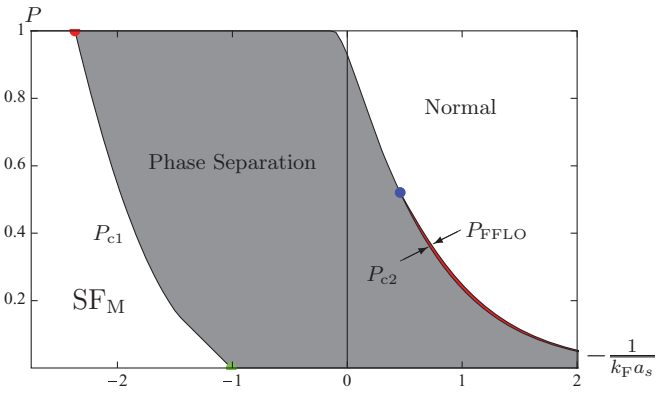

FIG. 1. (Color online) A mean-field zero-temperature phase diagram from Refs. [4,44] of an imbalanced Fermi gas, as a function of the inverse scattering length and normalized species imbalance $P = (N_\uparrow - N_\downarrow)/N \equiv \Delta N/N$, showing the magnetized (imbalanced) superfluid (SF_M), the FFLO state (approximated as the simplest FF state, confined to a narrow red sliver bounded by P_{FFLO} and P_{c2}), and the imbalanced normal Fermi liquid.

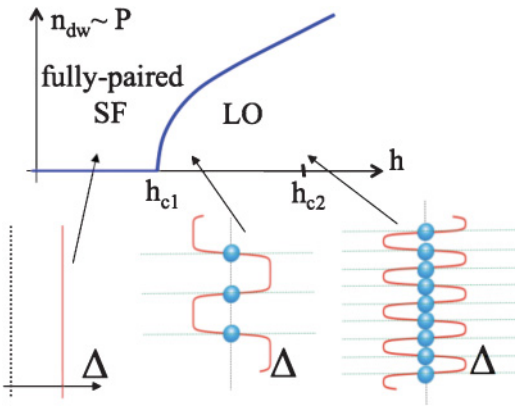

FIG. 2. (Color online) An illustration of a continuous commensurate-incommensurate (CI) transition at h_{c1} from a fully gapped (balanced) paired superfluid to an imbalanced Larkin-Ovchinnikov superfluid. The excess majority atoms are localized on the domain walls in (zeros of) the LO order parameter, whose number $n_{dw}(h)$ is then proportional to the imbalance $P(h)$ and grows continuously with the chemical potential difference (Zeeman energy) $h - h_{c1}$.

imbalance ΔN_{c2} or equivalently at the upper critical Zeeman field h_{c2} (corresponding to the chemical potential difference $\Delta\mu_{c2}$ of the two pairing species) no compromise is possible, and a transition to the normal state takes place.

2. *Mean-field energetic stability of FFLO states*

The original predictions by Fulde and Ferrell (FF), and by Larkin and Ovchinnikov (LO) were followed by extensive studies of the FFLO states [78–81], although exclusively confined to their energetics in the BCS limit. Stimulated by the aforementioned potential realization in imbalanced resonant Fermi gases, the recent revival of the subject extended the analysis to the full range of the BCS-BEC crossover [4,44,52,69,70,94]. As illustrated in Fig. 1, the key observation is that, despite strong interactions, within a single-$\mathbf{q}_0$ Bogoliubov–de Gennes (BdG) treatment the conventional FFLO state (as originally proposed by FF and LO) remains quite fragile, confined to a narrow sliver of polarization in the BCS regime [4,44].

However, motivated by earlier studies of the BdG equation [95–97], combined with the finding of a negative domain-wall energy in an otherwise fully paired singlet BCS superfluid in a Zeeman field [97,98], recent studies have quite convincingly argued that a more generic pair-density-wave state (that includes a larger set of collinear wave vectors) may be significantly more stable. Analogously to a strongly type-II superconductor that undergoes a continuous transition into a vortex state at a lower critical orbital field H_{c1} [99–101] (which is significantly below the thermodynamic field H_c), in the current system, a Zeeman field h (the chemical potential imbalance) can drive a nucleation of domain walls in the superfluid order parameter above the lower critical Zeeman field h_{c1} which is below the bulk mean-field value h_c. Thereby, the excess of the majority fermionic atoms (polarization) in an imbalanced system can be *continuously* accommodated by the subgap states localized on the self-consistently induced domain walls, through a continuous commensurate-incommensurate (CI) Pokrovsky-Talapov (PT) type of transition [102] from a fully paired s-wave superfluid to a Larkin-Ovchinnikov-like periodic state of domain walls [103,104]. This picture, illustrated in Fig. 2, resembles the soliton mechanism for doping of polyacetylene [105]. The $\pm\Delta$ domain-wall description, which is explicitly realized in one dimension (1D) through exact BdG [95] and Bethe ansatz [106,107] solutions and via bosonization [108,109], is complementary, but not qualitatively distinct from the more familiar single-cosine form of the LO state [77].

The latter, "soft," pair-density wave is a more appropriate description near the h_{c2} transition into the normal state, where the pair order parameter is naturally small, and a Landau expansion in the leading harmonic Δ_q is expected to be valid. On the other hand, clearly, far below h_{c2} (e.g., near the h_{c1} transition from the fully paired uniform singlet BCS state) the periodic soliton state is a quantitatively better description as it more accurately captures the strong pairing at Δ, confining the "normal" regions that accommodate the imposed fermion imbalance to the narrow gapless domain walls between $\pm\Delta$. Upon increasing h above h_{c1} the density of domain walls grows and the walls eventually overlap at h_{c2}, thereby continuously interpolating between the two limiting descriptions of the LO state. This picture is explicitly realized in the exact 1D solutions [95,106–108] and emerges from the numerical BdG studies [96,97]. Furthermore, the lack of a single-$\mathbf{q}$ nesting for $d > 1$, to which the fragility of the LO state is usually attributed, is irrelevant when the LO order parameter exhibits a broad spectrum of $\mathbf{q}$ (set by $1/\xi_0$), as in its soliton form above h_{c1}.

The LO state can be equivalently thought of as a periodically ordered *micro* phase separation between the normal and paired states, which naturally replaces the *macro* phase separation [40,81] ubiquitously found in the BCS-BEC detuning-imbalance phase diagram [4,44,47].

It is clear that the standard (even multiple-wave-vector) Landau treatments valid near h_{c2} and analytical BdG analysis of a single FF plane-wave state (exhibiting no amplitude nodes) [4] fail to capture the quantitatively important ingredients

described above. These treatments are therefore not necessarily quantitatively trustworthy in their prediction of the energetic range of stability (location of h_{c1}) of the LO state (they are, however, reliable for the prediction of h_{c2}), and in our view need to be reexamined.

3. *Fluctuation in the FFLO states*

The microscopic question of the energetic stability of FFLO states is certainly an extremely important one and has dominated most of the research on the subject to date. However, given the extensive 45-year history of the topic, it is astounding that the equally basic complementary question of the nature of the Goldstone modes and their fluctuations within the FFLO states received so little attention [110,111] until our study of the problem, reported in a recent Letter [112]. From general symmetry principles the FFLO states' low-energy phenomenology is expected to be significantly richer than that of a homogeneous fully gapped superconductor, whose low-energy phenomenological (Ginzburg-Landau and *XY* model) description long predated the microscopic theory by BCS [99–101]. That is, in addition to a local superfluid phase degree of freedom, the low-energy modes include the phonons (a single scalar one in the case of a uniaxial LO state) of the periodic superconducting structure, as well as gapless polarized (single-species) fermionic atoms confined to a fluctuating periodic array of two-dimensional domain walls [111,112].

In the isotropic realization (e.g., in cold atoms in an isotropic trap) of interest to us, the FFLO states *spontaneously* break a *continuous* rotational (in addition to the translational) symmetry akin to smectic liquid crystals, in contrast to their solid-state density-wave analogs. Consequently, as was originally anticipated by Shimahara [110] and was demonstrated in our recent work [112], to be explored in greater detail below, their Goldstone modes are qualitatively softer and therefore exhibit far stronger fluctuations. These can either completely destabilize the (otherwise energetically stable) FFLO state, or can qualitatively modify its mean-field form and properties. This general picture therefore reveals that the complexity of the FFLO state beyond its mean-field cartoon requires the understanding of a subtle interplay of superfluidity, liquid crystallization, and anisotropic Fermi surface physics.

With this motivation in mind, in a recent Letter [112] the questions discussed above were formulated and carefully explored. Namely, as illustrated in the schematic phase diagram in Fig. 3, supported by the aforementioned studies [95,96] and the exact 1D solutions [95,108,109], we assumed that a striped (unidirectional) FFLO state (which we refer to as the LO state), characterized by a collinear set of wave vectors, is *energetically* (microscopically) stable over an experimentally accessible portion of the detuning-imbalance phase diagram. We then formulated the model for the low-energy Goldstone mode fluctuations and fermionic excitations in the LO state and used it to study the stability of the state to quantum and thermal fluctuations, as well as to explore the fluctuation-driven phenomenology, topological defects, interesting quantum liquid crystal phases, and associated phase transitions [112]. In the present paper we present a significantly more extensive description of these findings and the details of the associated calculations.

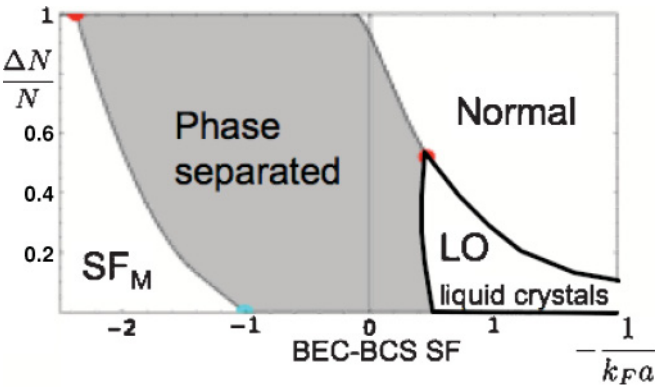

FIG. 3. (Color online) A proposed $\Delta N/N$ vs $1/(k_F a_s)$ phase diagram for an imbalanced resonant Fermi gas, showing the more stable LO liquid-crystal phases (discussed in the text and illustrated in detail in Fig. 4) replacing a portion of the phase-separated regime.

4. *Relation to other systems and studies*

Although physically quite distinct, some of our motivations and findings [112] are closely related to studies in solid-state realizations, such as the putative FFLO states in heavy-fermion ($CeCoIn_5$) and organic [κ-$(BEDT\text{-}TTF)_2Cu(NCS)_2$] superconductors [113,114], the striped (and spiral) states in high-T_c superconductors and nickelates and more generally in strongly correlated doped Mott insulators [115–120], spiral states in helimagnets [121–123], partially filled high-Landau-level 2D electron gases [124–126], charge-density waves in anisotropic metals [127], and others. Among a number of physical properties special to resonant atomic Fermi gases, one key qualitatively distinguishing feature in our study is that the FF and LO states spontaneously break *continuous* translational and orientational symmetries of an isotropically trapped Fermi gas. As first emphasized in Refs. [110,112], this latter property is responsible for the qualitatively enhanced fluctuations that lead to the predicted universal power-law correlations (5),(7) persisting throughout the 3D quasi-long-range-ordered FFLO phase, rather than just at a critical point. Thus, such FF and LO states (and their descendants) are qualitatively distinct from their mean-field forms [76,77], akin to a distinction between, e.g., a quasi-long-range ordered 2D ferromagnet (a 2D *XY* model) and a 3D ferromagnet. In contrast, the aforementioned states in the solid-state systems by their very definition only break *discrete* point-group crystal symmetries, and therefore exhibit quite tame Gaussian fluctuations inside the phase, with these periodic states only quantitatively distinct from their mean-field forms.

However, as we will see, despite enhanced fluctuations the LO state studied here does lead to a number of interesting features recently discussed in the literature, such as the fractional vortex-dislocation defects, charge-4 superfluidity, Andreev-like midgap states, and many others [113,118].

5. *Outline*

The rest of the paper is organized as follows. We conclude the Introduction with the summary of our main results. Then,

in Sec. II we use a microscopic description of the imbalanced resonant atomic Fermi gas to derive in the weakly interacting BCS limit the corresponding Landau theory (along with microscopic expressions for its parameters) valid near the h_{c2} transition to the normal state. In Sec. III we discuss symmetries of two generic classes of FFLO states, construct corresponding order parameters, and derive from the Landau theory the corresponding models for their Goldstone modes. As we argue, these models provide universal descriptions of low-energy fluctuations in the FF and LO classes of states, beyond the limit of validity of their microscopic BCS-limit derivation. In Sec. IV we complement this derivation (valid near h_{c2}) by an analysis of an array of fluctuating domain walls, valid near h_{c1}. In Sec. V we use these low-energy universal models to analyze quantum and thermal fluctuations in the FF and LO classes of states, paying particular attention to elastic nonlinearities that (as we show) are qualitatively important at a finite temperature. Then in Sec. VI we classify and discuss the energetics of topological defects in the LO state. In Sec. VII we use this information to uncover a variety of exotic "daughter" liquid-crystal phases that emerge as a result of unbinding different combinations of topological defects and discuss corresponding phase transitions. In Sec. VIII we extend the model to include the coupling of the Goldstone modes to gapless fermionic atoms and comment on their effects. In Sec. IX we use the local density approximation (LDA) to put our results in the context of trapped atomic gases and discuss experimental probes of our predictions. We conclude in Secs. X, XI, and XII with discussions of experimental probes, open questions, and a summary of our study. In Appendixes A and B we provide technical details for the microscopic derivation of the Ginzburg-Landau expansion near h_{c2} and finite-size scaling analysis of smectic fluctuations, respectively.

B. Results

Before turning to the derivation and analysis of the model, we summarize the key predictions of our work, previously reported in Ref. [112]. Because our predictions [128] are based on general symmetry principles, supported by detailed microscopic weak-coupling calculations, they are generic and robust to variation in microscopic details. At a very general level, we demonstrate that (in contrast to the conventional uniform superfluid and FF states) a unidirectional (striped) LO superfluid exhibits *two* Goldstone modes ϕ and θ. These correspond to two coupled smectic phonons, or equivalently the superfluid phase ϕ and a nonlinearly coupled smectic phonon mode $u = -\theta/q_0$, with $\mathbf{q}_0$ the wave vector characterizing the LO state.

Through robust symmetry arguments, complemented by an explicit microscopic derivation (valid in the BCS regime, near the LO to normal state transition at h_{c2}), we show that the low-energy universal (classical) LO Hamiltonian governing fluctuations of these Goldstone modes is given by

$$\mathcal{H}_{\rm LO}^{\rm GM} = \frac{K}{2}(\nabla^2 u)^2 + \frac{B}{2}\left(\partial_\parallel u - \frac{1}{2}(\boldsymbol{\nabla} u)^2\right)^2 + \frac{\rho_s^i}{2}(\nabla_i \phi)^2. \tag{1}$$

This Hamiltonian form, familiar from studies of conventional smectic liquid crystals, encodes the underlying rotational invariance through the vanishing of the $(\nabla_\perp u)^2$ modulus and the specific form of the nonlinear elastic terms in u [129–132]. Here, $\parallel$, $\perp$ refer to axes that are parallel and perpendicular to the LO ordering wave vector $\mathbf{q}_0$, respectively. In the weak-coupling BCS limit, we derive explicit expressions for the above Goldstone-mode moduli, K, B, and ρ_s^i ($i = \parallel, \perp$), given by

$$K \approx \frac{0.8 n \Delta_{\rm BCS}^2}{\epsilon_{\rm F} q_0^2} \ln(h/h_{c2}), \tag{2a}$$

$$B \approx q_0^2 \rho_s^\parallel \approx \frac{3.3 n \Delta_{\rm BCS}^2}{\epsilon_F} \ln(h/h_{c2}), \tag{2b}$$

$$\rho_s^\perp \approx \frac{0.8 n \Delta_{\rm BCS}^2}{\epsilon_{\rm F} q_0^2} \ln^2(h/h_{c2}), \tag{2c}$$

also given in Eqs. (80) and (81). Among these predictions, we find that the LO state is a highly anisotropic superfluid, with the ratio of superfluid stiffnesses given by

$$\rho_s^\perp/\rho_s^\parallel = \tfrac{3}{4}\left(\Delta_{q_0}/\Delta_{\rm BCS}\right)^2 \approx \tfrac{1}{4}\ln(h_{c2}/h) \ll 1, \tag{3}$$

vanishing on the approach to the upper critical Zeeman field $h \to h_{c2}^-$, which marks the mean-field transition to the normal state at which the LO order parameter Δ_{q_0} vanishes. $\Delta_{\rm BCS}$ is the zero-field BCS order parameter.

We find the FF state to be even more exotic. In contrast to other homogeneous superfluids (described by an XY model), its single superfluid Goldstone mode ϕ is described by the above smectic Hamiltonian, with an identically vanishing transverse superfluid stiffness $\rho_{s,\rm FF}^\perp = 0$, a reflection of the rotational invariance of the spontaneous current to an energy-equivalent ground state. Thus we show that a resonant imbalanced Fermi gas confined to an isotropic trap gives a natural realization of a quantum (superfluid) smectic liquid crystal.

As a consequence of the spontaneous breaking of continuous spatial symmetries (contrasting with its solid-state realizations, where only discrete point-group (lattice) symmetries are spontaneously broken) [113,115,118–121,123–125], the Goldstone-mode excitations in the FF and LO states are of *qualitatively* lower energy. As a result, the fluctuations in such superfluid smectic states are qualitatively stronger. Specifically, we find that while they are stable to quantum fluctuations, in 3D the LO and FF long-range orders are marginally unstable at any nonzero T, with the LO order parameter (with Dirichlet boundary conditions; for a more general case, see Sec. X)

$$\begin{aligned}\langle \Delta_{\rm LO}(\mathbf{r})\rangle_R &= \left\langle 2\Delta_{q_0} e^{i\phi(\mathbf{r})}\cos[\mathbf{q}_0\cdot\mathbf{r} + \theta(\mathbf{r})]\right\rangle_R \\ &\sim \frac{1}{R^\eta}\cos\mathbf{q}_0\cdot\mathbf{r} \;\to\; 0,\end{aligned} \tag{4}$$

vanishing in the thermodynamic limit (a large cloud with atom number N and cloud size $R \to \infty$), suppressed to zero by thermal phonon $u = -\theta/q_0$ fluctuations, and therefore strictly speaking homogeneous on long scales. The resulting superfluid state is thus an "algebraic topological" phase with no long-ranged translational order; namely, beyond mean-field theory it is instead characterized by power-law order-parameter correlations, distinguished from the spatially short-ranged disordered phase by confined topological defects (bound dislocations), not by a nonzero LO order parameter. It

is therefore a 3D analog of the more familiar quasi-long-range-ordered superfluid film and a 2D easy-plane ferromagnet.

There are a number of interesting consequences of this finding. For example, as illustrated in Fig. 21, we predict that in 3D [133] the static structure function $S(\mathbf{q})$ in the LO state exhibits universal anisotropic *quasi*-Bragg peaks (akin to a conventional smectic liquid crystal [134,135]), with nth-order peak given by

$$S(q_\parallel, \mathbf{q}_\perp = 0) \sim \frac{1}{|q_\parallel - 2nq_0|^{2-4n^2\eta}}, \tag{5}$$

rather than the true δ-function Bragg peaks of, e.g., a long-range-ordered pair-density wave in a crystalline environment. Here the anomalous Caillé exponent [134] is given by

$$\eta = \frac{q_0^2 T}{8\pi\sqrt{BK}}. \tag{6}$$

We similarly find that the momentum distribution function of pairs displays a power-law form around the reciprocal lattice momenta set of q_0,

$$n_{\mathbf{k}} \sim \frac{1}{|k_z - nq_0|^{2-n^2\eta}}, \tag{7}$$

as illustrated in Fig. 20. This power law is a reflection of a striking pair-condensate depletion to zero by the divergent finite-T LO Goldstone-mode fluctuations even in 3D, akin to the Landau-Peierls [136,137] behavior of films of a conventional superfluid and 2D crystals [138–141]. Such static correlations in the LO state can be computed asymptotically exactly, as was first done for a conventional smectic liquid crystal [131,132,134]. This fluctuation-driven 3D power-law phenomenology is a unique feature of a unidirectional (*collinear* wave vectors) FFLO state. It is not exhibited by crystalline FFLO phases with multiple *noncollinear* ordering wave vectors [78,79], which, in contrast, are characterized by the long-range positional order and a nonzero pair condensate that is stable to thermal fluctuations.

As with treatments of the LO state, where long-range order is assumed [113,118], in this algebraic LO phase we also find an unusual topological excitation—a half vortex bound to a half dislocation—in addition to integer vortices and dislocations. These are illustrated in Figs. 8, 9, and 10.

In 2D, at nonzero T the LO state is even more strongly disordered, at intermediate scales characterized by universal power-law phonon correlations and concomitant short-range positional order with Lorentzian structure function peaks, controlled by a nontrivial exactly calculable fixed point [132]. Asymptotically, however, at arbitrary low temperature the 2D LO state is unstable to proliferation of dislocations [142]. The state that results from such dislocated superfluid smectics is either a charge-4 (paired Cooper pairs) [143] nematic superfluid [112,119] or a nematic (possibly "fractionalized") Fermi liquid [117,126], the latter qualitatively the same as the deformed Fermi surface state [49].

More generally, while analyzing defect-driven continuous transitions out of the LO state, we uncover a rich array of descendant states that generically must intervene between the LO superfluid and a fully paired conventional (isotropic and homogeneous) superfluid and a conventional Fermi liquid. If indeed the 3D LO state is energetically stable, as argued above, we expect these unusual states to appear in the region collectively denoted "LO liquid crystals" in the detuning-polarization phase diagram of Fig. 3. They include a nonsuperfluid smectic ($\mathrm{FL}^{2q}_{\mathrm{Sm}}$, driven by an unbinding of integer 2π-vortices), a superfluid (SF^4_N, driven by a proliferation of integer a dislocations) and a nonsuperfluid (FL_N, driven by an unbinding of both vortices and dislocations) nematic, and the corresponding isotropic states, when disclinations also condense. In addition, we predict a variety of topologically ordered isotropic and nematic fractionalized Fermi-liquid states (FL^*_N, FL^{**}_N, FL^*_I, and others), that are distinguished from their more conventional fully disordered forms by *gapped* (bound) half-integer defects. These phases are summarized by a schematic phase diagram illustrated in Fig. 4. We now turn to the derivation of these predictions.

II. BCS THEORY OF IMBALANCED RESONANT FERMI GAS

A. Model

We begin with the one-channel model of two-species, resonantly interacting Fermi gas, appropriate for the experimentally relevant broad Feshbach resonance [4–6]. In the grand-canonical ensemble, it is described by a Hamiltonian

$$H = \sum_{\mathbf{k},\sigma} (\epsilon_k - \mu_\sigma) \hat{c}^\dagger_{\mathbf{k}\sigma} \hat{c}_{\mathbf{k}\sigma} + \frac{g}{V} \sum_{\mathbf{kqp}} \hat{c}^\dagger_{\mathbf{k}\uparrow} \hat{c}^\dagger_{\mathbf{p}\downarrow} \hat{c}_{\mathbf{k}+\mathbf{q}\downarrow} \hat{c}_{\mathbf{p}-\mathbf{q}\uparrow}, \tag{8}$$

with the two atomic species (labeling the hyperfine states $\sigma = \uparrow, \downarrow$) open-channel fermions created by the anticommuting operator $\hat{c}^\dagger_{\mathbf{k}\sigma}$,

$$\{\hat{c}_{\mathbf{k}\sigma}, \hat{c}^\dagger_{\mathbf{k}'\sigma'}\} = \delta_{\sigma,\sigma'} \delta_{\mathbf{k},\mathbf{k}'}, \tag{9}$$

with the single-particle energy $\epsilon_k = \hbar^2 k^2/2m$, mass m, and system's volume V (henceforth set to 1).

Above we introduced two distinct chemical potentials $\mu_\sigma = (\mu_\uparrow, \mu_\downarrow)$ to impose numbers of two separately conserved atomic species, $N_\sigma = (N_\uparrow, N_\downarrow)$, or equivalently the total fermion number $N = N_\uparrow + N_\downarrow$ and the atom species imbalance $\Delta N = N_\uparrow - N_\downarrow$. Equivalently, the two species chemical potentials $\mu_\uparrow = \mu + h$ and $\mu_\downarrow = \mu - h$ are related to the total-number chemical potential μ and the species-imbalance chemical potential h, the latter corresponding to the pseudo Zeeman energy. The imbalanced resonant Fermi gas thermodynamics as a function of $N, \Delta N, T, a_s$, i.e., the extension of the BEC-BCS crossover to a finite imbalance, can be computed by a variety of theoretical techniques, including quantum Monte Carlo [42], mean-field theory [4,44,45,47,69], the large-N_f (fermion flavor) [144,145], and ϵ expansions [146].

The attractive interaction is parametrized by a short-range s-wave pseudopotential with a strength $g < 0$. Through a standard T-matrix scattering calculation [147,148], that gives the two-atom s-wave scattering amplitude $f_s(k) = -\frac{m}{4\pi\hbar^2} T_k$, the pseudopotential parameter g can be related to the experimentally determined, magnetic-field-dependent [149] scattering length

$$\frac{m}{4\pi\hbar^2 a_s} = \frac{1}{g} + \frac{1}{V} \sum_{\mathbf{k}} \frac{1}{2\epsilon_k}, \tag{10}$$

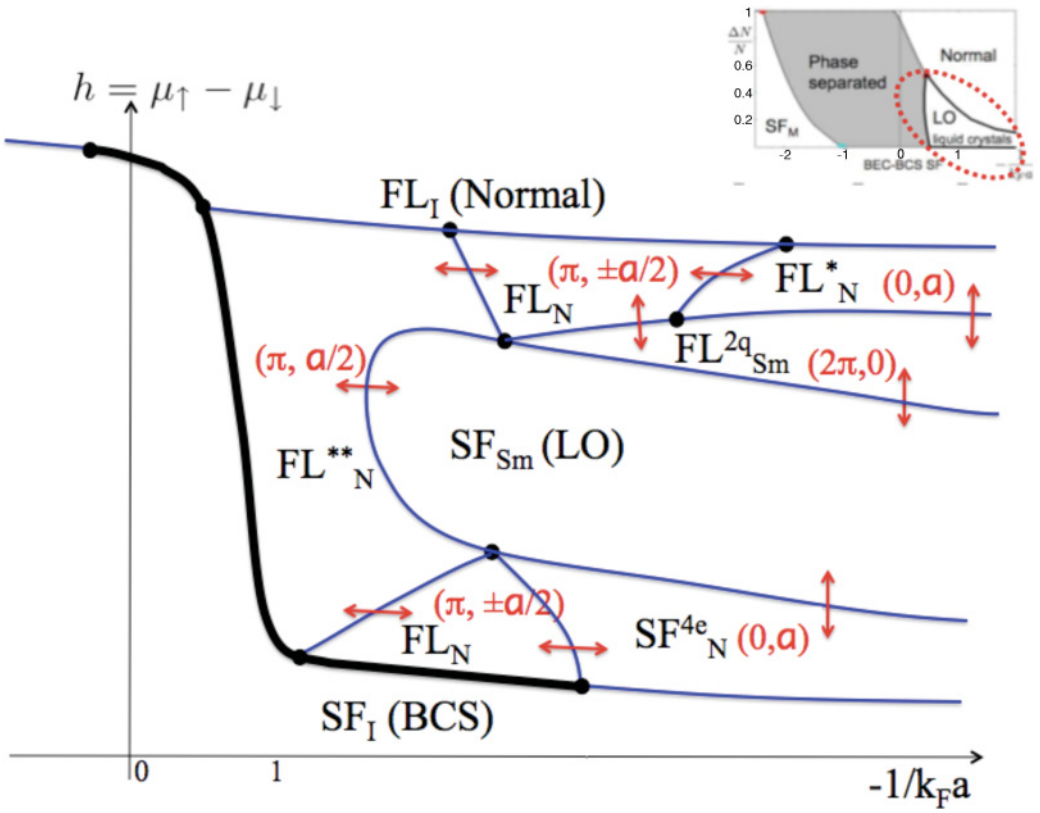

FIG. 4. (Color online) A schematic imbalance-chemical potential (Zeeman energy) $h = (\mu_\uparrow - \mu_\downarrow)/2$ vs detuning (interaction strength) $-1/k_F a$ phase diagram, illustrating the 3D LO smectic phase (SF_{Sm}) and its descendant (described in the text), driven by a proliferation of various combinations of topological defects. The inset shows the global imbalance-interaction BCS-BEC phase diagram, illustrating the location of these putative phases.

where the ultraviolet-divergent second term is regularized by a microscopic momentum cutoff scale $\Lambda \sim 1/d$ set by the range of the potential, d. This gives (with $\hbar = 1$ hereafter)

$$a_s(g) = \left(\frac{4\pi}{mg} + \frac{2\Lambda}{\pi}\right)^{-1} \equiv \frac{m}{4\pi} g_R \tag{11a}$$

$$= \frac{m}{4\pi} \frac{g}{1 + g/g_c}, \tag{11b}$$

where g_R is the effective screened coupling and $g_c = \frac{2\pi^2}{\Lambda m}$ is the critical coupling g (set by the zero-point energy at scale d) at which a molecular bound state appears and the scattering length diverges. The above relation allows a definition of the model and therefore a reexpression of physical observables in terms of the experimentally defined (uv-cutoff independent) scattering length a_s.

To treat the many-body problem (8), we utilize the standard mean-field analysis [4,44] (quantitatively valid deep in the BCS regime, $k_F a_s \ll 1$, but expected to be qualitatively valid throughout) by first assuming an expectation value

$$g\langle \hat{c}_\downarrow(\mathbf{r})\hat{c}_\uparrow(\mathbf{r})\rangle = \Delta(\mathbf{r}),$$
$$= \sum_{\mathbf{q}} \Delta_{\mathbf{q}} e^{i\mathbf{q}\cdot\mathbf{r}}, \tag{12}$$

corresponding to pair condensation at a superposition of finite momenta $\mathbf{q}$, with the set of $\Delta_{\mathbf{q}}$ and $\mathbf{q}$ to be self-consistently determined. With this mean-field assumption, H, in Eq. (8), reduces to the standard BCS mean-field form:

$$H = -\sum_{\mathbf{q}} \frac{|\Delta_{\mathbf{q}}|^2}{g} + \sum_{\mathbf{k}} (\epsilon_k - \mu_\sigma) \hat{c}^\dagger_{\mathbf{k}\sigma} \hat{c}_{\mathbf{k}\sigma}$$
$$+ \sum_{\mathbf{q},\mathbf{k}} \left(\Delta^*_{\mathbf{q}} \hat{c}_{\mathbf{k}+\frac{\mathbf{q}}{2}\downarrow} \hat{c}_{-\mathbf{k}+\frac{\mathbf{q}}{2}\uparrow} + \hat{c}^\dagger_{-\mathbf{k}+\frac{\mathbf{q}}{2}\uparrow} \hat{c}^\dagger_{\mathbf{k}+\frac{\mathbf{q}}{2}\downarrow} \Delta_{\mathbf{q}}\right), \tag{13}$$

which can equivalently be obtained using a Hubbard-Stratonovich transformation and a saddle-point approximation on the coherent-state path-integral formulation of the problem.

Although the resulting mean-field Hamiltonian is quadratic in the fermionic operators, its diagonalization for a generic $\Delta(\mathbf{r})$ (an arbitrary set of Fourier components $\Delta_{\mathbf{q}}$) is only possible through a numerical self-consistent solution of the Bogoliubov–de Gennes equations [95,96].

Analytical progress is, however, possible through two complementary approaches. One is to specialize to a single-Fourier-component $\Delta_{\mathbf{q}}$ FF state [76] that is self-consistently determined through the $\mathbf{q}$-dependent gap equation (12), equivalent to the ground-state energy minimization. This approach allows for a computation of the ground-state energy that is fully nonlinear in $\Delta_{\mathbf{q}}$. However, as emphasized in the Introduction with regard to learning about a more generic amplitude-modulated FFLO state this simplifying specialization to a single Fourier component is only harmless near the normal- to FFLO-state transition at the mean-field upper critical field

h_{c2}, where $\Delta_{\mathbf{q}}$ is small and physics is well approximated by the lowest dominant harmonic.

An alternative analytical approach is through the Ginzburg-Landau expansion, which allows a treatment of a general form of the superconducting order parameter, (12), but is again limited to the vicinity of h_{c2}, where $\Delta(\mathbf{r})$ is small, permitting Taylor expansion of the ground-state energy in terms of it [77].

B. Bogoliubov–de Gennes analysis of the Fulde-Ferrell state

1. Ground-state solution

Specializing to the Fulde-Ferrell (single-harmonic, $\Delta_{\mathbf{q}}$) state simplifies the mean-field Hamiltonian (8), allowing for a straightforward diagonalization [4,44,76] of the the associated Bogoliubov–de Gennes equations. A standard analysis [4] gives the (fermionic) Bogoliubov quasiparticle operators $\hat{\alpha}_{\mathbf{k}\sigma}$,

$$\hat{\alpha}_{\mathbf{k}\uparrow} = u_k \hat{c}_{-\mathbf{k}+\frac{\mathbf{q}}{2}\uparrow} + v_k \hat{c}^\dagger_{\mathbf{k}+\frac{\mathbf{q}}{2}\downarrow}, \tag{14a}$$

$$\hat{\alpha}^\dagger_{\mathbf{k}\downarrow} = -v^*_k \hat{c}_{-\mathbf{k}+\frac{\mathbf{q}}{2}\uparrow} + u^*_k \hat{c}^\dagger_{\mathbf{k}+\frac{\mathbf{q}}{2}\downarrow}, \tag{14b}$$

with the orthonormal coherence factors [99–101]

$$u_k = \frac{1}{\sqrt{2}}\sqrt{1+\frac{\varepsilon_k}{E_k}}, \tag{15a}$$

$$v_k = \frac{1}{\sqrt{2}}\sqrt{1-\frac{\varepsilon_k}{E_k}}, \tag{15b}$$

ensuring the canonical anticommutation relations $\{\hat{\alpha}_{\mathbf{k}\sigma},\hat{\alpha}^\dagger_{\mathbf{k}\sigma'}\} = \delta_{\sigma,\sigma'}$. In terms of these quasiparticles, the Hamiltonian reduces to a diagonal quadratic form,

$$H_{\rm FF} = \sum_{\mathbf{k}\sigma}[E_{\mathbf{k}\sigma}\Theta(E_{\mathbf{k}\sigma})\hat{\alpha}^\dagger_{\mathbf{k}\sigma}\hat{\alpha}_{\mathbf{k}\sigma} - E_{\mathbf{k}\sigma}\Theta(-E_{\mathbf{k}\sigma})\hat{\alpha}_{\mathbf{k}\sigma}\hat{\alpha}^\dagger_{\mathbf{k}\sigma}] + E^{\rm FF}_{\rm GS}(\Delta_{\mathbf{q}}), \tag{16}$$

with the ground-state energy given by

$$E^{\rm FF}_{\rm GS} = \sum_{\mathbf{k}}[\varepsilon_k - E_k + E_{\mathbf{k}\uparrow}\Theta(-E_{\mathbf{k}\uparrow}) + E_{\mathbf{k}\downarrow}\Theta(-E_{\mathbf{k}\downarrow})] - \frac{1}{g}|\Delta_{\mathbf{q}}|^2. \tag{17}$$

Here, we defined the excitation energy $E_{\mathbf{k}\sigma}$ for spin state σ,

$$E_{\mathbf{k}\uparrow} = E_k - h - \frac{\mathbf{k}\cdot\mathbf{q}}{2m}, \tag{18a}$$

$$E_{\mathbf{k}\downarrow} = E_k + h + \frac{\mathbf{k}\cdot\mathbf{q}}{2m}, \tag{18b}$$

with

$$\varepsilon_k \equiv \frac{k^2}{2m} - \mu + \frac{q^2}{8m}, \tag{19a}$$

$$E_k \equiv \left(\varepsilon_k^2 + \Delta_{\mathbf{q}}^2\right)^{1/2}, \tag{19b}$$

and $\mu = \frac{1}{2}(\mu_\uparrow + \mu_\downarrow)$, $h = \frac{1}{2}(\mu_\uparrow - \mu_\downarrow)$ the average and difference chemical potentials, respectively. The introduction of Θ functions in the above expressions divides the momentum space into three regions, for $h > 0$ given by (1) $\mathbf{k} \in \mathbf{k}_1$ such that $E_{\mathbf{k}\uparrow} > 0$ and $E_{\mathbf{k}\downarrow} > 0$, (2) $\mathbf{k} \in \mathbf{k}_2$ such that $E_{\mathbf{k}\uparrow} < 0$, and (3) $\mathbf{k} \in \mathbf{k}_3$ such that $E_{\mathbf{k}\downarrow} < 0$, (it is easy to see that the $E_{\mathbf{k}\sigma}$ cannot both be negative), and by construction ensures a positive-definite excitation spectrum $|E_{\mathbf{k}\sigma}|$ above the FF ground state,

$$|{\rm FF}_{\mathbf{q}}\rangle = \prod_{\mathbf{k}\in E_{\mathbf{k}\sigma}<0}\hat{\alpha}^\dagger_{\mathbf{k}\sigma}|{\rm BCS}_{\mathbf{q}}\rangle \tag{20a}$$

$$= \prod_{\mathbf{k}\in\mathbf{k}_3}\hat{c}^\dagger_{\mathbf{k}+\frac{\mathbf{q}}{2}\downarrow}\prod_{\mathbf{k}\in\mathbf{k}_2}\hat{c}^\dagger_{-\mathbf{k}+\frac{\mathbf{q}}{2}\uparrow}\prod_{\mathbf{k}\in\mathbf{k}_1}\left(u_{\mathbf{k}} + v_{\mathbf{k}}\hat{c}^\dagger_{\mathbf{k}+\frac{\mathbf{q}}{2}\downarrow}\hat{c}^\dagger_{-\mathbf{k}+\frac{\mathbf{q}}{2}\uparrow}\right)|0\rangle, \tag{20b}$$

with $|0\rangle$ the atom vacuum. The first form demonstrates that the FF ground state can be formally thought of as the Fermi sea of negative energy Bogoliubov quasiparticles added to the BCS state $|{\rm BCS}_{\mathbf{q}}\rangle$ (which is *not* the ground state) with the center-of-mass momentum $\mathbf{q}$. The second form, above, shows that equivalently the FF ground state corresponds to a finite center-of-mass momentum ($\mathbf{q}$) BCS state with unpaired atoms from the two momenta sets $\mathbf{k}_2$ and $\mathbf{k}_3$, defined above.

This analysis thus suggests a possibility of two distinct FF states, ${\rm FF}_{fs1}$ and ${\rm FF}_{fs2}$, that exhibit a single- and two-species Fermi surfaces, respectively, with their volume difference set by the imposed species imbalance [62].

2. Analysis near h_{c2}

The energetic stability of the state is controlled by $E^{\rm FF}_{\rm GS}(\Delta_{\mathbf{q}})$, which deep in the BCS limit was first computed by Fulde and Ferrell [76]. Its full behavior throughout the BCS-BEC crossover generally requires a combination of numerical and analytical analysis. This led to the prediction of a narrow sliver of stability of the FF state confined to the BCS side of the crossover, $-1/(k_F a_s) \gtrsim 0.46$ [4,44]. However, as discussed in the Introduction, given the expected unfavorable nature of the FF state (lacking the amplitude nodes necessary to accommodate the imbalanced atoms) this analysis is unlikely to shed light on the stability of other (e.g., LO-type) states far below the h_{c2} transition to them. Nevertheless, because the transition at the upper critical field h_{c2} (at least in mean-field theory) is expected to be continuous and therefore $\Delta_{\mathbf{q}}$ small, growing from 0, $E^{\rm FF}_{\rm GS}(\Delta_{\mathbf{q}})$ can be analyzed analytically by Taylor-expanding it in $\Delta_{\mathbf{q}}$.

Taking advantage of the extensive analysis in [4,44], near h_{c2} we obtain

$$E^{\rm FF}_{\rm GS} \approx \varepsilon_q|\Delta_{\mathbf{q}}|^2 + \tfrac{1}{2}\tilde{V}_{\mathbf{q},\mathbf{q},\mathbf{q},\mathbf{q}}|\Delta_{\mathbf{q}}|^4, \tag{21}$$

where

$$\varepsilon_q \approx \frac{3n}{4\epsilon_F}\left[-1 + \frac{1}{2}\ln\frac{v_{\rm F}^2q^2 - 4h^2}{\Delta^2_{\rm BCS}} + \frac{h}{v_{\rm F}q}\ln\frac{v_{\rm F}q + 2h}{v_{\rm F}q - 2h}\right], \tag{22}$$

and

$$\tilde{V}_{\mathbf{q},\mathbf{q},\mathbf{q},\mathbf{q}} = \frac{3n}{4\epsilon_{\rm F}}\frac{1}{v_{\rm F}^2q^2 - 4h^2}, \tag{23}$$

which agree with the Larkin-Ovchinnikov result [77] obtained via a direct Landau expansion in $\Delta_{\mathbf{q}}$. Here we used (10) to eliminate the interaction coupling g in favor of the scattering length a_s and then reexpressed the latter in terms of the BCS superfluid gap $\Delta_{\rm BCS}$ according to $-m/(4\pi a_s) = N(\epsilon_{\rm F})\ln(8e^{-2}/\Delta_{\rm BCS})$, with 3D density of states

$N(\epsilon) = m^{3/2}\sqrt{\epsilon}/(\sqrt{2}\pi^2)$. Near its minimum ε_q can be approximated quadratically in q,

$$\varepsilon_q \approx \varepsilon_0 + \tfrac{1}{2} J\left(q^2 - q_0^2\right)^2 + \cdots, \tag{24}$$

with

$$\varepsilon_0 = \frac{3n}{4\epsilon_F} \ln\left[2\sqrt{\alpha^2-1}\frac{h}{\Delta_{BCS}}\right] \equiv \frac{3n}{4\epsilon_F}\ln\left[\frac{h}{h_{c2}}\right], \tag{25a}$$

$$q_0 = 2\alpha\frac{h}{v_F}, \tag{25b}$$

$$J \approx \frac{1}{\alpha^2-1}\frac{3n\epsilon_F}{16k_F^2 q_0^2}\frac{1}{h^2}. \tag{25c}$$

Here, α is a solution of the equation arising from the minimization of the ground-state energy with respect to the center-of-mass momentum q [4,44],

$$\alpha = \frac{1}{2}\ln\frac{\alpha+1}{\alpha-1} \tag{26a}$$

$$\approx 1.200. \tag{26b}$$

Combining this value with the point at which $\varepsilon_0(h)$ vanishes, we obtain the N-FFLO upper critical transition field [76,77],

$$h_{c2} \equiv h_{FFLO} = \frac{\Delta_{BCS}}{2\sqrt{\alpha^2-1}} \tag{27a}$$

$$\approx 0.754\Delta_{BCS}. \tag{27b}$$

At this transition point we have

$$q_0 = \frac{\alpha}{\sqrt{\alpha^2-1}}\frac{\Delta_{BCS}}{v_F} \tag{28a}$$

$$= 1.81\frac{\Delta_{BCS}}{v_F} = \frac{0.58}{\xi_0} \quad \text{at the } h_{c2} \text{ transition,} \tag{28b}$$

$$J \approx \frac{\alpha^2}{\alpha^2-1}\frac{3n}{16\epsilon_F}\frac{1}{q_0^4} \tag{28c}$$

$$\approx 0.61\frac{n}{\epsilon_F}\frac{1}{q_0^4} \quad \text{at the } h_{c2} \text{ transition,} \tag{28d}$$

where the BCS coherence length is given by its standard expression $\xi_0 = v_F/(\pi\Delta_{BCS})$.

Near the h_{c2} transition the FF quartic vertex (23) also simplifies, giving

$$\tilde{V}_{\mathbf{q},\mathbf{q},\mathbf{q},\mathbf{q}} \approx \frac{3n}{4\epsilon_F}\frac{1}{\alpha^2-1}\frac{1}{4h^2} \tag{29a}$$

$$\approx \frac{3n}{4\epsilon_F}\frac{0.57}{h^2} \tag{29b}$$

$$\approx \frac{3n}{4\epsilon_F}\frac{1}{\Delta_{BCS}^2} \quad \text{at the } h_{c2} \text{ transition,} \tag{29c}$$

which agrees precisely with perturbative LO result [77].

As we will see shortly, in a single-plane-wave FF state the transverse superfluid stiffness for a supercurrent flowing transversely vanishes identically, enforced by a Ward identity. As mentioned in the Introduction this property is a special feature of a single-momentum-component FF state and is guaranteed by the underlying rotational invariance of the spontaneous current to an energy-equivalent ground state. Thus, to correctly (even qualitatively) capture a more general FFLO (e.g., the LO) state requires the inclusion of the multiple momentum components, as in (12) and an analysis beyond the lowest-order LO treatment [77]. This unfortunately cannot be calculated analytically through the Bogoliubov–de Gennes analysis, although it quite successfully can numerically [95,96] and through the Ginzburg-Landau expansion to which we now turn.

C. Ginzburg-Landau expansion near h_{c2}

The analytical treatment of the LO state near h_{c2} relies on the Ginzburg-Landau expansion in $\Delta_{\mathbf{q}}$, which is small near the (in mean-field) continuous h_{c2} normal to FFLO transition [77,150]. This expectation is explicitly supported by the exact 1D BdG solution [95] at high fields, where $\Delta(x)$ is indeed well approximated by a single harmonic, with an amplitude Δ_q that vanishes continuously near h_{c2}.

Based on these general arguments, near h_{c2} the Ginzburg-Landau expansion for the ground-state energy is expected to take a familiar form,

$$\mathcal{H} \approx \sum_{\mathbf{q}} \varepsilon_q |\Delta_{\mathbf{q}}|^2 + \frac{1}{2}\sum_{\mathbf{q}_1,\mathbf{q}_2,\mathbf{q}_3,\mathbf{q}_4} \tilde{V}_{\mathbf{q}_1,\mathbf{q}_2,\mathbf{q}_3,\mathbf{q}_4}\Delta^*_{\mathbf{q}_1}\Delta_{\mathbf{q}_2}\Delta^*_{\mathbf{q}_3}\Delta_{\mathbf{q}_4}, \tag{30}$$

where rotational invariance constrains ε_q to be a function of the magnitude of $\mathbf{q}$ only, $\mathbf{q}_4 = \mathbf{q}_1 - \mathbf{q}_2 + \mathbf{q}_3$, and $\Delta_{\mathbf{q}}$ is a Fourier transform of $\Delta(\mathbf{r})$.

It is straightforward to see that translational and rotational invariances and the quadratic form (in $\Delta_{\mathbf{q}}$) of the first term in $\mathcal{H}$ guarantee that ε_q is independent of the type of FFLO state, and is therefore identical to that of the FF state, (22) [4]. This observation guarantees that all harmonics with magnitude q_0 become unstable at the same imbalance field h_{c2}, h_{FFLO}, with the degeneracy only lifted by the quartic $\Delta_{\mathbf{q}}$ term in $\mathcal{H}$.

Following the standard prescription and guided by the seminal (lowest-order) analysis of Larkin and Ovchinnikov [77], we now derive the quartic vertex function $\tilde{V}_{\mathbf{q}_1,\mathbf{q}_2,\mathbf{q}_3,\mathbf{q}_4}$ appearing in Eq.(30). It, together with ε_q will then allow us to derive the key elastic moduli (compression modulus, bending rigidity, and superfluid stiffnesses) characterizing the Goldstone modes of the striped FFLO states. As first found in Ref. [112], one key observation is that a derivation of a generic Ginzburg-Landau form and consequently of a generic Goldstone-mode theory requires a calculation that is of higher order than that originally carried out by Larkin and Ovchinnikov [77]. In particular, as we will see below, the leading momentum dependence of the quartic coupling needs to be kept. It corresponds to an induced short-ranged current-current interaction $v_{ij}j_i j_j$, with the supercurrent given by the standard expression

$$j_i = \frac{1}{m}\mathrm{Re}[-\Delta^*(\mathbf{r})i\partial_i\Delta(\mathbf{r})]. \tag{31}$$

To derive the generic Ginzburg-Landau form, we use the imaginary-time fermionic coherent-state path-integral formulation of the BCS problem, by computing the partition function,

$$Z = \mathrm{Trace}[e^{-\beta H[\psi^*_\sigma,\psi_\sigma]}] \tag{32a}$$

$$= \int [d\psi^*_\sigma d\psi_\sigma] e^{-S_\tau[\psi^*_\sigma,\psi_\sigma]}, \tag{32b}$$

where H is the four-Fermi Hamiltonian (8), $\psi_\sigma(\tau,\mathbf{r})$ Grassmann (anticommuting) fields, and the imaginary-time action is given by

$$S_\tau[\psi_\sigma^*,\psi_\sigma] = \int d\tau d^d r[\psi_\sigma^*(\partial_\tau + \hat{\xi}_\sigma)\psi_\sigma + g\psi_\uparrow^*\psi_\downarrow^*\psi_\downarrow\psi_\uparrow], \tag{33}$$

where for notational shorthand we defined a space-time coordinate $\mathbf{x} \equiv (\tau,\mathbf{r})$ and a single-particle Hamiltonian operator $\hat{\xi}_\sigma = -\frac{\nabla^2}{2m} - \mu_\sigma$.

We use the Cooper-pair Hubbard-Stratonovich field $\Delta(\mathbf{x})$ to decouple the (quartic) pairing interaction g and to integrate out the fermionic atoms:

$$Z = \int [d\bar{\psi}_\sigma d\psi_\sigma d\bar{\Delta} d\Delta] e^{-S_\tau[\psi_\sigma^*,\psi_\sigma,\Delta^*,\Delta]} \tag{34a}$$

$$\equiv \int [d\Delta^* d\Delta] e^{-S_{\rm eff}[\Delta^*,\Delta]}, \tag{34b}$$

where $S_\tau = S_0 + S_{\rm int} - \frac{1}{g}\int_{\mathbf{x}} |\Delta|^2$,

$$S_0 = \int_{\mathbf{x}} \left[\psi_\sigma^*(\partial_\tau + \hat{\xi}_\sigma)\psi_\sigma - \frac{1}{g}|\Delta|^2\right], \tag{35a}$$

$$S_{\rm int} = \int_{\mathbf{x}} [\Delta\psi_\uparrow^*\psi_\downarrow^* + \psi_\downarrow\psi_\uparrow\Delta^*], \tag{35b}$$

and we defined the Ginzburg-Landau effective action

$$S_{\rm eff}[\Delta^*,\Delta] = -\ln\left[\int [d\bar{\psi}_\sigma d\psi_\sigma] e^{-S_\tau[\psi_\sigma^*,\psi_\sigma,\Delta^*,\Delta]}\right]. \tag{36}$$

Taylor-expanding S_τ in powers of $S_{\rm int}$, we compute $S_{\rm eff}$ in powers of Δ. Relegating all technical details to Appendix A and focusing on the time-independent quartic order [in $\Delta(\mathbf{r})$] contribution, given by the connected fourth cumulant $S_4 = \int d\tau H_4$, we find

$$H_4 = \frac{1}{2}\int_{\mathbf{r}_1\mathbf{r}_2\mathbf{r}_3\mathbf{r}_4} V(\mathbf{r}_1,\mathbf{r}_2,\mathbf{r}_3,\mathbf{r}_4)\Delta^*(\mathbf{r}_1)\Delta(\mathbf{r}_2)\Delta^*(\mathbf{r}_3)\Delta(\mathbf{r}_4), \tag{37}$$

where

$$V(\mathbf{r}_1,\mathbf{r}_2,\mathbf{r}_3,\mathbf{r}_4) = \int \frac{d\omega}{2\pi}\tilde{G}_\uparrow^0(\mathbf{r}_2-\mathbf{r}_1,\omega)\tilde{G}_\downarrow^0(\mathbf{r}_2-\mathbf{r}_3,-\omega)\tilde{G}_\uparrow^0(\mathbf{r}_4-\mathbf{r}_3,\omega)\tilde{G}_\downarrow^0(\mathbf{r}_4-\mathbf{r}_1,-\omega), \tag{38a}$$

$$\tilde{V}(\mathbf{q}_1,\mathbf{q}_2,\mathbf{q}_3,\mathbf{q}_4) = \int \frac{d\omega d^d k}{(2\pi)^{d+1}}\tilde{G}_\uparrow^0(\mathbf{k},\omega)\tilde{G}_\downarrow^0(\mathbf{q}_1-\mathbf{k},-\omega)\tilde{G}_\uparrow^0(\mathbf{k}-\mathbf{q}_1+\mathbf{q}_2,\omega)\tilde{G}_\downarrow^0(\mathbf{q}_4-\mathbf{k},-\omega), \tag{38b}$$

with the noninteracting fermionic Green's function (in Fourier space) as usual given by

$$G_\sigma^0(\omega_n,q) = -\langle\psi_\sigma\psi_\sigma^*\rangle_0 \tag{39a}$$

$$= \frac{1}{i\omega_n - \xi_{q\sigma}}. \tag{39b}$$

We focus on the FFLO-type order parameter

$$\Delta(\mathbf{r}) = \sum_{\mathbf{q}_n} \Delta_{\mathbf{q}_n}(\mathbf{r})\, e^{i\mathbf{q}_n\cdot\mathbf{r}}, \tag{40}$$

with Fourier transform given by

$$\Delta(\mathbf{q}) = \sum_{\mathbf{q}_n} \Delta_{\mathbf{q}_n}(\mathbf{q}-\mathbf{q}_n). \tag{41}$$

We note that to go beyond the mean field, here we included an additional long-scale positional dependence in the Larkin-Ovchinnikov order parameters $\Delta_{q_n}(\mathbf{r})$ on top of the short-scale mean-field periodic dependence at the LO wave vectors q_n encoded in the plane-wave factor.

Substitution of this form into H_4 gives

$$H_4 = \frac{1}{2}\sum_{\mathbf{q}_{n_i}}\int_{\tilde{\mathbf{q}}_i}(2\pi)^d\delta^d(\tilde{\mathbf{q}}_1-\tilde{\mathbf{q}}_2+\tilde{\mathbf{q}}_3-\tilde{\mathbf{q}}_4)\delta_{\mathbf{q}_{n_1}-\mathbf{q}_{n_2}+\mathbf{q}_{n_3}-\mathbf{q}_{n_4},0}$$

$$\times\,\tilde{V}\left(\mathbf{q}_{n_1}+\tilde{\mathbf{q}}_1,\mathbf{q}_{n_2}+\tilde{\mathbf{q}}_2,\mathbf{q}_{n_3}+\tilde{\mathbf{q}}_3,\mathbf{q}_{n_4}+\tilde{\mathbf{q}}_4\right)\Delta_{\mathbf{q}_{n_1}}^*(\tilde{\mathbf{q}}_1)\Delta_{\mathbf{q}_{n_2}}(\tilde{\mathbf{q}}_2)\Delta_{\mathbf{q}_{n_3}}^*(\tilde{\mathbf{q}}_3)\Delta_{\mathbf{q}_{n_4}}(\tilde{\mathbf{q}}_4), \tag{42}$$

with $\tilde{\mathbf{q}}_i \equiv \mathbf{q}_i - \mathbf{q}_{n_i} \ll \mathbf{q}_{n_i}$ [because $\Delta_{q_{n_i}}(\tilde{\mathbf{q}}_i)$ is expected to be sharply peaked around $\tilde{\mathbf{q}}_i = \mathbf{0}$], allowing us to disentangle the q sums and integrals, and the corresponding δ function above, without double-counting momentum states.

To lowest order in $\tilde{\mathbf{q}}_i$, we ignore its dependence on $\tilde{V}$, equivalent to the LO treatment [77], with $\tilde{V}(\mathbf{q}_{n_1}+\tilde{\mathbf{q}}_1,\mathbf{q}_{n_2}+\tilde{\mathbf{q}}_2,\mathbf{q}_{n_3}+\tilde{\mathbf{q}}_3,\mathbf{q}_{n_4}+\tilde{\mathbf{q}}_4) \approx \tilde{V}(\mathbf{q}_{n_1},\mathbf{q}_{n_2},\mathbf{q}_{n_3},\mathbf{q}_{n_4})$, and thereby obtain the quartic vertex that determines which set of reciprocal momenta $\mathbf{q}_{n_i}$ (satisfying the momentum conservation) minimizes the interaction energy, thereby defining the structure of the FFLO ground state. As found by LO [77], near h_{c2} it is the striped state of collinear $\mathbf{q}_{n_i}$'s that is energetically favored and is well approximated

by the lowest pair of harmonics, $\mathbf{q}_{n_i} = \pm\mathbf{q}$. Focusing on this energetically preferred (near h_{c2}) LO state reduces the general form of H_4 in Eq. (43) to

$$H_4 = \frac{1}{2}\int_{\tilde{\mathbf{q}}_i}(2\pi)^d\delta^d(\tilde{\mathbf{q}}_1-\tilde{\mathbf{q}}_2+\tilde{\mathbf{q}}_3-\tilde{\mathbf{q}}_4)\Bigg[\sum_{\mathbf{q}_1=\pm\mathbf{q}}\tilde{V}(\mathbf{q}_1+\tilde{\mathbf{q}}_1,\mathbf{q}_1+\tilde{\mathbf{q}}_2,\mathbf{q}_1+\tilde{\mathbf{q}}_3,\mathbf{q}_1+\tilde{\mathbf{q}}_4)\Delta^*_{\mathbf{q}_1}(\tilde{\mathbf{q}}_1)\Delta_{\mathbf{q}_1}(\tilde{\mathbf{q}}_2)\Delta^*_{\mathbf{q}_1}(\tilde{\mathbf{q}}_3)\Delta_{\mathbf{q}_1}(\tilde{\mathbf{q}}_4)$$

$$+4\tilde{V}(\mathbf{q}+\tilde{\mathbf{q}}_1,\mathbf{q}+\tilde{\mathbf{q}}_2,-\mathbf{q}+\tilde{\mathbf{q}}_3,-\mathbf{q}+\tilde{\mathbf{q}}_4)\Delta^*_{\mathbf{q}}(\tilde{\mathbf{q}}_1)\Delta_{\mathbf{q}}(\tilde{\mathbf{q}}_2)\Delta^*_{-\mathbf{q}}(\tilde{\mathbf{q}}_3)\Delta_{-\mathbf{q}}(\tilde{\mathbf{q}}_4)\Bigg]. \tag{43}$$

Taylor-expansion of $\tilde{V}(\mathbf{q}_{n_1}+\tilde{\mathbf{q}}_1,\mathbf{q}_{n_2}+\tilde{\mathbf{q}}_2,\mathbf{q}_{n_3}+\tilde{\mathbf{q}}_3,\mathbf{q}_{n_4}+\tilde{\mathbf{q}}_4)$ in $\tilde{\mathbf{q}}_i$ then gives $H_4 = H_4^{(0)} + H_4^{(2)}$, with

$$H_4^{(0)} = \frac{1}{2}\int_{\mathbf{r}}[v^{(0)}_{++}(|\Delta_{\mathbf{q}}(\mathbf{r})|^4+|\Delta_{-\mathbf{q}}(\mathbf{r})|^4)+4v^{(0)}_{+-}|\Delta_{\mathbf{q}}(\mathbf{r})|^2|\Delta_{-\mathbf{q}}(\mathbf{r})|^2], \tag{44}$$

where

$$v^{(0)}_{++} = \tilde{V}(\mathbf{q},\mathbf{q},\mathbf{q},\mathbf{q}) = \int\frac{d\omega d^dk}{(2\pi)^{d+1}}\tilde{G}^0_\uparrow(\mathbf{k},\omega)^2\tilde{G}^0_\downarrow(\mathbf{q}-\mathbf{k},-\omega)^2, \tag{45a}$$

$$v^{(0)}_{+-} = \tilde{V}(\mathbf{q},\mathbf{q},-\mathbf{q},-\mathbf{q}) = \int\frac{d\omega d^dk}{(2\pi)^{d+1}}\tilde{G}^0_\uparrow(\mathbf{k},\omega)^2\tilde{G}^0_\downarrow(\mathbf{q}-\mathbf{k},-\omega)\tilde{G}^0_\downarrow(-\mathbf{q}-\mathbf{k},-\omega), \tag{45b}$$

already computed by LO in their mean-field approximation and in Ref. [4] from the expansion of the BdG ground-state energy of the FF state discussed in Sec. II B.

In computing the higher-order $H_4^{(2)}$ term that contains the essential current-current interaction $v_{ij}j_ij_j$ discussed in the previous section, we will neglect contributions from the first set of terms in Eq.(43) (++ and −− terms), because they lead to $\mathbf{j}^2_{\mathbf{q}}$ (positive $\mathbf{q}$ current) and $\mathbf{j}^2_{-\mathbf{q}}$ (negative $\mathbf{q}$ current) contributions whose coefficients are enforced either by rotational invariance (which for transverse current each are 1/2 of the coefficient of the $\mathbf{j}_{\mathbf{q}}\mathbf{j}_{-\mathbf{q}}$ term, required to keep the smectic phonon field u soft), or for the longitudinal pieces are small, i.e., higher-order, subleading corrections to the nonzero quadratic (in Δ) terms computed in the previous section.

To proceed we focus on the second term in Eq. (43), and Taylor-expand it to second order in $\tilde{\mathbf{q}}_i$

$$\tilde{V}(\mathbf{q}+\tilde{\mathbf{q}}_1,\mathbf{q}+\tilde{\mathbf{q}}_2,-\mathbf{q}+\tilde{\mathbf{q}}_3,-\mathbf{q}+\tilde{\mathbf{q}}_4) \approx v^{(0)}_{+-}+\frac{v^{(2)}_{ij}(\mathbf{q})}{4m^2}(\tilde{q}_{1i}\tilde{q}_{4j}+\tilde{q}_{1i}\tilde{q}_{3j}+\tilde{q}_{2i}\tilde{q}_{4j}+\tilde{q}_{2i}\tilde{q}_{3j}), \tag{46}$$

taking advantage of momentum conservation $\mathbf{q}_1-\mathbf{q}_2+\mathbf{q}_3-\mathbf{q}_4=\mathbf{0}$ to generate four equivalent terms such that the expression is explicitly real. Here we defined the current-current coupling matrix

$$v^{(2)}_{ij} = m^2\int\frac{d\omega d^dk}{(2\pi)^{d+1}}\tilde{G}^0_\uparrow(\mathbf{k},\omega)^2\partial_i\tilde{G}^0_\downarrow(\mathbf{q}-\mathbf{k},-\omega)\partial_j\tilde{G}^0_\downarrow(-\mathbf{q}-\mathbf{k},-\omega) \tag{47a}$$

$$= g_1\delta_{ij}+g_2\hat{\mathbf{q}}_i\hat{\mathbf{q}}_j, \tag{47b}$$

where

$$g_1 = \frac{N(\epsilon_F)k_F^2}{2v_F^4q_0^4}\alpha_1\left(\frac{2h}{v_Fq_0}\right) \tag{48a}$$

$$\approx 2.07\frac{N(\epsilon_F)k_F^2}{2v_F^4q_0^4} \quad \text{at the } h_{c2} \text{ transition}, \tag{48b}$$

$$g_2 = \frac{N(\epsilon_F)k_F^2}{2v_F^4q_0^4}\alpha_2\left(\frac{2h}{v_Fq_0}\right) \tag{48c}$$

$$\approx -5.75\frac{N(\epsilon_F)k_F^2}{2v_F^4q_0^4} \quad \text{at the } h_{c2} \text{ transition}, \tag{48d}$$

are computed in Appendix A. Conversion of this Fourier-space expression into real space gives

$$H_4^{(2)} \approx \frac{1}{2}\int_{\mathbf{r}}4v^{(2)}_{ij}\left[\frac{1}{m}\mathrm{Re}[-\Delta^*_{\mathbf{q}}i\partial_i\Delta_{\mathbf{q}}(\mathbf{r})]\frac{1}{m}\mathrm{Re}[-\Delta^*_{-\mathbf{q}}i\partial_j\Delta_{-\mathbf{q}}(\mathbf{r})]\right] \tag{49a}$$

$$\approx \frac{1}{2}\int_{\mathbf{r}}4v^{(2)}_{ij}j^i_{\mathbf{q}}j^j_{-\mathbf{q}} \tag{49b}$$

$$\approx \frac{1}{2}\int_{\mathbf{r}} 2v_{ij}^{(2)}(\mathbf{j_q}+\mathbf{j_{-q}})_i(\mathbf{j_q}+\mathbf{j_{-q}})_j \tag{49c}$$

$$\approx \frac{1}{2}\int_{\mathbf{r}} 8v_{ij}^{(2)} j_i j_j, \tag{49d}$$

where we reconstructed the $j^i_{\mathbf{q}} j^j_{\mathbf{q}}$ and $j^i_{-\mathbf{q}} j^j_{-\mathbf{q}}$ transverse pieces (by rotational invariance) and defined the total supercurrent $\mathbf{j} = (\mathbf{j_q} + \mathbf{j_{-q}})/2$.

It is important to note already at this stage that the positivity of $g_1 > 0$ in Eq. (48) generates a positive *transverse* superfluid stiffness $\rho_s^\perp$ and therefore a well-defined LO state. Furthermore, we note that (as we will see in Sec. III) the fact that g_2 and even $g_1 + g_2$ are negative does not cause any stability difficulties as they lead to $O((\Delta_{q_0}/\Delta_{\rm BCS})^4)$ corrections to the longitudinal superfluid stiffness $\rho_s^\parallel$, a correction that is subdominant near h_{c2}. However, the opposite signs do suggest that below h_{c2}, $\rho_s^\perp$ grows, while $\rho_s^\parallel$ decreases with decreasing chemical potential difference h. It is thus conceivable that the anisotropy ratio $\rho_s^\perp/\rho_s^\parallel$ (starting at 0 just below h_{c2}) may actually grow above 1, i.e., that the superfluid anisotropy may reverse, something that would have striking experimental consequences.

Putting the ingredients derived above together, we finally obtain the sought-after Ginzburg-Landau Hamiltonian

$$\mathcal{H}_{\rm GL} = J[|\nabla^2\Delta|^2 - 2q_0^2|\nabla\Delta|^2] + r|\Delta|^2 + \tfrac{1}{2}\lambda_1|\Delta|^4 + \tfrac{1}{2}\lambda_2\mathbf{j}^2 + \cdots, \tag{50}$$

where as just derived, deep in the BCS limit (large positive detuning, $k_F a_s \ll 1$) and near the h_{c2} transition to the polarized normal state the model parameters are given by

$$J \approx \frac{0.61n}{\epsilon_F q_0^4}, \tag{51a}$$

$$q_0 \approx \frac{1.81\Delta_{\rm BCS}}{\hbar v_F}, \tag{51b}$$

$$r \approx \frac{3n}{4\epsilon_F}\ln\left[\frac{9h}{4h_{c2}}\right], \tag{51c}$$

$$h_{c2} \approx \frac{3}{4}\Delta_{\rm BCS}, \tag{51d}$$

$$\lambda_1 \approx \frac{3n}{4\epsilon_F\Delta_{\rm BCS}^2}, \tag{51e}$$

$$\lambda_2 \approx \frac{1.83nm^2}{\epsilon_F\Delta_{\rm BCS}^2 q_0^2}. \tag{51f}$$

Based on the discussion following Eq. (49), we approximated the anisotropic tensor coupling $v_{ij}^{(2)}$, Eq. (47), by an isotropic one of strength set by the transverse part of $v_{ij}^{(2)}$, namely, g_1, with the difference a subleading correction near h_{c2}. More generally (away from the weak-coupling BCS limit) these couplings can be taken as phenomenological parameters to be determined experimentally.

III. THEORY OF GOLDSTONE MODES IN STRIPED FFLO STATES

A. Landau theory

The general form of the Ginzburg-Landau model (50) derived in the previous section has a much broader range of applicability, even if our derivation and microscopic predictions for the associated coupling constants in Eq. (51) only apply in the BCS regime, near h_{c2}. Independent of the microscopics, the key ingredient of $\mathcal{H}_{\rm GL}$ is that it captures the imbalanced atomic Fermi system's energetic tendency to pair at a finite momentum, and thereby forms a pair-density wave characterized by a reciprocal lattice vector with magnitude q_0 and spontaneously chosen orientation. More generally, we expect the quadratic [in $\Delta(\mathbf{r})$] part of $\mathcal{H}_{\rm GL}$,

$$\mathcal{H}^0_{\rm GL} = \Delta^*\hat{\varepsilon}\Delta, \tag{52}$$

to be characterized by a more generic differential kernel [specialized to a quadratic form, $\hat{\varepsilon} = J(-\nabla^2 - q_0^2)^2 + r - Jq_0^4$ in (50)], exhibiting a minimum at a finite momentum with a magnitude q_0 and an arbitrary orientation. However, it can be shown [151] that this generalization adds little new physics to the Lifshitz-like normal- to FFLO-state (PDW) transition and to the emerging Goldstone-mode theory, which is our main interest. We will therefore work directly with the simpler form in (50).

With the minimum in the dispersion $\hat{\varepsilon}(q)$ located at a finite momentum magnitude q_0, for $r < r_c$ (which in the mean-field BCS approximation is given by $r_c = Jq_0^4 \approx 0.61n/\varepsilon_F$, or equivalently at $h < h_{c2} \approx \frac{3}{4}\Delta_{\rm BCS}$) the gap in $\hat{\varepsilon}(q)$ closes and $\mathcal{H}_{\rm GL}$ in (50) develops an instability to a nonzero superconducting (pairing) order parameter $\Delta(\mathbf{r}) = \sum_{\mathbf{q}_n}\Delta_{\mathbf{q}_n}e^{i\mathbf{q}_n\cdot\mathbf{r}}$ at a set of nonzero wave vectors $\mathbf{q}_n$ with a magnitude of the fundamental given by the dispersion minimum q_0.

As with other crystallization problems, the nontrivial question of the choice of the set of the momenta $\mathbf{q}_n$ is determined by the details of the interaction (terms higher than quadratic order in Δ) and will not be addressed here. Instead, motivated by the LO findings and by the more recent analyses [77,95–98], we will focus on the *unidirectional* pair-density-wave (Cooper-pair stripe) order, characterized by a *collinear* set of $\mathbf{q}_n$'s. That is, we will assume that such states are energetically stable, will develop their Goldstone-mode low-energy description, and will analyze their stability to fluctuations.

As we will see below, within this *unidirectional* pair-density wave class of FFLO states, the FF and LO states are representatives of two qualitatively distinct universality classes and therefore must be treated separately. Although (as argued in the Introduction) it is the latter that is expected to

be significantly more stable, for completeness and potential of other microscopic realizations (where FF states may be stable) we will treat both universality classes.

The low-energy properties of the FF and LO states are described by a periodically spatially modulated order parameter $\Delta(\mathbf{r})$, that in its simplest form, quantitatively valid near h_{c2}, is well captured with a single $\pm\mathbf{q}$ pair of ordering momenta,

$$\Delta_{\mathrm{FFLO}}(\mathbf{r}) = \Delta_+(\mathbf{r})\, e^{i\mathbf{q}\cdot\mathbf{r}} + \Delta_-(\mathbf{r})\, e^{-i\mathbf{q}\cdot\mathbf{r}}, \tag{53}$$

where $\Delta_\pm(\mathbf{r})$ are two complex scalar order parameters, the dominant Fourier coefficients of $\Delta(\mathbf{r})$,

$$\Delta_\pm(\mathbf{r}) = \Delta^0_\pm(\mathbf{r})\, e^{i\phi_\pm(\mathbf{r})}, \tag{54}$$

and amplitudes $\Delta^0_\pm$ distinguishing between the FF and LO states. We first focus on the amplitudes of these two order parameters, for now ignoring the corresponding Goldstone modes $\phi_\pm$. Taking $\Delta_\pm(\mathbf{r})$ as spatially independent (to be justified *a posteriori*), we use the Ginzburg-Landau theory (50) to determine their magnitudes. To this end we find

$$\begin{aligned}\mathcal{H}_{\mathrm{Landau}} = {}& \tilde{r}(|\Delta_+|^2 + |\Delta_-|^2) + \frac{3}{4}\lambda_1(|\Delta_+|^2 + |\Delta_-|^2)^2 \\ & + \frac{1}{2}\left(\lambda_2\frac{q^2}{m^2} - \frac{1}{2}\lambda_1\right)(|\Delta_+|^2 - |\Delta_-|^2)^2,\end{aligned} \tag{55}$$

where $\tilde{r} = r - Jq_0^4 + J(q^2 - q_0^2)^2$. The quadratic coupling $\tilde{r}$ dictates that the most unstable momentum mode is $q = q_0$, which condenses when $\tilde{r}$ becomes negative, i.e., r falls below $r_c = Jq_0^4$, corresponding to $h = h_{c2}$. Since the first and second terms are "rotationally invariant" in the Δ_+-Δ_- space, i.e., O(4) invariant, it is the last term that breaks this symmetry down to the physical $\mathrm{U}(1)\otimes\mathrm{U}(1)$ and thereby determines the relative size of these critical $\pm\mathbf{q}_0$ momenta order parameters, $\Delta_\pm$.

Clearly, for $\lambda_1 > \lambda_2\frac{2q_0^2}{m^2}$, $\mathcal{H}_{\mathrm{Landau}}$ is minimized by the FF state with only one of the two order parameters nonzero, e.g., with $\Delta^{\mathrm{FF}}_- = 0$, and

$$\Delta^{\mathrm{FF}}_+ = \sqrt{\frac{|\tilde{r}|}{\lambda_1 + \lambda_2 q_0^2/m^2}} \quad \text{for } \lambda_1 > \lambda_2\frac{2q_0^2}{m^2}. \tag{56}$$

In the opposite limit of $\lambda_1 < \lambda_2 2q_0^2/m^2$, the last quartic term in $\mathcal{H}_{\mathrm{Landau}}$ instead selects the LO state, with the two order parameters equal and nonzero,

$$\Delta^{\mathrm{LO}}_+ = \Delta^{\mathrm{LO}}_- = \sqrt{|\tilde{r}|/(3\lambda_1)} \quad \text{for } \lambda_1 < \lambda_2\frac{2q_0^2}{m^2} \tag{57a}$$

$$= \frac{1}{3}\Delta^2_{\mathrm{BCS}}\ln(h/h_{c2}) \tag{57b}$$

$$\equiv \Delta^{\mathrm{LO}}_{q_0}(h). \tag{57c}$$

As first found by LO [77] and discussed in the previous section, in the current system the microscopics dictates that it is the latter, LO state that is the more stable one.

B. Symmetries and order parameters

The fundamental FFLO order parameter (53) that characterizes the FF and LO states clearly distinguishes these two symmetry-distinct states.

1. The Fulde-Ferrell state

The FF state is characterized by a single (independent) nonzero complex order parameter,

$$\Delta_{\mathrm{FF}}(\mathbf{r}) = \Delta_{q_0} e^{i\mathbf{q}_0\cdot\mathbf{r} + i\phi}, \tag{58}$$

which is a plane wave with the momentum $\mathbf{q}_0$ and a single Goldstone mode

$$\phi = \phi_+, \tag{59}$$

corresponding to the local superconducting phase. The state carries a nonzero, uniform spontaneously directed supercurrent

$$\mathbf{j}_{\mathrm{FF}} = \frac{1}{m}|\Delta_{q_0}|^2(\mathbf{q}_0 + \nabla\phi), \tag{60}$$

and thereby breaks the time-reversal and rotational symmetry, chosen spontaneously along $\mathbf{q}_0$, as well as the global gauge symmetry, corresponding to the total atom conservation. Although the FF order parameter itself is not translationally invariant, under translation by an arbitrary vector $\mathbf{a}$ it transforms by a multiplication by a global phase $e^{i\mathbf{q}_0\cdot\mathbf{a}}$. It is therefore invariant under a modified transformation of an arbitrary translation followed by a gauge transformation. Thus, in the FF state all gauge-invariant observables and therefore the state are translationally invariant; namely, the FF state is a uniform orientationally ordered (polar) superfluid. Under an infinitesimal rotation of the FF current axis $\mathbf{q}_0 \to \mathbf{q}_0 + \delta\mathbf{q}_0$, its phase transforms as $\phi \to \phi + \delta\mathbf{q}_0\cdot\mathbf{r}$, costing zero energy. Thus the underlying rotational symmetry of the FF state requires the corresponding Goldstone-mode Hamiltonian of the superconducting phase $\phi = \phi_+$ to be invariant under such a transformation, which for an infinitesimal rotation corresponds to a phase shift *linear* in $\mathbf{r}$ transverse to $\mathbf{q}_0$. A generic Goldstone-mode Hamiltonian that is well known to satisfy these properties is that of a smectic [112,129], to harmonic order given by

$$\mathcal{H}^{\mathrm{FF}}_0 = \tfrac{1}{2}\tilde{K}(\nabla^2_\perp\phi)^2 + \tfrac{1}{2}\rho^{\parallel}_s(\hat{\mathbf{q}}_0\cdot\nabla\phi)^2. \tag{61}$$

Its key qualitative feature is the strict (symmetry-enforced) vanishing of the $(\nabla_\perp\phi)^2$ stiffness, with $\perp$ designating axes transverse to the spontaneous current ($\hat{r}_\parallel \equiv \hat{\mathbf{z}} \equiv \hat{\mathbf{q}}_0$) axis. Thus, despite its uniform density (i.e., it is an orientationally ordered *superfluid*, rather than a density wave) the FF state is characterized by a smectic Goldstone-mode Hamiltonian, which is qualitatively distinct from that of a conventional uniform and isotropic superfluid, described by an *XY* model,

$$\mathcal{H}_{XY} = \tfrac{1}{2}\rho_s(\nabla\phi)^2. \tag{62}$$

Namely, as is evident from Eq. (61) the FF state is infinitely anisotropic, characterized by an identically vanishing transverse superfluid stiffness

$$\rho^{\mathrm{FF}}_{s,\perp} = 0, \tag{63}$$

a reflection of its underlying rotational symmetry that is *spontaneously* broken by the ground-state supercurrent $\mathbf{j}_{\mathrm{FF}}$. Its longitudinal superfluid stiffness $\rho_{s,\parallel}$ is nonzero, measuring the energetic cost of a deviation from the ground-state current magnitude of $j^0_{\mathrm{FF}} = \frac{1}{m}|\Delta_{q_0}|^2 q_0$.

In the next section (after discussing the LO state), we will support these symmetry-based arguments by an explicit

derivation from the generic Ginzburg-Landau theory (50) for the FF state.

2. The Larkin-Ovchinnikov state

As illustrated through the Landau analysis, the LO state is described by a nonzero (standing-wave-like) pair-density-wave order parameter. That is, taking the magnitudes of the two order parameters $\Delta_+ = \Delta_- = \Delta_{q_0}$ in (53) to be the same (as dictated by the last quartic term for $\lambda_1 < \lambda_2 \frac{2q_0^2}{m^2}$) the LO order parameter reduces to a physically appealing form,

$$\Delta_{\rm LO}(\mathbf{r}) = 2\Delta_{q_0} e^{i\frac{1}{2}(\phi_+ + \phi_-)} \cos\left[\mathbf{q}_0 \cdot \mathbf{r} + \tfrac{1}{2}(\phi_+ - \phi_-)\right] \quad (64a)$$

$$= 2\Delta_{q_0} e^{i\phi} \cos[\mathbf{q}_0 \cdot \mathbf{r} + \theta], \quad (64b)$$

which is a product of a superfluid and a unidirectional density-wave order parameter, respectively characterized by two Goldstone modes

$$\phi = \tfrac{1}{2}(\phi_+ + \phi_-), \quad (65a)$$

$$\theta = \tfrac{1}{2}(\phi_+ - \phi_-). \quad (65b)$$

In a qualitative contrast to the FF state and to a conventional superfluid or a superconductor, the LO state's density and other physical quantities are periodic along $\hat{\mathbf{q}}_0$, exhibiting periodic uniaxial stripe order. The position of the associated pair-density wave is characterized by the smectic phonon

$$u = -\theta/q_0, \quad (66)$$

giving physical interpretation to the second Goldstone mode θ as the phase of the pair-density wave.

We also note that unlike a conventional smectic [129] [e.g., in liquid-crystal materials, where one instead is dealing with a real mass density $\rho(\mathbf{r})$ not a pair-condensate wave function], here, because $\Delta(\mathbf{r})$ is complex, the phases of $\Delta_\pm$ are independent (though interacting) Goldstone modes [152].

The mean-field LO order parameter $\Delta_{\rm LO}$ thus simultaneously exhibits the off-diagonal long-range order (ODLRO) (superfluid) and the smectic (unidirectional density-wave) orders. It thus spontaneously breaks the rotational, translational, and global gauge symmetries, and is therefore realizes a form of a paired supersolid. However, it is distinguished from a conventional purely bosonic supersolid [87–90], where homogeneous superfluid order and periodic density wave coexist, by the vanishing of the ("charge"-2 two-atom) zero momentum ($\mathbf{q} = \mathbf{0}$) superfluid component in the LO condensate [91].

The supercurrent in the LO state is given by

$$\mathbf{j}_{\rm LO} = \frac{2|\Delta_{q_0}|^2}{m} \nabla\phi[1 + \cos(2\mathbf{q} \cdot \mathbf{r} + 2\theta)] \quad (67a)$$

$$\approx \frac{2|\Delta_{q_0}|^2}{m} \nabla\phi, \quad (67b)$$

where in the last form we neglected its periodic contribution. As expected, in contrast to the FF state (60), the supercurrent vanishes in the LO ground state where $\nabla\phi = \mathbf{0}$.

Similarly to the FF state, the underlying rotational symmetry of the LO state strongly restricts the form of the Goldstone-mode Hamiltonian. Under an infinitesimal rotation of $\mathbf{q}_0$, which defines the spontaneously chosen orientation of the pair-density wave, the phase of the LO state transforms according to

$$\theta \to \theta + \delta\mathbf{q}_0 \cdot \mathbf{r}. \quad (68)$$

Hence the $\theta = -q_0 u$ sector of the LO Goldstone-mode Hamiltonian must be invariant under this symmetry and must therefore be described by a smectic form [129–131]. On the other hand, because a rotation of the LO state leaves the superconducting phase ϕ unchanged, the ϕ sector of the Hamiltonian generically does not experience any such restriction. We thus expect it to be described by a generic anisotropic XY model form, with the full harmonic Goldstone-mode Hamiltonian given by

$$\mathcal{H}_0^{\rm LO} = \frac{K}{2}(\nabla_\perp^2 u)^2 + \frac{B}{2}(\partial_\parallel u)^2 + \frac{1}{2}\rho_s^\perp(\nabla_\perp\phi)^2 + \frac{1}{2}\rho_s^\parallel(\partial_\parallel\phi)^2. \quad (69)$$

Thus, unlike the FF state, the LO state is characterized by nonzero, but unequal, superfluid stiffnesses $\rho_s^\perp \neq \rho_s^\parallel$.

Another feature of the LO state is that in addition to the primary order parameter, $\Delta_{\rm LO}$ (64), it is characterized by a uniform charge-4 superconducting order parameter and by a neutral $2\mathbf{q}_0$-smectic secondary order parameter,

$$\Delta_{\rm sc}^{(4)} = \Delta_{\rm LO}^2 \approx 2\Delta_{q_0}^2 e^{i2\phi}, \quad (70a)$$

$$\Delta_{\rm Sm}^{(2q)} = |\Delta_{\rm LO}|^2 \approx 2|\Delta_{q_0}|^2 \cos[2\mathbf{q} \cdot \mathbf{r} + 2\theta], \quad (70b)$$

where we neglected the subdominant contributions. As we will see in subsequent sections, these order parameters become particularly important when the primary order parameter $\Delta_{\rm LO}$ vanishes either due to divergent fluctuations (as, e.g., for $T > 0$ in two and three dimensions) or via a disordering transition driven by unbinding of topological defects.

C. Goldstone-mode Hamiltonian

To support the above symmetry-based arguments, we will now use the Ginzburg-Landau theory (50) to explicitly derive the Goldstone-mode Hamiltonians for the FF and the LO states.

1. The Fulde-Ferrell Hamiltonian

To this end we use $\Delta_{\rm FF}(\mathbf{r})$ inside the $\mathcal{H}_{\rm GL}$ (50), but in contrast to the earlier mean-field calculation that determined the value of Δ_{q_0}, focus on the spatially dependent Goldstone mode $\phi(\mathbf{r})$. However, we will neglect the spatial dependence of the amplitude Δ_{q_0}, valid in the ordered phase, where its deviations from the average condensate value are gapped, controlled by a finite susceptibility.

Working out the gradients of $\Delta_{\rm FF}(\mathbf{r})$ under these conditions and using the expression for $\mathbf{j}_{\rm FF}$ inside $\mathcal{H}_{\rm GL}$, we find

$$\mathcal{H}_{\rm FF} = J|\Delta_{q_0}|^2[(\nabla^2\phi)^2 + [2\mathbf{q} \cdot \nabla\phi + (\nabla\phi)^2]^2] + \left[J|\Delta_{q_0}|^2(q^2 - q_0^2) + \frac{\lambda_2}{2m^2}|\Delta_{q_0}|^4\right][2\mathbf{q} \cdot \nabla\phi + (\nabla\phi)^2] \quad (71a)$$

$$= \frac{1}{2}\tilde{K}(\nabla^2\phi)^2 + \frac{1}{2}\rho_s^\parallel\left[\partial_\parallel\phi + \frac{1}{2}q_0^{-1}(\nabla\phi)^2\right]^2. \quad (71b)$$

Here, we dropped constant pieces, used the FF amplitude Δ_{q_0} (computed in the previous section), defined a longitudinal derivative $\partial_\parallel \equiv \hat{\mathbf{q}}_0 \cdot \boldsymbol{\nabla}$, and in going to the final form (71b) chose q according to

$$q^2 = q_0^2 - \frac{\lambda_2}{2m^2 J}|\Delta_{q_0}|^2 \tag{72a}$$

$$\approx q_0^2 \quad \text{near } h_{c2}, \tag{72b}$$

in order to eliminate the terms linear in the fluctuation-current nonlinear form

$$\delta j_\parallel = \partial_\parallel \phi + \tfrac{1}{2} q_0^{-1} (\boldsymbol{\nabla}\phi)^2 \tag{73}$$

as a standard minimization condition for the FF ground-state current $j_{\rm FF}$. This condition is closely analogous to the choice of an order parameter magnitude to eliminate terms linear in fluctuations. As expected from the earlier mean-field analysis, near h_{c2} (where Δ_{q_0} is small) this corresponds to the choice of $q \approx q_0$. However, as usual with a magnitude of an order parameter (here the spontaneous current $j_{\rm FF}$), the nonuniversal magnitude of $\mathbf{q}$ (proportional to $j_{\rm FF}$) will be modified by fluctuations. Ultimately it is determined by the requirement that the coefficient of the term linear in $\delta j_\parallel$ vanishes.

Within this derivation, the Goldstone-mode moduli in $\mathcal{H}_{\rm FF}$ are given by

$$\tilde{K} = 2J\left|\Delta_{q_0}\right|^2, \tag{74a}$$

$$\rho_s^\parallel = 8Jq_0^2\left|\Delta_{q_0}\right|^2, \tag{74b}$$

but more generally are two independent parameters characterizing the energetics of the single Goldstone mode of the FF state. The Hamiltonian form $\mathcal{H}_{\rm FF}$ (valid beyond its weak-coupling microscopic derivation) is familiar from studies of conventional smectic liquid crystals [129–131], with the rotational invariance encoded in two ways. First, to the quadratic order in $\boldsymbol{\nabla}\phi$ it reduces to the harmonic form $\mathcal{H}^0_{\rm FF}$ (61), invariant under an *infinitesimal* rotation of the FF current state. Namely, by the strict vanishing of the $(\nabla_\perp\phi)^2$ superfluid stiffness, $\rho_s^\perp = 0$ (resulting in the softer transverse Laplacian energetics, $(\nabla_\perp^2\phi)^2$), it exhibits a vanishing energy cost for transverse (to $\mathbf{q}_0$) current fluctuations, with the stiffness for the change in current *magnitude* (along $\mathbf{q}_0$) controlled by $\rho_s^\parallel$. Second, $\mathcal{H}_{\rm FF}$ is an expansion in a fully rotationally invariant longitudinal current fluctuation $\delta j_\parallel$ (73), whose nonlinearities ensure that it is fully rotationally invariant even for large reorientations in $\mathbf{q}_0$ [129–131] that defines the FF ground state.

To see the latter we note that under a rotation of $\mathbf{q}_0 = q_0\hat{\mathbf{z}}$ by an angle α in the $\hat{\mathbf{z}}$-$\hat{\mathbf{x}}$ plane,

$$q_0\hat{\mathbf{z}} \to \mathbf{q} = q_0(\hat{\mathbf{z}}\cos\alpha + \hat{\mathbf{x}}\sin\alpha) \tag{75}$$

generates a nontrivial, spatially dependent phase

$$\phi^0(\mathbf{r}) = z(\cos\alpha - 1) + x\sin\alpha, \tag{76}$$

even though the system is clearly in its ground state. Simple algebra demonstrates that the fully nonlinear form of the longitudinal current $\delta j_\parallel$ ensures that it and the corresponding energy $\mathcal{H}_{\rm FF}$ vanish for $\phi^0(\mathbf{r})$, as required by the rotational invariance.

One might question the necessity of keeping nonlinearities in $\mathcal{H}_{\rm FF}$ (71b). As we will see shortly, because of the vanishing transverse superfluid stiffness in the FF state, the fluctuations in the purely harmonic description $\mathcal{H}^0_{\rm FF}$ (61) are infrared divergent in three and lower dimensions. Consequently these nonlinearities are in fact absolutely essential for a well-defined description of such a state.

2. *The Larkin-Ovchinnikov Hamiltonian*

The derivation of the Larkin-Ovchinnikov Goldstone-mode Hamiltonian follows a similar route to that for the FF state of the previous section, with many common features, but also some essential qualitative differences in the results. To this end, we insert the LO order parameter $\Delta_{\rm LO}(\mathbf{r})$ inside $\mathcal{H}_{\rm GL}$ (50), use the earlier mean-field values of the amplitude Δ_{q_0}, Eq. (57) (that vanishes at h_{c2} and grows as $|h_{c2} - h|^\beta$ below h_{c2}), ignoring its subdominant spatial dependence, and track the resulting energetics of two spatially dependent Goldstone modes $\phi(\mathbf{r})$ and $\theta(\mathbf{r}) = -q_0 u(\mathbf{r})$. We thereby obtain

$$\mathcal{H}_{\rm LO} = J|\Delta_{q_0}|^2\left[(\nabla^2\phi_+)^2 + [2\mathbf{q}_0\cdot\boldsymbol{\nabla}\phi_+ + (\boldsymbol{\nabla}\phi_+)^2]^2 + (\nabla^2\phi_-)^2 + [2\mathbf{q}_0\cdot\boldsymbol{\nabla}\phi_- - (\boldsymbol{\nabla}\phi_-)^2]^2\right] + \frac{\lambda_2|\Delta_{q_0}|^4}{2m^2}(\boldsymbol{\nabla}\phi_+ + \boldsymbol{\nabla}\phi_-)^2 \tag{77a}$$

$$= \sum_{\alpha=\pm}\left[\frac{1}{4}K(\nabla^2 u_\alpha)^2 + \frac{1}{4}B\left[\partial_\parallel u_\alpha - \frac{1}{2}(\boldsymbol{\nabla}u_\alpha)^2\right]^2\right] + \frac{1}{8}\rho_s^\perp q_0^2(\boldsymbol{\nabla}u_+ - \boldsymbol{\nabla}u_-)^2 \tag{77b}$$

$$= \frac{1}{2}K(\nabla^2 u)^2 + \frac{1}{2}B\left[\partial_\parallel u - \frac{1}{2}(\boldsymbol{\nabla}u)^2\right]^2 + \frac{1}{2}\rho_s^\parallel(\partial_\parallel\phi)^2 + \frac{1}{2}\rho_s^\perp(\nabla_\perp\phi)^2 + \mathcal{H}_{\rm LO}^{\rm subdom}, \tag{77c}$$

where we dropped the constant and fast-oscillating parts that average away upon spatial integration of the energy density, introduced two phonon fields

$$u_\pm = \mp\phi_\pm/q_0, \tag{78}$$

and chose $q = q_0$ in order to eliminate the term linear in the nonlinear, rotationally invariant strain tensor [the analog of $\delta j_\parallel$ in (73)]

$$u^\pm_{qq} = \hat{\mathbf{q}}\cdot\boldsymbol{\nabla}u_\pm - \tfrac{1}{2}(\boldsymbol{\nabla}u_\pm)^2 \tag{79}$$

whose nonlinearities in $u_\pm$ ensure that it is fully rotationally invariant even for large rotations. We also defined the bend K and the compressional B smectic elastic moduli

$$K = 4Jq_0^2|\Delta_{q_0}|^2 \tag{80a}$$

$$\approx \frac{0.8n\Delta_{\rm BCS}^2}{\epsilon_{\rm F}q_0^2}\ln(h/h_{c2}), \tag{80b}$$

$$B = 16Jq_0^4|\Delta_{q_0}|^2 \tag{80c}$$

$$\approx \frac{3.3n\Delta_{\rm BCS}^2}{\epsilon_{\rm F}}\ln(h/h_{c2}), \tag{80d}$$

and identified the longitudinal, $\rho_s^{\parallel}$, and transverse, $\rho_s^{\perp}$, superfluid stiffnesses given by

$$\rho_s^{\parallel} = B/q_0^2 = \frac{9.8n}{\epsilon_F}\frac{\Delta_{q_0}^2}{q_0^2} \tag{81a}$$

$$\approx \frac{3.3n\Delta_{BCS}^2}{\epsilon_F q_0^2}\ln(h/h_{c2}), \tag{81b}$$

$$\rho_s^{\perp} = \frac{4\lambda_2}{m^2}|\Delta_{q_0}|^4 \tag{81c}$$

$$\approx \frac{7.3n}{\epsilon_F}\frac{\Delta_{q_0}^2}{q_0^2}\left(\frac{\Delta_{q_0}}{\Delta_{BCS}}\right)^2 \tag{81d}$$

$$\approx \frac{0.8n\Delta_{BCS}^2}{\epsilon_F q_0^2}\ln^2(h/h_{c2}). \tag{81e}$$

A nonzero transverse superfluid coupling $\rho_s^{\perp}$ (minimized by a vanishing supercurrent $\mathbf{j} \propto \nabla\phi_+ + \nabla\phi_-$) removes the two independent rotational symmetries, orientationally locking the two incommensurate ($u_\pm$) smectics. As argued above based on symmetry, (69), this leads to the superconducting phase combination $\phi = \frac{1}{2}(\phi_+ + \phi_-)$ of a conventional *XY* (as opposed to soft smectic) gradient type, (77c).

Within the superconductor context, this coupling of $\nabla\phi_\pm$ (*XY*- rather than smectic stiffness of the ϕ Goldstone mode) is straightforward to understand. The LO state effectively corresponds to two FF states, each carrying a supercurrent along $\mathbf{q} + \nabla\phi_+$ and $-\mathbf{q} + \nabla\phi_-$. A superfluid stiffness measures the nonzero kinetic energy cost of a total current $\mathbf{j}$. The latter results from either a transverse *orientational* misalignment of $\nabla\phi_\pm$, measured by the $\rho_s^{\perp}$, or a mismatch between the $\nabla\phi_+$ and $\nabla\phi_-$ *magnitudes* (even if directed along $\pm\mathbf{q}$, respectively), measured by the $\rho_s^{\parallel}$. These two distinct LO-state distortions are schematically illustrated in Fig. 5.

As advertised in the Introduction we thus find from (81) that the LO state is a highly anisotropic superfluid (though less so than the FF state, where $\rho_s^{\perp} = 0$), with

$$\frac{\rho_s^{\perp}}{\rho_s^{\parallel}} = \frac{3}{4}\left(\frac{\Delta_{q_0}}{\Delta_{BCS}}\right)^2 \approx \frac{1}{4}\ln\left(\frac{h_{c2}}{h}\right) \ll 1, \tag{82}$$

a ratio that vanishes for $h \to h_{c2}^-$.

Because (in contrast to the FF state) the $\rho_s^{\perp}$ is indeed nonzero for $h < h_{c2}$, the nonlinearities in $\nabla\phi$ and the soft term $(\nabla^2\phi)^2$ [contained in the $\mathcal{H}_{LO}^{subdom}$ of (77c)] are subdominant on long scales, and can (and will) therefore be neglected [153].

We stress that, while the detailed expressions for the moduli above are specific to the weak-coupling BCS limit near h_{c2}, the general form of $\mathcal{H}_{LO}$, (77c), including the structure of the symmetry-enforced nonlinearities in the u (smectic) sector, is valid beyond our microscopic derivation, and holds throughout the LO phase. Specifically, as argued in the previous section based on symmetry, in contrast to the superconducting ϕ sector, the vanishing of the $(\nabla_\perp u)^2$ coupling is a reflection of the underlying rotational invariance of the LO striped state. Thus the soft transverse elastic form of the smectic sector and the form of the nonlinear strain tensor u_{qq} [analogous to $\delta j_\parallel$ (73)] are strictly protected by this symmetry. As we will see in Sec. V (and is well known for conventional smectic liquid crystals [129–131]), because of this harmonic elastic softness, in the presence of thermal fluctuations these smectic nonlinearities are qualitatively important at long length scales for the description of the FF and LO states.

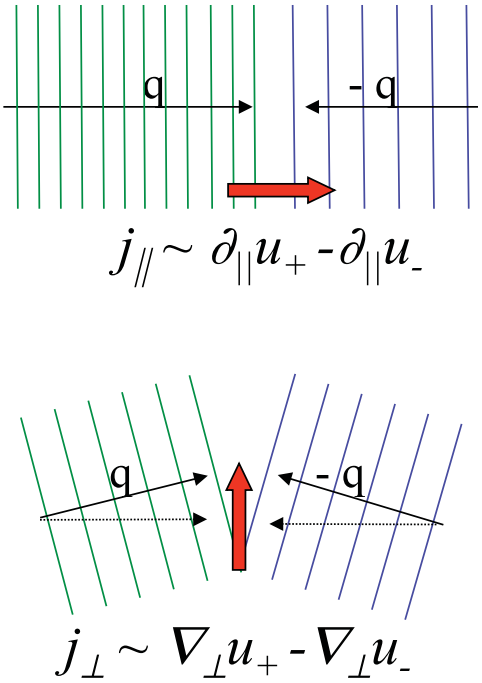

FIG. 5. (Color online) An illustration of longitudinal and transverse (to $\mathbf{q}$) LO nonzero supercurrent configuration controlled by the corresponding superfluid stiffnesses $\rho_s^{\parallel}$,$\rho_s^{\perp}$. Because there is no change in the effective period associated with the transverse current excitation, it is qualitatively energetically "cheaper," scaling as $\Delta_{q_0}^4$, as compared to the longitudinal excitation that scales as $\Delta_{q_0}^2$. As indicated in Eq. (82), the ratio therefore vanishes as h approaches the transition into a nonsuperfluid phase at h_{c2}.

D. Quantum dynamics

The bosonic Hamiltonian density $\mathcal{H}_{GL}$ (50) determines the classical thermodynamics and equal-time finite-temperature correlation functions of the FFLO system [154], which in the ordered state reduces to $\mathcal{H}_{FF/LO}$, in (71b) and (77c).

The dynamics is controlled by the Lagrangian density. Focusing on quantum thermodynamics, the partition function $Z = \mathrm{Trace}[e^{-\beta H[\hat\Delta^\dagger,\hat\Delta]}]$ is formulated in a standard way as a path integral over coherent states labeled by the c fields $\Delta(\tau,\mathbf{r})$ and $\Delta^*(\tau,\mathbf{r})$,

$$Z = \int [d\Delta^* d\Delta] e^{-S[\Delta^*,\Delta]}, \tag{83}$$

with $\tau = it$ the imaginary time $0 \leqslant \tau < \beta \equiv 1/k_B T$ ($\hbar \equiv 1$). The coherent-state action $S[\Delta^*,\Delta]$ is given by

$$S[\Delta^*,\Delta] = \int_0^\beta d\tau \int d^d r \mathcal{L}[\Delta^*,\Delta], \tag{84}$$

with the Lagrangian density given by

$$\mathcal{L} = \Delta^*\partial_\tau\Delta + \mathcal{H}[\Delta^*,\Delta]. \tag{85}$$

Using the density-phase representation

$$\Delta = (n_0 + \delta n_+)^{1/2} e^{i\mathbf{q}\cdot\mathbf{r}+i\phi_+} + (n_0 + \delta n_-)^{1/2} e^{-i\mathbf{q}\cdot\mathbf{r}+i\phi_-}, \tag{86}$$

with $\delta n_\pm$ the fluctuating Cooper-pair density about its ground state value $n_0 = |\Delta_{q_0}|^2$, and at low energies neglecting the subdominant terms (e.g., fast-oscillating pieces or spatial dependence of gapped amplitude fields) the Lagrangian density reduces to

$$\mathcal{L} = i\delta n_+ \partial_\tau \phi_+ + i\delta n_- \partial_\tau \phi_- + \mathcal{H}[\delta n_\pm, \phi_\pm]. \tag{87}$$

Integrating these Berry's phase terms [155,156] over the "massive" (nonzero compressibility χ_0) $\delta n_\pm$ fluctuations, we obtain

$$\mathcal{L} = \frac{\chi_0}{2}(\partial_\tau \phi_+)^2 + \frac{\chi_0}{2}(\partial_\tau \phi_-)^2 + \mathcal{H}[\phi_+, \phi_-], \tag{88}$$

with $\mathcal{H}$ given by the $\mathcal{H}_{\rm LO}$ in the LO ground state, and the FF state treated similarly using $\mathcal{H}_{\rm FF}$. For the LO state, this analysis then predicts the existence of two anisotropic low-frequency modes with dispersions

$$\omega_\phi(\mathbf{k}) = \sqrt{\left(\rho_s^\perp k_\perp^2 + \rho_s^\parallel k_z^2\right)/\chi_0}, \tag{89a}$$

$$\omega_u(\mathbf{k}) = \sqrt{\left(K k_\perp^4 + B k_z^2\right)/\chi_0}, \tag{89b}$$

that can be read off from the analytical continuation of the Lagrangian into real time, $t = -i\tau$. These modes respectively correspond to the zeroth sound (the Bogoliubov mode as in a conventional superfluid) and the smectic phonon, unique to the LO state. In cold atomic gases, these should in principle be measurable via the Bragg spectroscopy technique [157–159].

With the Goldstone-mode Lagrangian in hand, we can now calculate the effects of quantum and thermal fluctuations as well as equilibrium correlation and response functions [155].

IV. LARKIN-OVCHINNIKOV STATE NEAR h_{c1}

As emphasized earlier the general form of the action for the description of the LO state, Eq. (88), is expected to hold universally throughout the ordered state. However, its derivation above and therefore the expressions for the associated couplings Eqs. (51), (80), and (81) are limited to the weak-coupling BCS regime and near the high-chemical-potential imbalance (Zeeman field) normal- to FFLO-state transition at h_{c2}.

An estimate of these couplings outside 1D throughout the FFLO phases can only be done numerically. However, in the complementary, low-chemical-potential imbalance (Zeeman field) regime, just above the transition from the fully paired superfluid (BCS-BEC) state to the LO state at h_{c1}, qualitative estimates are possible based on an analysis of a "dilute gas" of fluctuating $\pm\Delta$ domain walls. We carry out this analysis below by focusing on the LO state, treating it as a periodic array of fluctuating domain walls in $\Delta(\mathbf{r})$, akin to the lyotropic phases in soft condensed matter [129,130].

A. Macro- vs microphase separation: Stability of the LO state

Implicit in our analysis below is the assumption that as the domain-wall surface energy becomes negative [95–98] for $h > h_{c1}$, their interaction remains *repulsive*, and so the domain walls proliferate *continuously* as a periodic array inside the LO state. Under this assumptions (which warrants further study) the domain-wall density $n_{\rm dw}$ and the associated species imbalance $P \propto n_{\rm dw}$ [$\approx q_0(h)$] is then set by a balance between the negative surface energy and the domain-wall repulsion, growing continuously as a function of $h - h_{c1}$ according to the Pokrovsky-Talapov commensurate-incommensurate (CI) transition phenomenology [102]. This behavior is clearly exhibited in 1D [95,108] through an exact solution and bosonization methods, and has been argued to persist in higher dimensions [95–98]. The CI route for a transition to the LO state contrasts sharply with the Landau theory [4,44,77] of two independent order parameters Δ_0, Δ_q, which always predicts a first-order BCS-LO transition. The latter corresponds to the case of an *attractive* domain-wall interaction, and therefore proliferate discontinuously above h_{c1}, leading to the ubiquitous phase separation found in mean-field theory [4,44]. It is currently unclear what dimensionless microscopic parameter, analogous to Abrikosov's κ (distinguishing between type-I and type-II superconductors) [99,100], controls these two alternatives of the macrophase separation (a first-order transition) and the microphase-separated LO state [a continuous transition out of the gapped superfluid (SF) state] [103].

B. SF-LO transition at h_{c1}

The phenomenology of the domain-wall proliferation above h_{c1} and the associated (fully gapped, singlet) SF to LO transition can be captured by a domain-wall energy functional, extended to a general dimension d:

$$E[n_{\rm dw}]/L^{d-1} = \int_z \left[\varepsilon_{\rm dw}^0 - h m_N(h)\xi_{\rm dw}\right] n_{\rm dw} + \frac{1}{2}\int_{z,z'} V(z-z') n_{\rm dw}(z) n_{\rm dw}(z') \tag{90a}$$

$$= \int_z m_N(h)\xi_{\rm dw}(h_{c1} - h) n_{\rm dw} + \frac{1}{2}\int_{z,z'} V(z-z') n_{\rm dw}(z) n_{\rm dw}(z'), \tag{90b}$$

where $\varepsilon_{\rm dw}^0$ is the domain-wall surface energy at $h = 0$, $V(z)$ is the domain-wall interaction energy per unit of area, and $n_{\rm dw}(z) = \sum_i \tilde{\delta}(z - z_i)$ [$\tilde{\delta}(z)$ and z_i are the profile of width $\xi_{\rm dw}$ and the position (along z) of the ith domain wall]. Here, we used an approximate relation between the domain-wall 1D density $n_{\rm dw}(h)$ and the magnetization density $m(h) = n_\uparrow - n_\downarrow$,

$$m(h) \approx m_N(h)\xi_{\rm dw} n_{\rm dw}(h), \tag{91}$$

where $m_N(h)$ is the magnetization density (per d-dimensional volume) of the normal state, which is approximately nucleated in the zeros of the (locally BCS-like) gap function, i.e., on the domain wall of width $\xi_{\rm dw}$; $m_N\xi_{\rm dw}$ is the fermion number imbalance per unit area (L^{d-1}) per domain wall. In the Pauli (weak-imbalance) limit, we expect the former to be approximately given by $k_{\rm F}^{d-1} h/h_{c1}$, through a string of relations: $m_N\xi_{\rm dw} \approx \chi_P h \xi_0 \approx (n h_{c1}/\epsilon_{\rm F})(\hbar v_{\rm F}/\Delta_{\rm BCS})(h/h_{c1}) \approx k_{\rm F}^{d-1} h/h_{c1} \approx k_{\rm F}^{d-1}$ (using $n \approx k_{\rm F}^d$). This is indeed the case in

the noninteracting Fermi-gas limit, where $m_N(h)$ is given as the solution of

$$m_N(h) = \frac{n}{2}\left[(\hat{\mu}+\hat{h})^{\frac{3}{2}}\Theta(\hat{\mu}+\hat{h}) - (\hat{\mu}-\hat{h})^{\frac{3}{2}}\Theta(\hat{\mu}-\hat{h})\right], \tag{92}$$

with the normalized chemical potential $\hat{\mu} \equiv \mu/\epsilon_F$ determined in terms of the normalized chemical-potential difference (Zeeman energy) $\hat{h} \equiv h/\epsilon_F$ by the number-density equation

$$1 = \tfrac{1}{2}\left[(\hat{\mu}+\hat{h})^{\frac{3}{2}}\Theta(\hat{\mu}+\hat{h}) + (\hat{\mu}-\hat{h})^{\frac{3}{2}}\Theta(\hat{\mu}-\hat{h})\right]. \tag{93}$$

The set above reduces to the Pauli expression $m_N \approx \chi_P h$ for weak $h \ll \mu$ [$\chi_P = 3n/(2\epsilon_F)$] and $m_N \approx n$ for large $h \gg \mu$. In either case the h dependence of $m_N(h)$ is weak around h_{c1} and therefore can be neglected, along with other weak h dependences, such as the soliton width $\xi_{dw}(h)$.

Ignoring fluctuations [160], the domain-wall interaction $V(z) \approx V_0 e^{-|z|/\xi_{dw}}$ is expected to be short ranged with the scale set by the soliton width ξ_{dw}. Thus, for low soliton density $n_{dw}\xi_{dw} \ll 1$, its strength is a strong function of $z - z'$, whose typical value is given by the domain-wall spacing itself, $1/n_{dw}$. Thus, just above h_{c1} a good approximation for the above energy density is given by

$$\begin{aligned}\varepsilon(n_{dw}) &\approx m_N(h)\xi_{dw}(h_{c1}-h)n_{dw} + \frac{\xi_{dw}}{2}V(n_{dw})n_{dw}^2 \\ &\approx m_N(h)\xi_{dw}(h_{c1}-h)n_{dw} + \frac{\xi_{dw}}{2}V_0 e^{-\frac{1}{\xi_{dw}n_{dw}}}n_{dw}^2.\end{aligned} \tag{94}$$

A minimization then gives the domain-wall density $n_{dw}(h)$ and [through Eq. (91)] the imbalance density $m(h)$ as a function of chemical-potential difference h:

$$n_{dw}(h) \approx \xi_{dw}^{-1}\begin{cases}\frac{1}{\ln[h_0/(h-h_{c1})]} & \text{for } n_{dw}\xi_{dw} \ll 1, \\ (h-h_{c1})/h_0 & \text{for } n_{dw}\xi_{dw} \gg 1,\end{cases} \tag{95}$$

where $\xi_{dw} \approx \xi_0$ and $h_0 \approx V_0/(\xi_{dw}m_N) \approx V_0/(\chi_P h_{c1}\xi_0) \approx \Delta_{BCS}$ [since $V_0 \approx k_F^{d-1}h_{c1} \approx k_F^{d-1}\Delta_{BCS}$ is the energy lost per fermion per unit of area (with separation $1/k_F$); for a 1D exact solution, one indeed has $h_{c1} = 2\Delta_{BCS}/\pi$, consistent with this estimate].

Note that for large imbalance (high domain-wall density) the interaction part reduces to a simple quadratic dependence on n_{dw} and thus gives the expected linear growth of the density with $h - h_{c1}$ (second line above). In contrast, for low density the interaction is exponentially weak and domain walls enter the state as a quickly growing (with a divergent slope) function of $h - h_{c1}$, though not as discontinuously as in a first-order transition. These limits are illustrated in Fig. 2.

1. LO elastic moduli at $T = 0$

For $h > h_{c1}$ a 1D lattice of domain walls, i.e., the LO state, forms. Because of the underlying rotational invariance its elasticity is generically given by that of a smectic, Eq. (77c). The energy of the deviation δn_{dw} from the minimum domain-wall density $n_{dw}(h)$, Eq. (95), is a quadratic function of δn_{dw}, given by

$$\varepsilon(\delta n_{dw}) \approx \varepsilon_0 + \tfrac{1}{2}\varepsilon''(n_{dw}(h))(\delta n_{dw})^2 \tag{96a}$$

$$\approx \varepsilon_0 + \tfrac{1}{2}B(h)(\partial_z u)^2, \tag{96b}$$

where the smectic bulk modulus is given by

$$B(h) \approx n_{dw}(h)^2\varepsilon''(n_{dw}(h)) \tag{97a}$$

$$\approx (h-h_{c1})n_{dw}(h)k_F^{d-1}. \tag{97b}$$

Here, to deduce $B(h)$ we used the relation between the density n_{dw} and the displacement field $\delta n_{dw} = -n_{dw}(h)\partial_z u$, the relation $m_N \approx k_F^{d-1}/\xi_{dw}$, and went to the continuum limit via $\int n_{dw}(h)dz \cdots = \sum_i \cdots$. As expected, $B(h)$ grows strongly just above h_{c1}, but quickly asymptotes to $B(h \gg h_{c1}) \approx \Delta_{BCS}k_F^{d-1}/\xi_0 \approx n\Delta_{BCS}/\epsilon_F$, in scale consistent with its form found below h_{c2}, Eq. (80).

A detailed estimate of the bend modulus K is more difficult in this regime. However, we can take advantage of the relation in Eq. (80) to deduce K via the $K \approx B/q_0^2$ mean-field relation. Thus we find

$$K(h) \approx B(h)/n_{dw}(h)^2 \tag{98a}$$

$$\approx \Delta_{BCS}k_F^{d-1}\xi_0 \approx \epsilon_F k_F^{d-2} \quad \text{for} \quad h \gg h_{c1}. \tag{98b}$$

From these, we deduce the key smectic penetration length

$$\lambda(h) = \sqrt{K(h)/B(h)} \tag{99a}$$

$$\approx 1/n_{dw}(h) \tag{99b}$$

$$\approx \xi_0 \quad \text{for} \quad h \gg h_{c1}. \tag{99c}$$

2. LO elastic moduli at $T > 0$

Because the microscopic repulsive domain-wall interaction is short ranged (exponentially weak at long scales), sufficiently close to h_{c1} (where solitons are dilute) thermal fluctuations *always* qualitatively modify the above $T = 0$ predictions. To understand this we first derive the Helfrich [102,161] interaction between two $(d-1)$-dimensional fluctuating, curvature-dominated (tensionless) domain walls, separated by an average distance z. The corresponding energy functional of the instantaneous local domain-wall separation $u(\mathbf{x})$ is given by

$$E_{dw}[u(\mathbf{x})] = \frac{1}{2}\kappa\int d^{d-1}x(\nabla_\perp^2 u)^2, \tag{100}$$

where the curvature modulus is related to that of the smectic via $\kappa = K/n_{dw}$. The average transverse domain-wall spacing is determined by the root-mean-squared fluctuations, given by

$$\langle u^2\rangle \equiv z_T^2 = \frac{T}{\kappa}\int\frac{d^{d-1}q_x}{q_x^4} \tag{101a}$$

$$\sim \frac{T}{\kappa}x_T^{5-d}. \tag{101b}$$

This gives the thermal collision length x_T as a function of separation,

$$x_T \approx \left(\frac{\kappa}{T}\right)^{1/(5-d)} z_T^{2/(5-d)}. \tag{102}$$

To deduce the entropic (Helfrich) interaction, we note that domain walls separated by distance z reduce each other's fluctuation entropy by an amount s_0 (of order 1) per collision. For a pair of domain walls of linear extent L_x there are $(L_x/x_T)^{d-1}$ collisions, and thus the entropic part of the free energy is raised (relative to the infinite separation) by

$$\delta F_T \approx T s_0\left(\frac{L_x}{x_T}\right)^{d-1}, \tag{103}$$

leading to the Helfrich curvature-controlled interaction

$$V_H(z) \approx L_x^{d-1} \frac{T^\alpha}{\kappa^\beta} \frac{1}{z^\gamma} \tag{104a}$$

$$\approx L_x \frac{T^{4/3}}{\kappa^{1/3}} \frac{1}{z^{2/3}} \quad \text{for the 2D LO smectic state,} \tag{104b}$$

with

$$\alpha = \frac{4}{5-d}, \tag{105a}$$

$$\beta = \frac{d-1}{5-d}, \tag{105b}$$

$$\gamma = \frac{2d-2}{5-d}. \tag{105c}$$

Clearly, asymptotically close to the h_{c1} transition, where the domain-wall array is sufficiently dilute, the above thermal-fluctuation-induced steric interaction $V_H(z)$ always dominates over the short-range microscopic interaction. The crossover density $n_{\rm dw}^T$ is set by a separation $1/n_{\rm dw}^T \equiv z_{\rm dw}^T$ at which these are comparable, given by

$$n_{\rm dw}^T \approx \frac{1}{\xi_{\rm dw} \ln\left(V_0 \kappa^\beta \xi_{\rm dw}^\gamma / T^\alpha\right)}. \tag{106}$$

The corresponding Zeeman field range is $h_{c1} < h < h_T \approx h_{c1} + T^\alpha/(k_{\rm F}^{d-1} \xi_{\rm dw}^\gamma \kappa^\beta)$, with the energy density in this regime given by

$$\varepsilon_T(n_{\rm dw}) \approx m_N(h) \xi_{\rm dw} (h_{c1} - h) n_{\rm dw} + V_H(n_{\rm dw}) n_{\rm dw} \tag{107a}$$

$$\approx m_N(h) \xi_{\rm dw} (h_{c1} - h) n_{\rm dw} + \frac{T^\alpha}{\kappa^\beta} n_{\rm dw}^{\gamma+1}. \tag{107b}$$

A minimization then gives $n_{\rm dw}(h)$,

$$n_{\rm dw}(h,T) \approx \frac{(m_N \xi_{\rm dw} \kappa^\beta)^{1/\gamma}}{T^{\alpha/\gamma}} (h - h_{c1})^{1/\gamma} \quad \text{for } h_{c1} < h < h_T, \tag{108a}$$

$$\approx \frac{k_{\rm F}^{(5-d)/2} \kappa^{1/2}}{T^{2/(d-1)}} (h - h_{c1})^{\frac{5-d}{2d-2}} \quad \text{for } h_{c1} < h < h_T. \tag{108b}$$

As expected it shows that a fluctuation-enhanced Helfrich domain-wall repulsion leads to a significantly slower [than the $T = 0$, Eq. (95)] power law, and $1/\gamma$ increase in the domain-wall density and therefore of the species imbalance $P(h)$. Correspondingly, for this low range of Zeeman field $h < h_T$, this enhances the smectic bulk modulus, $B(h,T)$ through Eq. (97b).

For $h > h_T$ the microscopic exponential interaction takes over and the growths of $n_{\rm dw}(h)$ and $B(h,T)$ cross over to that of the $T = 0$ result, Eq. (95).

V. GOLDSTONE-MODE FLUCTUATIONS

A. Gaussian fluctuations

As an estimate of the role of Goldstone-mode fluctuations, we first study them at the Gaussian level, namely, we approximate the Goldstone-mode action $S[u,\phi]$ at the quadratic level, $S^0[u,\phi] = S^0_{\rm Sm}[u] + S^0_{\rm sc}[\phi]$ by dropping the nonlinearities in $\mathcal{H}_{\rm LO}$, (77c). Combining with (88) and focusing on the LO state (leaving the straightforward extension for the FF state for later), the LO harmonic action is given by

$$S^0_{\rm LO} = \int_0^\beta d\tau \int dz d^{d-1} r_\perp \left[\frac{\kappa}{2}(\partial_\tau u)^2 + \frac{B}{2}(\partial_z u)^2 + \frac{K}{2}(\nabla_\perp^2 u)^2 + \frac{\chi}{2}(\partial_\tau \phi)^2 + \frac{1}{2}\rho_s^\parallel (\partial_z \phi)^2 + \frac{1}{2}\rho_s^\perp (\nabla_\perp \phi)^2\right], \tag{109}$$

where (for later mathematical convenience) we generalized the model to d dimensions, with a single LO modulation-ordering axis $\hat{\mathbf{z}} \equiv \hat{r}_\parallel$ along $\mathbf{q}_0$ and $d-1$ space $\mathbf{r}_\perp$ transverse to $\mathbf{q}_0$, and introduced $\kappa = 2q_0^2\chi_0$, $\chi = 2\chi_0$. The harmonic (imaginary-time-ordered) correlations of the decoupled modes $u(\tau,\mathbf{r}),\phi(\tau,\mathbf{r})$ can be easily computed exactly for two-point correlation functions giving

$$G_u(\tau,\mathbf{r}) = \langle u(\tau,\mathbf{r}) u(0,0)\rangle_0 = \frac{1}{\beta}\sum_{\omega_n} \int^{\Lambda_\perp} \frac{d^d k}{(2\pi)^d} \frac{e^{-i\omega_n \tau + i\mathbf{k}\cdot\mathbf{r}}}{\kappa\omega_n^2 + Bk_z^2 + Kk_\perp^4}, \tag{110a}$$

$$G_\phi(\tau,\mathbf{r}) = \langle \phi(\tau,\mathbf{r}) \phi(0,0)\rangle_0 = \frac{1}{\beta}\sum_{\omega_n} \int^{\Lambda} \frac{d^d k}{(2\pi)^d} \frac{e^{-i\omega_n \tau + i\mathbf{k}\cdot\mathbf{r}}}{\kappa\omega_n^2 + \rho_s^\parallel k_z^2 + \rho_s^\perp k_\perp^2}. \tag{110b}$$

The averaging above was done with the Euclidean probability distribution $e^{-S^0_{\rm LO}}/Z_0$, using the harmonic action above, and $\omega_n = 2\pi n/\beta$ is the standard Matsubara frequency. Λ is the uv cutoff for the Goldstone-mode action, set by the inverse coherence length $1/\xi \approx q_0$. While the full expression above can be computed asymptotically in terms of special functions or numerically, it is more revealing to analyze these in special limits of interest. The simplest measure of fluctuations is given by the root-mean-squared (rms) fluctuations of these Goldstone modes, given by $G_u(0,0) = \langle u^2\rangle, G_\phi(0,0) = \langle \phi^2\rangle$.

1. $T = 0$ *quantum fluctuations*

At zero temperature, the Matsubara summations in the above expressions reduce to frequency integrals over ω in d dimensions giving

$$\langle u^2\rangle_0^Q = \int^{\Lambda_\perp} \frac{d\omega d^d k}{(2\pi)^{d+1}} \frac{1}{\kappa\omega^2 + Bk_z^2 + Kk_\perp^4} \approx \frac{\Lambda_\perp^{d-1}}{(2\pi)^d \sqrt{\kappa B}} \quad \text{for} \quad d > 1, \tag{111a}$$

$$\langle \phi^2\rangle_0^Q = \int^{\Lambda} \frac{d\omega d^d k}{(2\pi)^{d+1}} \frac{1}{\kappa\omega^2 + \rho_s^\parallel k_z^2 + \rho_s^\perp k_\perp^2} \approx \frac{\Lambda_\perp^{d-1}}{(2\pi)^d \sqrt{\kappa \rho_s^\parallel}} \quad \text{for} \quad d > 1. \tag{111b}$$

Because of the integrand's anisotropies, the details of above expressions are sensitive to microscopic ultraviolet (uv) and infrared (ir) cutoffs. However, the key unambiguous finding above is that in any physical dimension of interest here ($d > 1$) quantum Goldstone-mode fluctuations in the LO state are finite, set by the short (uv) length scale and therefore are qualitatively unimportant within the ordered LO state. That is, the LO state has a nonzero range of stability to quantum fluctuations, and therefore at $T = 0$ is well approximated by its

mean-field form [162]. Quantum fluctuations will, of course, give quantitative corrections to the properties of the LO state and will be important near quantum transitions to other putative phases.

The above findings are consistent with known results for mathematically related systems. The action (109) for the d-dimensional $T = 0$ LO quantum phonon is isomorphic to a classical Hamiltonian of a generalized $(d+1)$-dimensional columnar liquid crystal [129,130], characterized by two spatial stiff directions (z and τ) and $d-1$ transverse soft $\mathbf{r}_\perp$ axes. The latter is known (by simple power counting) to exhibit long-range order down to $d+1 = 5/2$ dimensions, which is consistent with our finding for $\langle u^2\rangle$, above. Similarly, (110c) is also consistent with the well-known property of the XY model exhibiting long-range order down to $d+1 = 2$ dimensions. Thus, at $T = 0$ we conclude, as advertised in the Introduction, that a $(d+1)$-dimensional superfluid smectic, i.e., the LO ground state, is stable to quantum fluctuations for $d > 1$.

2. $T > 0$ *thermal fluctuations*

At nonzero T the Goldstone modes u and ϕ exhibit classical thermal fluctuations. By the identification of the corresponding sectors with the well-studied smectic and anisotropic XY models, we can conveniently take advantage of the large body of literature on these systems [129,130,134]. However, for completeness we will work out some of the key findings.

Returning to the full expressions for the harmonic correlation functions (110a) and (110c) at nonzero T, we separate out the dominant classical $\omega_{n=0} = 0$ contribution,

$$\langle u^2\rangle_0^T = \int_{L_\perp^{-1}}^{\Lambda_\perp} \frac{d^dk}{(2\pi)^d} \frac{T}{Bk_z^2 + Kk_\perp^4} \tag{112a}$$

$$\approx \begin{cases} \frac{T}{2\sqrt{BK}} C_{d-1} L_\perp^{3-d}, & d < 3, \\ \frac{T}{4\pi\sqrt{BK}} \ln q_0 L_\perp, & d = 3, \end{cases} \tag{112b}$$

$$\langle \phi^2\rangle_0^T = \int_{L_\perp^{-1}}^{\Lambda_\perp} \frac{d^dk}{(2\pi)^d} \frac{T}{\rho_s^\parallel k_z^2 + \rho_s^\perp k_\perp^2} \tag{112c}$$

$$\approx \begin{cases} \frac{T}{\sqrt{\rho_s^\parallel \rho_s^\perp}} C_d L_\perp^{2-d}, & d < 2, \\ \frac{T}{2\pi\sqrt{\rho_s^\parallel \rho_s^\perp}} \ln q_0 L_\perp, & d = 2, \end{cases} \tag{112d}$$

where we neglected the subdominant quantum contribution (worked out above), defined a constant $C_d = S_d/(2\pi)^d = 2\pi^{d/2}/[(2\pi)^d \Gamma(d/2)]$, with S_d the surface area of a d-dimensional sphere, and introduced an infrared cutoff by considering a system of finite extent $L_\perp \times L_z$, with L_z the length of the system along the ordering (z) axis and $L_\perp$ transverse to z. Unless it has a huge aspect ratio, such that $L_z \sim L_\perp^2/\lambda \gg L_\perp$, any large system ($L_\perp, L_z \gg \lambda$) will have $\lambda L_z \ll L_\perp^2$.

The key observation here is that the smectic phonons exhibit fluctuations that diverge, growing logarithmically in 3D and linearly in 2D with system size $L_\perp$. The superconductor phase fluctuations ϕ exhibit well-known 2D logarithmic divergences [138,139,141]. Because (aside from the superfluid stiffness anisotropy) these are the same as in an ordinary superconductor and in the bulk 3D case will be finite, indicating a long-range off-diagonal order, we will focus on the smectic phonon fluctuations special to the LO (and FF) states.

The expression for the root-mean-squared phonon fluctuations in (112b) leads to the emergence of important crossover length scales $\xi_\perp, \xi_z$, related by

$$\xi_\perp = (\xi_z\sqrt{K/B})^{1/2} \tag{113a}$$

$$\equiv \sqrt{\xi_z \lambda}, \tag{113b}$$

that characterize the finite-temperature LO state. These are defined as scales $L_\perp, L_z$ at which phonon fluctuations are large, comparable to the LO period $a = 2\pi/q_0$. That is, setting

$$\langle u^2\rangle_0^T \approx a^2 \tag{114}$$

in Eq. (112b), we find

$$\xi_\perp \approx \begin{cases} \frac{a^2\sqrt{BK}}{T} \sim \frac{K}{Tq_0}, & d = 2, \\ ae^{4\pi a^2\sqrt{BK}/T} \sim ae^{\frac{cK}{Tq_0}}, & d = 3, \end{cases} \tag{115a}$$

where in the second form of the above expressions we took the simplest approximation for the smectic anisotropy length $\lambda = \sqrt{K/B}$ to be $\lambda = a \sim 1/q_0$, and introduced an order-1 Lindemann constant c [163] that depends on the somewhat arbitrary definition of "large" phonon rms fluctuations.

The thermal connected correlation function of LO phonons,

$$C_u(\mathbf{r}_\perp, z) = \langle [u(\mathbf{r}_\perp, z) - u(\mathbf{0}, 0)]^2\rangle_0, \tag{116}$$

is also straightforwardly worked out, in 3D giving the logarithmic Caillé form [134]

$$C_u^{3D}(\mathbf{r}_\perp, z) = 2T \int \frac{d^2q_\perp dq_z}{(2\pi)^3} \frac{1 - e^{i\mathbf{q}\cdot\mathbf{r}}}{Kq_\perp^4 + Bq_z^2}$$

$$= \frac{T}{2\pi\sqrt{KB}} g_T^{3D}\left(\frac{z\lambda}{r_\perp^2}, \frac{r_\perp}{a}\right)$$

$$= \frac{T}{2\pi\sqrt{KB}} \left[\ln\left(\frac{r_\perp}{a}\right) - \frac{1}{2}\mathrm{Ei}\left(\frac{-r_\perp^2}{4\lambda|z|}\right)\right] \tag{117a}$$

$$\approx \frac{T}{2\pi\sqrt{KB}} \begin{cases} \ln\left(\frac{r_\perp}{a}\right), & r_\perp \gg \sqrt{\lambda|z|}, \\ \ln\left(\frac{4\lambda z}{a^2}\right), & r_\perp \ll \sqrt{\lambda|z|}, \end{cases} \tag{117b}$$

where $\mathrm{Ei}(x)$ is the exponential-integral function. As indicated in the last form, in the asymptotic limits of $r_\perp \gg \sqrt{\lambda z}$ and $r_\perp \ll \sqrt{\lambda z}$ this 3D correlation function reduces to logarithmic growth with $r_\perp$ and z, respectively.

In 2D we instead have [142]

$$C_u^{2D}(x, z) = 2T \int \frac{dq_x dq_z}{(2\pi)^2} \frac{1 - e^{i\mathbf{q}\cdot\mathbf{r}}}{Kq_x^4 + Bq_z^2}$$

$$= \frac{T}{2\pi\sqrt{KB}} g_T^{2D}\left(\frac{z\lambda}{x^2}, \frac{x}{a}\right)$$

$$= \frac{2T}{B}\left[\left(\frac{|z|}{4\pi\lambda}\right)^{1/2} e^{-x^2/(4\lambda|z|)} + \frac{|x|}{4\lambda}\mathrm{erf}\left(\frac{|x|}{\sqrt{4\lambda|z|}}\right)\right] \tag{118a}$$

$$\approx \frac{2T}{B} \begin{cases} \left(\frac{|z|}{4\pi\lambda}\right)^{1/2}, & x \ll \sqrt{\lambda|z|}, \\ \frac{|x|}{4\lambda}, & x \gg \sqrt{\lambda|z|}, \end{cases} \tag{118b}$$

where $\mathrm{erf}(x)$ is the error function.

This divergence of smectic phonon fluctuations at nonzero temperature has immediate drastic implications for the properties of the LO (and FF) states. As emphasized in the Introduction, the most important of these is that the thermal average of the Landau LO order parameters (64) vanishes in the thermodynamic limit,

$$\begin{aligned}\langle\Delta_{\rm LO}(\mathbf{r})\rangle_0 &= 2\Delta_{q_0}\langle e^{i\phi}\cos[\mathbf{q}_0\cdot\mathbf{r}+\theta]\rangle_0\\ &= 2\Delta_{q_0}e^{-\frac{1}{2}\langle\phi^2\rangle_0-\frac{1}{2}q_0^2\langle u^2\rangle_0}\cos(\mathbf{q}_0\cdot\mathbf{r})\\ &= 2\tilde{\Delta}_{q_0}(L_\perp)\cos(\mathbf{q}_0\cdot\mathbf{r}),\end{aligned}\tag{119}$$

with the thermally suppressed order parameter amplitude given by

$$\tilde{\Delta}_{q_0}(L_\perp) = \Delta_{q_0}e^{-\frac{1}{2}\phi_{\rm rms}^2}\begin{cases}e^{-L_\perp/\xi_\perp}, & d=2,\\ \left(\frac{a}{L_\perp}\right)^{\eta/2}, & d=3,\end{cases}\tag{120a}$$

$$\to 0 \quad \text{for} \quad L_\perp\to\infty,\tag{120b}$$

where $\phi_{\rm rms}^2\equiv\langle\phi^2\rangle_0$. Here we used results for the phonon and phase fluctuations, (112b) and (112d) and defined the Caillé exponent

$$\eta=\frac{q_0^2T}{8\pi\sqrt{BK}}.\tag{121}$$

We also neglected the subdominant quantum phonon fluctuations and included all finite (quantum and thermal) superconducting phase fluctuations inside the nonzero Debye-Waller factor $e^{-\frac{1}{2}\phi_{\rm rms}^2}$. Thus, in qualitative contrast to its mean-field description, at long scales (longer than $\xi_{\perp,z}$) a LO state is characterized by a *uniform* superconducting order parameter and density.

To further characterize a finite-temperature LO state, we compute the Cooper-pair momentum distribution function,

$$n_{\mathbf{k}}^{\rm LO}=\int_{\mathbf{r},\mathbf{r}'}\langle\Delta_{\rm LO}^*(\mathbf{r})\Delta_{\rm LO}(\mathbf{r}')\rangle e^{i\mathbf{k}\cdot\mathbf{r}-i\mathbf{k}\cdot\mathbf{r}'}\tag{122a}$$

$$\approx\sum_{q_n=nq_0}|\Delta_{q_n}|^2\int_{\mathbf{r},\mathbf{r}'}\langle e^{i(\phi_{\mathbf{r}}-\phi'_{\mathbf{r}})}e^{iq_n(u_{\mathbf{r}'}-u_{\mathbf{r}})}\rangle e^{i\mathbf{k}\cdot(\mathbf{r}-\mathbf{r}')+iq_n(z-z')}\tag{122b}$$

$$\approx\sum_{q_n=nq_0}V|\Delta_0|^2\int_{\mathbf{r}}e^{-\frac{1}{2}C_\phi(\mathbf{r})}e^{-\frac{1}{2}q_n^2C_u(\mathbf{r})}e^{i(\mathbf{k}-q_n\hat{\mathbf{z}})\cdot\mathbf{r}},\tag{122c}$$

where V is the system's volume and we generalized the LO order parameter to include high harmonics q_n. To lowest order we neglected the subdominant coupling between the superfluid phase and the LO phonons and ignored the nonlinear effects, approximating u and ϕ as Gaussian fields. The asymptotic form of $n_{\mathbf{k}}^{\rm LO}$ can then be readily obtained analytically. As we saw above, in the 3D superfluid phase, ϕ exhibits only finite fluctuations about an ordered state, with

$$C_\phi^{\rm 3D}(r\gg\xi)\approx\frac{T}{2\xi\sqrt{\rho_s^\parallel\rho_s^\perp}},\tag{123}$$

where we took the coherence length ξ as the short-scale cutoff. These phase fluctuations then simply give a finite Debye-Waller factor suppression of the momentum distribution function amplitude, corresponding to the usual fluctuation-driven condensate depletion, with a fraction of atoms pushed out of the $\mathbf{q}_0$ condensate.

In contrast, the 3D LO phonon fluctuations diverge logarithmically, (117b), strongly modifying $n_{\mathbf{k}}$ from its mean-field δ-function form. We thus find $n_{\mathbf{k}}$ to exhibit a power-law peak around the ordering wave vector $\mathbf{q}_0$ (and its harmonics $\mathbf{q}_n$), reminiscent of (1+1)D Luttinger liquids and two-dimensional crystals [136–138,141],

$$n_{\mathbf{k}}^{\rm LO}\approx\sum_{q_n\neq0}\frac{n_{q_n}}{|k_z-nq_0|^{2-n^2\eta}}\quad\text{for}\quad d=3,\tag{124}$$

where for simplicity we specialized to $\mathbf{k}=k_z\hat{\mathbf{z}}$. The form-factor amplitude is approximately given by $n_{q_n}\approx V|\Delta_{q_n}|^2e^{-\frac{T}{4\xi\sqrt{\rho_s^\parallel\rho_s^\perp}}}$.

An additional characterization of the LO state is through a structure function $S(\mathbf{q})$, a Fourier transform of the density correlation function, that in 3D is given by

$$S^{\rm LO}(\mathbf{q})=\int d^3r\langle\delta\rho(\mathbf{r})\delta\rho(0)\rangle e^{-i\mathbf{q}\cdot\mathbf{r}}\tag{125a}$$

$$\approx\int d^3r\langle|\Delta_{\rm LO}(\mathbf{r})|^2|\Delta_{\rm LO}(0)|^2\rangle e^{-i\mathbf{q}\cdot\mathbf{r}}\tag{125b}$$

$$\approx\sum_{q_n}|\Delta_{q_n}|^4\int_{\mathbf{r}}\langle e^{i2q_n(u_0-u_{\mathbf{r}})}\rangle_0 e^{-i(\mathbf{q}-2q_n\hat{\mathbf{z}})\cdot\mathbf{r}}\tag{125c}$$

$$\approx\sum_n\frac{|\Delta_{q_n}|^4}{|q_z-2nq_0|^{2-4n^2\eta}}\quad\text{for}\quad d=3,\tag{125d}$$

where we approximated phase and phonon fluctuations by Gaussian statistics (in 3D valid up to weak logarithmic corrections [131]) and replaced atomic density fluctuations by (twice) the LO condensate density. The latter neglects a contribution from the imbalanced atoms, without qualitatively modifying the result (since atomic density is locked to the condensate density) and is furthermore quantitatively subdominant for $h\ll h_{c2}$, where the imbalance is low. As for $n_{\mathbf{k}}$, we find that the logarithmically divergent 3D phonon fluctuations lead to a structure function with highly anisotropic ($q_z\sim q_\perp^2/\lambda$) quasi-Bragg peaks (see Fig. 21) replacing the true Bragg peaks characteristic of the mean-field long-range periodic order. These predictions are a reflection of the well-known [129,130] and experimentally tested [135] behavior of conventional smectic liquid crystals.

In two dimensions, the LO order is even more strongly suppressed by thermal fluctuations. The linear growth of the 2D phonon fluctuations leads to exponentially short-ranged correlations in the LO order parameter and in the density. Because it is the soft smectic Goldstone mode that is responsible for these interesting properties they are necessarily also shared by the FF state [110].

As discussed in the Introduction, another fascinating consequence of the thermal vanishing of $\langle\Delta_{\rm LO}\rangle$, (120b), is that the leading nonzero Landau order parameter characterizing the LO state is the translationally invariant charge-4 (four-atom pairing) superconducting order parameter $\Delta_{\rm sc}$, introduced in (70a). Thus in the presence of thermal fluctuations the LO phase corresponds to an exotic state in which the off-diagonal order is exhibited by pairs of Cooper pairs, i.e., a bound quartet of atoms, rather than by the conventional two-atom Cooper pairs [119]. In 2D and 3D this higher-order pairing is driven by arbitrary low-T fluctuation, rather than by a fine-tuned

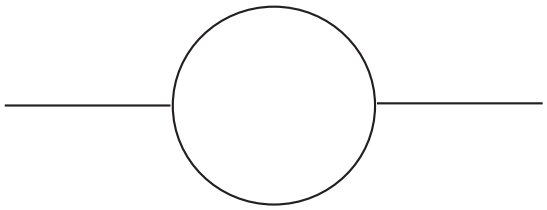

FIG. 6. Feynman graph that renormalizes the elastic moduli K and B of the LO superfluid.

attractive interaction between Cooper pairs, and therefore has no mean-field description. We will discuss these and other fluctuation-induced phases as well as transitions between them in Sec. VII.

B. Nonlinear elasticity: Beyond Gaussian fluctuations

1. Perturbation theory

As is clear from the derivation of the previous section, the restoration of the translational symmetry [a uniform LO state with a vanishing $\langle \Delta_{\rm LO}(\mathbf{r})\rangle$, etc.] by thermal fluctuations is a robust prediction of the quadratic theory that cannot be overturned by the left-out nonlinearities. However, the asymptotic form of the correlation functions computed within the harmonic approximation only extends out to the nonlinear length scales $\xi_{\perp,z}$, beyond which the divergently large LO-phonon fluctuations invalidate the neglect of the nonlinear phonon operators

$$\mathcal{H}_{\rm nonlinear} = -\tfrac{1}{2}B(\partial_z u)(\nabla u)^2 + \tfrac{1}{8}B(\nabla u)^4. \tag{126}$$

These will necessarily qualitatively modify predictions (117b), (118b), (124), and (125) on scales longer than the crossover scales $\xi_{\perp,z}^{\rm NL}$, which we compute next.

To see this, we use a perturbative expansion in the nonlinear operators (126) to assess the size of their contribution to, e.g., the free energy. Following a standard field-theoretic analysis, these can be accounted for as corrections to the compressional B and bend K elastic moduli, with the leading contribution to δB summarized graphically in Fig. 6 and given by

$$\delta B = -\frac{1}{2}TB^2\int_{\mathbf{q}} q_\perp^4 G_u(\mathbf{q})^2 \tag{127a}$$

$$\approx -\frac{1}{2}TB^2\int_{-\infty}^{\infty}\frac{dq_z}{2\pi}\int_{L_\perp^{-1}}\frac{d^{d-1}q_\perp}{(2\pi)^{d-1}}\frac{q_\perp^4}{\left(Kq_\perp^4+Bq_z^2\right)^2}$$

$$\approx -\frac{1}{8}\frac{C_{d-1}T}{3-d}\left(\frac{B}{K^3}\right)^{1/2}L_\perp^{3-d}B. \tag{127b}$$

Here, we neglected the subdominant contribution from quantum fluctuations, i.e., used the thermal equal-time correlator $G_u(\mathbf{q})$, focused on $d \leqslant 3$ (which allowed us to drop the uv-cutoff- (Λ-) dependent part that vanishes for $\Lambda \to \infty$), and cut off the divergent contribution of the long-wavelength modes via the infrared cutoff $q_\perp > 1/L_\perp$ by considering a system of a finite extent $L_\perp$. Clearly the anharmonicity become important when the fluctuation corrections to the elastic constants (e.g., δB above) become comparable to the bare microscopic values. The divergence of this correction as $L_\perp \to \infty$ signals the breakdown of the conventional harmonic elastic theory on length scales longer than a crossover scale $\xi_\perp^{\rm NL}$

$$\xi_\perp^{\rm NL} \approx \begin{cases} \frac{1}{T}\left(\frac{K^3}{B}\right)^{1/2}, & d=2, \\ ae^{\frac{c}{T}\left(\frac{K^3}{B}\right)^{1/2}}, & d=3, \end{cases} \tag{128}$$

which we define here as the value of $L_\perp$ at which $|\delta B(\xi_\perp^{\rm NL})| = B$. Within the approximation of the smectic screening length $\lambda = a$, these nonlinear crossover lengths reduce to the phonon disordering lengths (115) and (113b), defined by a Lindemann-like criterion. Clearly, on scales longer than $\xi_{\perp,z}^{\rm NL}$ the perturbative contributions of nonlinearities diverge and therefore cannot be neglected. Their contributions are thus expected to qualitatively modify the harmonic predictions of the previous section.

2. Renormalization group analysis in $d = 3 - \epsilon$ dimensions

To describe the physics beyond the crossover scales $\xi_{\perp,z}^{\rm NL}$—i.e., to make sense of the infrared-divergent perturbation theory found in Eq. (127b)–requires a renormalization group analysis. This was first performed in the context of conventional liquid crystals and Lifshitz points in a seminal work by Grinstein and Pelcovits (GP) [131]. For completeness, we complement GP's treatment with Wilson's momentum-shell renormalization group (RG) analysis, extending it to an arbitrary dimension d, so as to connect to the behavior in 2D, which has an exact solution [132].

To this end we integrate (perturbatively in $\mathcal{H}_{\rm nonlinear}$) short-scale Goldstone modes in an infinitesimal cylindrical shell of wave vectors, $\Lambda e^{-\delta\ell} < q_\perp < \Lambda$ and $-\infty < q_z < \infty$ ($\delta\ell \ll 1$ is infinitesimal). The leading perturbative momentum-shell coarse-graining contributions come from terms found in direct perturbation theory above, but with the system size divergences controlled by the infinitesimal momentum shell. The thermodynamic averages can then be equivalently carried out with an effective coarse-grained Hamiltonian of the same form (77c), but with all the couplings infinitesimally corrected by the momentum shell. For smectic moduli B and K this gives

$$\delta B \approx -\tfrac{1}{8}gB\delta\ell, \tag{129a}$$

$$\delta K \approx \tfrac{1}{16}gK\delta\ell, \tag{129b}$$

where the dimensionless coupling is given by

$$g = C_{d-1}\Lambda_\perp^{3-d}T\left(\frac{B}{K^3}\right)^{1/2} \tag{130a}$$

$$\approx \frac{T}{2\pi}\left(\frac{B}{K^3}\right)^{1/2}, \tag{130b}$$

and in the second form we approximated g by its value in 3D. Because it is only the smectic nonlinearities that are qualitatively important, no other stiffnesses experience corrections that accumulate at long scales. Equations (129) show that B is softened and K is stiffened by the nonlinearities in the presence of thermal fluctuations, making the system effectively more isotropic.

For convenience we then rescale the lengths and the remaining long-wavelength part of the fields $u^<(\mathbf{r})$ according to $r_\perp = r'_\perp e^{\delta\ell}$, $z = z'e^{\omega\delta\ell}$, and $u^<(\mathbf{r}) = e^{\phi\delta\ell}u'(\mathbf{r}')$, so as to restore the ultraviolet cutoff $\Lambda_\perp e^{-\delta\ell}$ back up to $\Lambda_\perp$. The

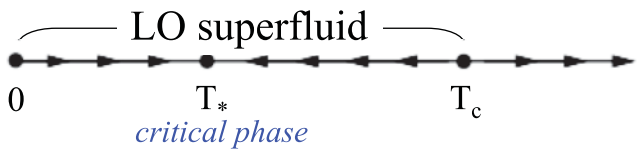

FIG. 7. (Color online) Renormalization group flow for a LO state in $d < 3$ dimensions, illustrating that at low T it is a "critical phase" displaying universal power-law phenomenology, controlled by a nontrivial infrared stable fixed point.

underlying rotational invariance ensures that the graphical corrections preserve the rotationally invariant strain operator $[\partial_z u - \frac{1}{2}(\nabla_\perp u)^2]$, renormalizing it as a whole. It is therefore convenient (but not necessary) to choose the dimensional rescaling that also preserves this form. It is easy to see that this choice leads to

$$\phi = 2 - \omega. \tag{131}$$

The leading (one-loop) changes to the effective coarse-grained and rescaled action can then be summarized by differential RG flows

$$\frac{dB(\ell)}{d\ell} = \left(d + 3 - 3\omega - \frac{1}{8}g(\ell)\right) B(\ell), \tag{132a}$$

$$\frac{dK(\ell)}{d\ell} = \left(d - 1 - \omega + \frac{1}{16}g(\ell)\right) K(\ell). \tag{132b}$$

From these we readily obtain the flow of the dimensionless coupling $g(\ell)$,

$$\frac{dg(\ell)}{d\ell} = (3-d)g - \frac{5}{32}g^2, \tag{133}$$

whose flow for $d < 3$ away from the $g = 0$ Gaussian fixed point encodes the long-scale divergences found in the direct perturbation theory above. As summarized in Fig. 7 for $d < 3$, the flow terminates at a nonzero fixed-point coupling $g_* = \frac{32}{5}\epsilon$ (with $\epsilon \equiv 3 - d$), which determines the nontrivial long-scale behavior of the system (see below). As with treatments of critical points [164], but here extending over the whole LO phase, the RG procedure is quantitatively justified by the proximity to $d = 3$, i.e., smallness of ϵ.

We can now use a standard matching calculation to determine the long-scale asymptotic form of the correlation functions on scales beyond $\xi^{\rm NL}_{\perp,z}$. Namely, applying above coarse-graining RG analysis to a computation of correlation functions allows us to relate a correlation function at long length scales of interest to us (which, because of infrared divergences is impossible to compute via a direct perturbation theory) to that at short scales, evaluated with coarse-grained couplings, $B(\ell), K(\ell), \ldots$. In contrast to the former, the latter is readily computed via a perturbation theory that because of the shortness of the length scale is convergent. The result of this matching calculation to lowest order gives correlation functions from an effective Gaussian theory,

$$G_u(\tau = 0, \mathbf{k}) \approx \frac{T}{B(\mathbf{k})k_z^2 + K(\mathbf{k})k_\perp^4}, \tag{134}$$

with moduli $B(\mathbf{k})$ and $K(\mathbf{k})$ that are singularly wave-vector dependent, the latter determined by the solutions $B(\ell)$ and $K(\ell)$ of the RG flow equations (132a) and (132b) with initial conditions the microscopic values B and K, e.g., as given by the BCS predictions, Eq. (80).

2D analysis. In $d = 2$, at long scales $g(\ell)$ flows to a nontrivial infrared stable fixed point $g_* = 32/5$, and the matching analysis predicts correlation functions characterized by anisotropic wave-vector-dependent moduli,

$$K(\mathbf{k}) = K(k_\perp \xi^{\rm NL}_\perp)^{-\eta_K} f_K\left[k_z \xi^{\rm NL}_z / (k_\perp \xi^{\rm NL}_\perp)^\zeta\right] \sim k_\perp^{-\eta_K}, \tag{135a}$$

$$B(\mathbf{k}) = B(k_\perp \xi^{\rm NL}_\perp)^{\eta_B} f_B\left[k_z \xi^{\rm NL}_z / (k_\perp \xi^{\rm NL}_\perp)^\zeta\right] \sim k_\perp^{\eta_B}. \tag{135b}$$

Thus, on scales longer than $\xi^{\rm NL}_{\perp,z}$ these qualitatively modify the real-space correlation function asymptotics of the harmonic analysis in the previous section. In Eqs. (135) the universal anomalous exponents are given by

$$\eta_B = \tfrac{1}{8}g_* = \tfrac{4}{5}\epsilon \approx \tfrac{4}{5} \quad \text{for } d = 2, \tag{136a}$$

$$\eta_K = \tfrac{1}{16}g_* = \frac{2}{5}\epsilon \approx \tfrac{2}{5} \quad \text{for } d = 2, \tag{136b}$$

determining the $z - \mathbf{r}_\perp$ anisotropy exponent via (134) to be

$$\zeta \equiv 2 - (\eta_B + \eta_K)/2 \tag{137a}$$

$$= \tfrac{7}{5} \quad \text{for} \quad d = 2, \tag{137b}$$

as expected reduced by thermal fluctuations down from its harmonic value of 2. The $\mathbf{k}_\perp - k_z$ dependence of $B(\mathbf{k}), K(\mathbf{k})$ is determined by universal scaling functions $f_B(x), f_K(x)$ that we will not compute here. The underlying rotational invariance (special to a LO state realized in an isotropic trap) gives an *exact* relation between the two anomalous $\eta_{B,K}$ exponents [165],

$$3 - d = \frac{\eta_B}{2} + \frac{3}{2}\eta_K, \tag{138a}$$

$$1 = \frac{\eta_B}{2} + \frac{3}{2}\eta_K \quad \text{for } d = 2, \tag{138b}$$

which is obviously satisfied by the anomalous exponents Eqs. (136b), and (136a), computed here to first order in $\epsilon = 3 - d$ [165].

Thus, as advertised in the Introduction, we find that a finite-temperature 2D LO state is highly nontrivial and qualitatively distinct from its mean-field perfectly periodic form. In addition to a vanishing LO order parameter and associated fluctuation-restored translational symmetry, it is characterized by a universal nonlocal length-scale-dependent modulus, Eq. (135). Consequently its Goldstone-mode theory and the associated correlations are not describable by a local field theory, which is an analytic expansion in local field operators. Instead, in 2D, on length scales beyond $\xi^{\rm NL}_{\perp,z}$, thermal fluctuations and correlations of the LO state are controlled by a nontrivial fixed point, characterized by universal anomalous exponents $\eta_{K,B}$ and scaling functions $f_{B,K}(x)$ defined above.

Above we obtained this nontrivial structure from an RG analysis and estimated these exponents within a controlled but approximate ϵ expansion. Remarkably, in 2D an exact solution of this problem was discovered by Golubovic and Wang [132]. It predicts an anomalous phenomenology in

qualitative agreement with the RG predictions above, and gives exact exponents

$$\eta_B^{2D} = 1/2, \tag{139a}$$
$$\eta_K^{2D} = 1/2, \tag{139b}$$
$$\zeta^{2D} = 3/2. \tag{139c}$$

3D analysis. In $d = 3$, the nonlinear coupling $g(\ell)$ is marginally irrelevant, flowing to 0 at long scales. Despite this, the marginal flow to the Gaussian fixed point is sufficiently slow (logarithmic in lengths) that (as usual at a marginal dimension [164]) its power-law-in-ℓ dependence leads to a universal, asymptotically *exact* logarithmic wave-vector dependence [131]

$$K(\mathbf{k}_\perp, k_z = 0) \sim K \left|1 + \frac{5g}{64\pi} \ln(1/k_\perp a)\right|^{2/5}, \tag{140a}$$
$$B(\mathbf{k}_\perp = 0, k_z) \sim B \left|1 + \frac{5g}{128\pi} \ln(\lambda/k_z a^2)\right|^{-4/5}. \tag{140b}$$

This translates into equal-time LO order parameter correlations given by

$$n(z, \mathbf{r}_\perp = 0) = \langle \Delta^*_{\rm LO}(\mathbf{r}) \Delta_{\rm LO}(0)\rangle \tag{141a}$$
$$\sim e^{-c_1 (\ln z)^{6/5}} \cos(q_0 z) \tag{141b}$$

(with c_1 a nonuniversal constant) as discovered in the context of conventional smectics by Grinstein and Pelcovits [131]. Although these 3D anomalous effects are less dramatic and likely to be difficult to observe in practice, theoretically they are quite significant as they represent a qualitative breakdown of the mean-field and harmonic descriptions, which respectively ignore interactions and thermal fluctuations.

We conclude this section by noting that all of the above analysis is predicated on the validity of the purely elastic model, Eq. (77c), which neglects topological defects, such as vortices and dislocations. If these unbind (as they undoubtedly do in 2D at any nonzero temperature [142]), then our predictions above only hold on scales shorter than the separation ξ_v, ξ_d between these defects.

VI. TOPOLOGICAL DEFECTS IN A LARKIN-OVCHINNIKOV STATE

We now turn to the discussion of the topological defects, followed in the subsequent section by an analysis of phases and transitions accessible by their unbinding. As discussed in Sec. III, the LO superfluid is distinguished by two independent order-parameter components $\Delta_{\pm\mathbf{q}_0}$, corresponding to $\pm\mathbf{q}_0$ finite center-of-mass momentum pairing [152]. These complex order parameters $\Delta_{\pm\mathbf{q}_0} = |\Delta_{q_0}| e^{i\phi_\pm}$ in turn lead to two independent phase Goldstone modes $\phi_\pm$ [or equivalently $\phi, \theta = -q_0 u$ (65)], controlled by a long-scale Hamiltonian, which at harmonic level is given by

$$H^0_{\rm LO} = \int dz d^{d-1} r_\perp \left[\sum_{\sigma=\pm} \left(\frac{\rho_s^\parallel}{4} (\partial_z \phi_\sigma)^2 + \frac{K}{4q_0^2} (\nabla_\perp^2 \phi_\sigma)^2 \right) + \frac{\rho_s^\perp}{8} (\nabla_\perp \phi_+ + \nabla_\perp \phi_-)^2 \right] \tag{142a}$$

$$= \int dz d^{d-1} r_\perp \left[\frac{B}{2} (\partial_z u)^2 + \frac{K}{2} (\nabla_\perp^2 u)^2 + \frac{1}{2} \rho_s^\parallel (\partial_z \phi)^2 + \frac{1}{2} \rho_s^\perp (\nabla_\perp \phi)^2 \right], \tag{142b}$$

with the couplings given in Eqs. (80) and (81) and in obtaining Eq. (142) we dropped the subdominant higher-gradient (K) term in ϕ. The analysis of this Hamiltonian in the absence of topological defects was discussed in the previous section. We now use it to understand the energetics of defects beyond that "spin-wave" approximation.

As in an ordinary superfluid, because $\phi_\pm$ are *compact* phase fields ($\phi_\pm$ and $\phi_\pm + 2\pi$ are physically identified), in addition to their smooth configurations, there are vortex topological excitations, corresponding to non-single-valued configurations of $\phi_\pm(\mathbf{r})$. These are defined by two corresponding integer-valued closed line integrals enclosing a vortex line:

$$\oint d\vec{\ell} \cdot \vec{\nabla} \phi_\pm = 2\pi n_\pm, \tag{143}$$

that we collectively designate by a two-component integer-valued vector $\vec{N}_v = (n_+, n_-)$, with $n_\pm \in \mathbb{Z}$. These integer vector defects $\vec{N}_v$ are associated with the fundamental group Π_1 of the torus $\mathrm{U}(1) \otimes \mathrm{U}(1)$ [166] that characterizes the low-energy manifold of Goldstone modes of the LO state. In this respect the LO superfluid has similarities to other $\mathrm{U}(1) \otimes \mathrm{U}(1)$ systems, such as easy-plane spinor-1 condensates [167] and two-gap superconductors, e.g., MgB_2 [168].

In a differential form, the line defects are equivalently encoded as

$$\nabla \times \nabla \phi_\pm = \mathbf{m}_\pm, \tag{144}$$

with vortex line topological charge density given by

$$\mathbf{m}_\pm(\mathbf{r}) = 2\pi \sum_i \int n^i_\pm \hat{\mathbf{t}}_i(s_i) \delta^3(\mathbf{r} - \mathbf{r}_i(s_i))\, ds_i, \tag{145}$$

where s_i parametrizes the ith vortex line (or loop), $\mathbf{r}_i(s_i)$ gives its positional conformation, $\hat{\mathbf{t}}_i(s_i)$ is the local unit tangent, and vortex "charges" $n^i_\pm$ are independent of s_i, since the charge of a given line is constant along the defect. Furthermore,

$$\nabla \cdot \mathbf{m}(\mathbf{r}) = 0 \tag{146}$$

enforces the condition that vortex lines cannot end in the bulk of the sample; they must either form closed loops or extend entirely through the system.

A. Vortices and dislocations

As with the Goldstone modes in (64), where it was more convenient to work with the more physical sum and difference modes $\phi(\mathbf{r}) = \frac{1}{2}(\phi_+ + \phi_-)$ and $\theta(\mathbf{r}) = \frac{1}{2}(\phi_+ - \phi_-)$, Eqs. (65) and (142b), we consider topological defects associated with singularities in $\phi(\mathbf{r})$ and $\theta(\mathbf{r})$ [166], defined by

$$\oint d\vec{\ell} \cdot \vec{\nabla} \phi = 2\pi n_v, \tag{147a}$$
$$\oint d\vec{\ell} \cdot \vec{\nabla} \theta = 2\pi n_d. \tag{147b}$$

Given the definitions of ϕ, θ, the corresponding vortex (v) and dislocation (d) defect "charges" $n_{v,d}$ are related to the

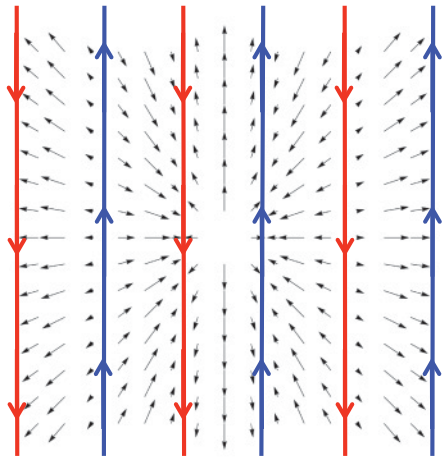

FIG. 8. (Color online) A 2π-vortex defect in a LO state. The 2D arrows indicate the corresponding complex condensate LO wave function $\Delta^{v}_{\rm LO}(\mathbf{r})$, with orientations characterizing the phase $\phi(\mathbf{r})$.

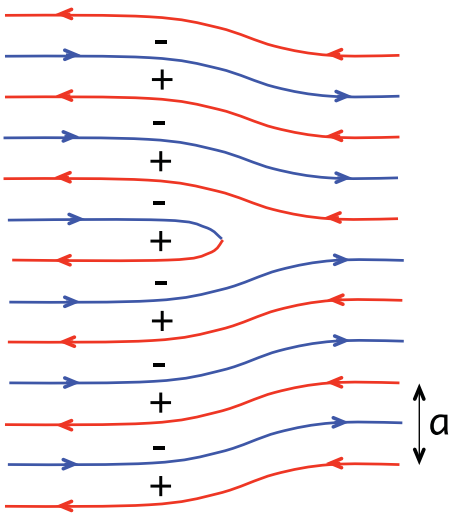

FIG. 9. (Color online) An integer a-dislocation defect in the LO layered structure, with no defects in its superfluid phase.

integer-valued $n_\pm$ according to

$$n_v = \tfrac{1}{2}(n_+ + n_-), \tag{148a}$$
$$n_d = \tfrac{1}{2}(n_+ - n_-), \tag{148b}$$

and therefore admit half-integer and integer topological "charges", collectively designated by a vortex flavor vector $\vec{\mathcal{N}} = (n_v, n_d)$. The minimal values of $n_+ = \pm 1, n_- = \pm 1$ lead to four fundamental defects (eight counting the overall $\pm$ signs of each)

$$\vec{\mathcal{N}}_v = (\pm 1, 0) \leftrightarrow \vec{N}_{v,v} = (\pm 1, \pm 1), \tag{149a}$$
$$\vec{\mathcal{N}}_d = (0, \pm 1) \leftrightarrow \vec{N}_{v,-v} = (\pm 1, \mp 1), \tag{149b}$$
$$\vec{\mathcal{N}}_{v\text{-}d,} = (\pm 1/2, \pm 1/2) \leftrightarrow \vec{N}_{v,0} = (\pm 1, 0), \tag{149c}$$
$$\vec{\mathcal{N}}^{*}_{v\text{-}d,} = (\pm 1/2, \mp 1/2) \leftrightarrow \vec{N}_{0,v} = (0, \pm 1), \tag{149d}$$

where the first two defects $\vec{\mathcal{N}}_v, \vec{\mathcal{N}}_d$ are ordinary 2π-vortices in ϕ_+ *and* in ϕ_-, which respectively correspond to a 2π-vortex in ϕ superimposed on defect-free LO layers (Fig. 8) and an integer a dislocation in the periodic LO smectic state.

As illustrated in Fig. 9 for a 2D state, the latter of these two corresponds to a LO state with an edge dislocation of a smectic layer, or equivalently, two missing adjacent $\pm$ domain walls, with no additional phase winding in ϕ. In 2D the LO order parameter in the presence of these point defects is given by

$$\Delta^{v}_{\rm LO} = 2e^{i\varphi(y,z)}\cos(q_0 z) \quad \text{for} \quad \vec{\mathcal{N}}_v = (1,0), \tag{150a}$$
$$\Delta^{d}_{\rm LO} = 2\cos[q_0 z + \theta_d(y,z)] \quad \text{for} \quad \vec{\mathcal{N}}_d = (0,1), \tag{150b}$$

where $\varphi(y,z) = \tan^{-1}(z/y)$ is the azimuthal coordinate angle creating the singular vortex, and $\theta_d(y,z) = \varphi(y,x) + \theta_0(y,x)$ the corresponding dislocation angle with a nonsingular part $\theta_0(y,x)$ accounting for smectic anisotropic elasticity. As can be seen from their form in terms of the $\vec{N}_v = (n_+, n_-)$ description, these two seemingly simpler integer defects in Eqs. (149a) and (149b) are actually composites of the fundamental $\vec{\mathcal{N}}_{v,0} = (1,0)$ and $\vec{\mathcal{N}}_{0,v} = (0,1)$ defects.

The $\vec{\mathcal{N}}_{v,-d} = (\pm 1/2, \pm 1/2)$, $\vec{\mathcal{N}}_{v,-d} = (\pm 1/2, \mp 1/2)$ defects are half-integer vortex-dislocation composites, where a $\pm\pi$-vortex is bound to half of a single domain wall, an $a/2$ dislocation, illustrated in Fig. 10. In terms of the two coupled phase fields ϕ_+, ϕ_- these half-integer defects correspond to an *integer* vortex in one but not both $\phi_\pm$ phases. In 2D the LO

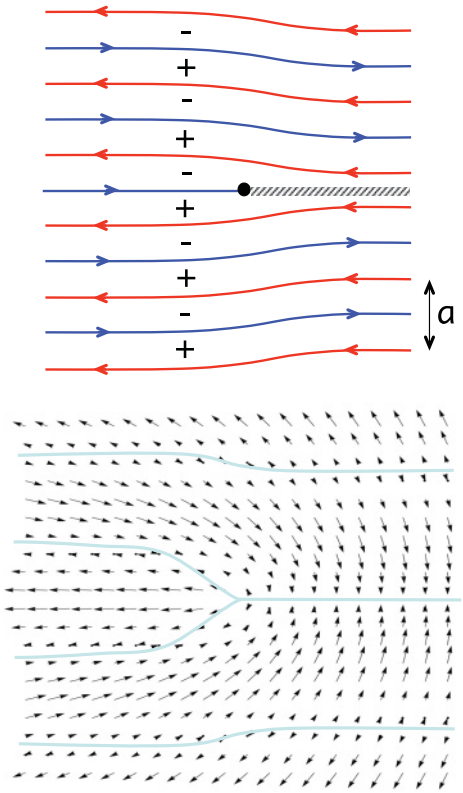

FIG. 10. (Color online) Two complementary forms illustrating a half-integer vortex-dislocation $(\pi, a/2)$ defect in the LO state. The 2D arrows indicate the corresponding complex condensate LO wave function $\Delta^{v-d}_{\rm LO}(\mathbf{r})$, with orientations characterizing the phase $\phi(\mathbf{r})$.

order parameter in the presence of such a half-integer defect is given by

$$\Delta_{\rm LO}^{v,-d} = 2e^{i\varphi(y,z)/2}\cos[q_0 z + \varphi(y,z)/2] \ \text{ for } \ \vec{\mathcal{N}}_v = (1/2,1/2). \tag{151}$$

In contrast to a conventional uniform superfluid or a standard smectic density wave, here the product form of the pair-density-wave LO order parameter (64) allows this composite half-integer defect. Namely, although the superfluid and the smectic density-wave order-parameter components each change by a minus sign (wind by a phase of π), the product LO order-parameter $\Delta_{\rm LO}$, Eq. (64), remains single-valued in the presence of such $(\pm 1/2, \pm 1/2)$ and $(\pm 1/2, \mp 1/2)$ fractional composite defects.

B. Energetics

The energy cost of these vortices and dislocations can be computed with straightforward extensions of standard analyses [130,142].

1. 2π-vortex: $\vec{\mathcal{N}}_v = (1,0)$

The 2π-vortex in the LO superfluid is obtained via a solution of the Euler-Lagrange equation for $\phi(\mathbf{r})$,

$$\rho_s^{\parallel}\partial_z^2\phi^v + \rho_s^{\perp}\nabla_{\perp}^2\phi^v = 0, \tag{152}$$

under the condition of a 2π-vortex line singularity,

$$\nabla\times\nabla\phi^v = 2\pi\int \hat{\mathbf{t}}(s)\delta^3(\mathbf{r}-\mathbf{r}(s))\,ds, \tag{153}$$

located at $\mathbf{r}(s)$ with a unit tangent $\hat{\mathbf{t}}(s)$. The smectic layers remained undistorted at long scales, $u = 0$ (equivalently $\phi_+ = \phi_-$). The solution displays a qualitatively standard form, but with distortions associated with a large anisotropy ratio $\rho_{\parallel}/\rho_{\perp}$, that, as we demonstrated dramatically diverges at the upper critical field h_{c2}. This is reflected in the anisotropy of the mass current flow around a vortex line running within the LO (smectic, xy) layers (a mass flow with velocity component along the smectic layer normal, $\hat{\mathbf{q}}_0 = \hat{\mathbf{z}}$), illustrated in Fig. 11. For concreteness we look at two straight vortex line configurations.

2π-vortex line $||\mathbf{q}_0$. For a straight vortex line running along $\mathbf{q}_0$ (z axis) the above equations reduce to

$$\nabla_{\perp}^2\phi^v = 0, \tag{154a}$$

$$\nabla\times\nabla\phi^v = 2\pi\hat{\mathbf{z}}\delta^2(\mathbf{r}_{\perp}), \tag{154b}$$

which gives $\phi^v(\mathbf{r}) = \varphi(x,y)$, where $\varphi(x,y) = \tan^{-1}(y/x)$ is the azimuthal coordinate angle within a smectic layer (xy plane). The corresponding superfluid "velocity" $\mathbf{v}_v = \nabla\phi^v$ for such a 2π-vortex line directed along $\hat{\mathbf{q}}_0 = \hat{\mathbf{z}}$ (flowing in the xy $\perp$ plane) is isotropic, given by a standard $\hat{\varphi}/r_{\perp}$ form:

$$\mathbf{v}_v^{\parallel} = \frac{1}{r_{\perp}^2}(-y,x,0). \tag{155}$$

Integrating the kinetic energy density Eq. (142b) in a system of dimensions $L_{\perp}\times L_{\perp}\times L_z$, we readily find the energy to be given by the familiar 3D (linear-logarithmic) form,

$$E_v^{\parallel} = \pi\rho_s^{\perp}L_z\ln(L_{\perp}/a), \tag{156}$$

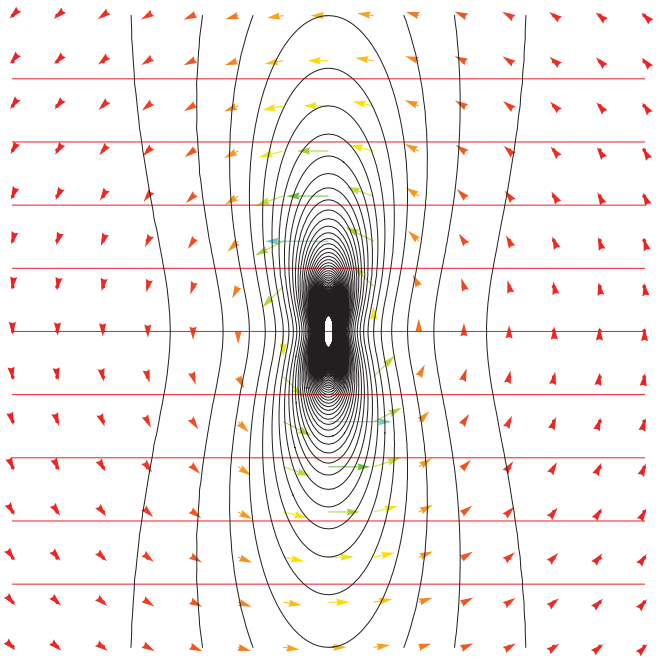

FIG. 11. (Color online) Anisotropic superfluid flow around a 2π-vortex near h_{c2}, predicted to be characterized by an anisotropic superfluid ratio $\rho_s^{\parallel}/\rho_s^{\perp}$ that diverges at h_{c2}.

diverging linearly with the vortex line's length L_z and logarithmically with the system's in-plane extent $L_{\perp}$.

2π-vortex line $\perp \mathbf{q}_0$. In contrast, a vortex line directed along the smectic layers (taken here to be along the x axis, with flow confined to the anisotropic y-z plane), characterized by

$$\nabla\times\nabla\phi^v = 2\pi\hat{\mathbf{x}}\delta(y)\delta(z), \tag{157}$$

is described by $\phi(\mathbf{r}) = \varphi(\sqrt{\rho_s^{\parallel}}y, \sqrt{\rho_s^{\perp}}z) = \tan^{-1}(\frac{z}{y}\sqrt{\frac{\rho_s^{\perp}}{\rho_s^{\parallel}}})$ and a velocity field

$$\mathbf{v}_v^{\perp} = \frac{\sqrt{\rho_s^{\parallel}\rho_s^{\perp}}}{\rho_s^{\parallel}y^2 + \rho_s^{\perp}z^2}(0,-z,y), \tag{158}$$

illustrated in Fig. 11.

As expected from the superfluid-stiffness anisotropy near h_{c2}, where $\rho_s^{\perp}/\rho_s^{\parallel} \ll 1$, the superflow around a vortex falls off much more slowly across the LO layers (along z) than within them (along $\mathbf{r}_{\perp}$). This leads to (near h_{c2} a highly) anisotropic ellipticlike superflow with the major axis oriented along the LO layers normal (along $\mathbf{q}_0$) and a velocity flow that is *not* everywhere tangent to the equipotential flows, as illustrated in Fig. 11.

Substituting this flow inside the Hamiltonian (142b), the corresponding vortex energy is then readily shown to be given by

$$E_v^{\perp} = \pi\sqrt{\rho_s^{\parallel}\rho_s^{\perp}}L_{\perp}\ln\left[\left(\rho_s^{\parallel}L_{\perp}^2 + \rho_s^{\perp}L_z^2\right)^{1/2}/a\right]. \tag{159}$$

In 2D it reduces to a familiar logarithmic form by replacement of the $L_{\perp}$ factor by the sample thickness.

2. *a-dislocation:* $\vec{\mathcal{N}}_d = (0,1)$

An integer dislocation defect in the LO superfluid is similarly obtained via a solution of the Euler-Lagrange equation for $u = -\theta/q_0$, obtained by minimizing Eq. (142b), with a condition of $\phi = 0$ (equivalently $\phi_+ = -\phi_-$):

$$B\partial_z^2 u_d - K\nabla_\perp^4 u_d = 0, \tag{160}$$

and the singularity and continuity conditions

$$\nabla \times \mathbf{v}_d = \mathbf{m}_d, \tag{161a}$$

$$\nabla \cdot \mathbf{m}_d = 0, \tag{161b}$$

with the singular strain

$$\mathbf{v}_d = \nabla u_d, \tag{162}$$

and the dislocation "charge" density

$$\mathbf{m}_d(\mathbf{r}) = a\sum_i \int n_d^i \hat{\mathbf{t}}_i(s_i)\delta^3(\mathbf{r} - \mathbf{r}_i(s_i))\, ds_i. \tag{163}$$

As for the vortex, s_i parametrizes the ith dislocation loop, $\mathbf{r}_i(s_i)$ is the conformation of that loop, $\hat{\mathbf{t}}_i(s_i)$ is its local unit tangent, and n_d^i is the number of excess layers associated with the dislocation. Note that n_d^i is independent of s_i, since the charge of a given dislocation line is constant along the line defect.

The dislocation solution is most straightforwardly obtained in Fourier space, where the equations reduce to

$$q_z v_d^z + \lambda^2 q_\perp^2 \mathbf{q}_\perp \cdot \mathbf{v}_d = 0, \tag{164a}$$

$$i\mathbf{q} \times \mathbf{v}_d = \mathbf{m}_d, \tag{164b}$$

and the general solution is given by

$$\mathbf{v}_d = \frac{i\mathbf{q} \times \mathbf{m}_d}{q^2} + i\mathbf{q}\chi(\mathbf{q}), \tag{165}$$

with $\chi(\mathbf{q})$ a smooth elastic distortion around the dislocation line that is obtained via the Euler-Lagrange equation (160) and is given by

$$\chi = -\frac{q_z(1-\lambda^2 q_\perp^2)}{\Gamma_q^{\mathrm{Sm}} q^2}\epsilon_{zij} q_i m_j^d. \tag{166}$$

The superfluid phase remains uniform at long scales, $\phi = 0$ (equivalently $\phi_+ = -\phi_-$). Here we defined the inverse of the LO phonon propagator,

$$\Gamma_{\mathbf{q}}^{\mathrm{Sm}} \equiv q_z^2 + \lambda^2 q_\perp, \tag{167}$$

with $\lambda = \sqrt{K/B}$ a length characterizing the LO domain-wall deformations. Insertion of the above expression for $\mathbf{v}_d$ into the original elastic Hamiltonian Eq. (142b) gives the Coulomb-gas-like Hamiltonian that determines the energy of an arbitrary dislocation configuration,

$$H_d = \frac{1}{2}\int_{\mathbf{q}} \left[\frac{Kq_\perp^2}{\Gamma_{\mathbf{q}}^{\mathrm{Sm}}} P_{ij}^\perp(\mathbf{q}) + \mathcal{E}_c\delta_{ij}\right] m_i^d(\mathbf{q}) m_j^d(-\mathbf{q}), \tag{168}$$

where $P_{ij}^\perp(\mathbf{q}) = \delta_{ij}^\perp - q_i^\perp q_j^\perp/q_\perp^2$ is the in-(xy) plane transverse projection operator, with $\perp$ indicating projection onto the smectic layers. Here we also added the dislocation core energy determined by its short-scale ($a = 2\pi/q_0$) configuration, at which the above continuum analysis no longer applies. A simplest estimate (up to possibly nontrivial dimensionless factors set by λ/a, which can only be determined through a microscopic calculation) of this core energy density $\mathcal{E}_c$ is given by K.

In 3D, two limiting dislocation line configurations are the screw and edge dislocations,

$$\mathbf{m}_d^{\mathrm{screw}}(\mathbf{r}) = a\hat{\mathbf{z}}\delta^2(\mathbf{r}_\perp), \tag{169a}$$

$$\mathbf{m}_d^{\mathrm{edge}}(\mathbf{r}) = a\hat{\mathbf{x}}\delta(y)\delta(z), \tag{169b}$$

running perpendicular to and along smectic layers, respectively. Within the above harmonic continuum approximation, the long-scale elastic contribution [the first term in (168)] to the energy of a screw dislocation vanishes identically [because of $P_{ij}^\perp(\mathbf{q})$], physically because of the smectic's soft in-plane curvature elasticity and due to the absence of long-scale compressional distortion in a screw dislocation, as can be readily verified. Thus its energy is determined by short-scale core energetics inaccessible to harmonic elastic analysis.

For a single edge dislocation along $\hat{\mathbf{x}}$ (169b) $\vec{m}^d(\mathbf{q}) = a\hat{\mathbf{x}}2\pi\delta(q_x)$, giving for the elastic part of the energy

$$E_{d,\mathrm{el}}^{\mathrm{3D\ edge}} = L_\perp a^2 \int_{\mathbf{q}} \frac{Kq_\perp^2}{\Gamma_{\mathbf{q}}^{\mathrm{Sm}}}(1 - q_x^2/q_\perp^2)2\pi\delta(q_x) \tag{170a}$$

$$= L_\perp a^2 \int \frac{dq_y dq_z}{(2\pi)^2}\frac{Kq_y^2}{q_z^2 + \lambda^2 q_y^4} \tag{170b}$$

$$= \frac{Ka}{2\lambda}L_\perp, \tag{170c}$$

where the factor of $L_\perp$ came from the regularized identity $2\pi\delta(q_x)\delta(q_x) = L_\perp\delta(q_x)$. Although the first "elastic" contribution in Eq. (168) no longer vanishes, the above energy is dominated by the short cutoff scale a and therefore in principle indistinguishable from the core energy. Thus, based on this analysis we can only provide an estimate of the 3D dislocation energies,

$$E_d^{\mathrm{3D\ screw}} \approx KL_z, \tag{171a}$$

$$E_d^{\mathrm{3D\ edge}} \approx \frac{Ka}{\lambda}L_\perp \approx (BK)^{1/2}aL_\perp \approx KL_\perp, \tag{171b}$$

diverging linearly with its length.

Correspondingly, as first demonstrated by Toner and Nelson [142], in two dimensions the energy of a smectic edge dislocation is constant, i.e., system-length independent, given by

$$E_d^{\mathrm{2D}} \approx a\sqrt{BK} \approx K. \tag{172}$$

As we will see in the next section, this observation has crucial implications for the instability of a finite-temperature 2D LO state [142].

3. *Half-integer vortex-dislocation defect:* $\vec{\mathcal{N}}_{v\text{-}d} = (1/2,1/2)$

As discussed above [112], on general grounds a LO (but not a FF) superconductor allows half-integer defects that are a composite of a π-vortex and an $a/2$ dislocation, illustrated in Fig. 10. The form and the energy associated with this defect

requires a solution of Euler-Lagrange equations for $\phi_\pm$,

$$-\rho_s^\parallel \partial_z^2 \phi_\pm + \frac{K}{q_0^2}\nabla_\perp^4 \phi_\pm - \frac{1}{2}\rho_s^\perp \nabla_\perp^2 \phi_\pm - \frac{1}{2}\rho_s^\perp \nabla_\perp^2 \phi_\mp = 0, \tag{173}$$

with singularity conditions

$$\boldsymbol{\nabla} \times \boldsymbol{\nabla}\phi_+ = 2\pi \hat{\mathbf{x}}\delta(y)\delta(z), \tag{174a}$$

$$\boldsymbol{\nabla} \times \boldsymbol{\nabla}\phi_- = \mathbf{0}, \tag{174b}$$

for concreteness taken to be a straight vortex line in ϕ_+ running parallel to LO layers, along the $\hat{\mathbf{x}}$ axis, and $\phi_- = 0$.

Solving these equations gives the defect's shape from which the energy is readily computed:

$$E_{\pi\text{-}a/2} \approx \tfrac{1}{4} L_\perp \left[\pi \sqrt{\rho_s^\parallel \rho_s^\perp}\, \ln\left[\left(\rho_s^\parallel L_\perp^2 + \rho_s^\perp L_z^2\right)^{1/2}/a\right] + K\right]. \tag{175}$$

Because the energy scales as a square of the defect's topological charge $n_{v,d}$, as expected, the above energy of the half vortex-dislocation defect is one-quarter of the sum of the energies of the unit vortex and dislocation.

C. Dual description: Coupled *XY*-smectic models

In characterizing phases in terms of topological defects, it is often useful to have a continuum field-theoretic description of defects and of the corresponding transitions associated with their unbinding. Such a description, which complements the LO Goldstone model (142), is obtained through a duality transformation that we develop here. In 3D the analysis is somewhat complicated and results in two coupled U(1) gauge theories, whose derivation and analysis we leave to a future presentation [151]. Here, for simplicity we will exclusively focus on two dimensions.

To this end, starting with $H_{\rm LO}$, (142b), allowing for singular configurations of ϕ (vortices) and u (dislocations) discussed in the previous section, and integrating out the smooth parts of Goldstone modes, we obtain a Coulomb-gas description of a finite density of topological defects,

$$H_{\rm CG}^{XY\text{-Sm}} = \frac{1}{2}\int_{\mathbf{q}} \left[\frac{\sqrt{\rho_s^\perp \rho_s^\parallel}}{\Gamma_{\mathbf{q}}^{XY}}|m_{\mathbf{q},v}|^2 + \frac{K q_\perp^2}{\Gamma_{\mathbf{q}}^{\rm Sm}}|m_{\mathbf{q},d}|^2\right] + \sum_{\mathbf{r}_i}\left(E_c^v n_{\mathbf{r}_i,v}^2 + E_c^d n_{\mathbf{r}_i,d}^2\right), \tag{176}$$

where

$$\Gamma_{\mathbf{q}}^{XY} = q_\perp^2\sqrt{\rho_s^\perp/\rho_s^\parallel} + q_z^2\sqrt{\rho_s^\parallel/\rho_s^\perp}, \tag{177a}$$

$$\Gamma_{\mathbf{q}}^{\rm Sm} = q_z^2 + \lambda^2 q_\perp^4. \tag{177b}$$

Here, $m_{\mathbf{q},v}, m_{\mathbf{q},d}$ are the Fourier transforms of the vortex and dislocation densities $m_v(\mathbf{r}) = \sum_i 2\pi n_{\mathbf{r}_i}^v \delta^2(\mathbf{r} - \mathbf{r}_i^v)$, $m_d(\mathbf{r}) = \sum_i a n_{\mathbf{r}_i}^d \delta^2(\mathbf{r} - \mathbf{r}_i^d)$, with $n_{\mathbf{r}_i}^{v,d} = \frac{1}{2}(n_{\mathbf{r}_i}^+ \pm n_{\mathbf{r}_i}^-)$, and $n_{\mathbf{r}_i}^\pm \in \mathbb{Z}$ the independent elementary integer defects, defined in the previous section. We also introduced the vortex and dislocation core energy $E_c^{v,d}$ to account for short-scale core physics not accounted for by the above continuum description. Although by time-reversal symmetry the core energies of the elementary defects $n^\pm$ are identical, those of the vortex and dislocation composites will generically be distinct with $E_c^v \neq E_c^d$.

To obtain a continuum description of these integer-valued fields, it is convenient to decouple interaction of these defects using a Hubbard-Stratonovich transformation by introducing a pair of dual real fields (corresponding potentials) $\tilde{\phi},\tilde{\theta}$ with the Hamiltonian

$$\tilde{H}[\tilde{\phi},\tilde{\theta},n_{v,d}] = \tilde{H}_0[\tilde{\phi},\tilde{\theta}] + i\int_{\mathbf{r}}(\tilde{\phi}(\mathbf{r})m_v(\mathbf{r}) + q_0\tilde{\theta}(\mathbf{r})m_d(\mathbf{r})) + \sum_{\mathbf{r}_i}\left(E_c^v n_{\mathbf{r}_i,v}^2 + E_c^d n_{\mathbf{r}_i,d}^2\right), \tag{178}$$

where

$$\tilde{H}_0[\tilde{\phi},\tilde{\theta}] = \frac{1}{2}\int_{\mathbf{q}}\left[\frac{\Gamma_{\mathbf{q}}^{XY}}{\sqrt{\rho_s^\perp\rho_s^\parallel}}|\tilde{\phi}_{\mathbf{q}}|^2 + \frac{\Gamma_{\mathbf{q}}^{\rm Sm} q_0^2}{K q_\perp^2}|\tilde{\theta}_{\mathbf{q}}|^2\right]. \tag{179}$$

The thermodynamics is characterized by a partition function

$$Z = \int [d\tilde{\phi}d\tilde{\theta}]\prod_{\mathbf{r}_i^{v,d}}\sum_{n_{\mathbf{r}_i}^{v,d}} e^{-\tilde{H}[\tilde{\phi},\tilde{\theta},n_{\mathbf{r}_i}^{v,d}]} \tag{180a}$$

$$= \int [d\tilde{\phi}d\tilde{\theta}]e^{-\tilde{H}_0[\tilde{\phi},\tilde{\theta}]}\prod_{\mathbf{r}_i^{v,d}}\sum_{n_{\mathbf{r}_i}^{v,d}} e^{i2\pi n_{\mathbf{r}_{i,v}}\tilde{\phi}(\mathbf{r}_{i,v}) + i2\pi n_{\mathbf{r}_{i,d}}\tilde{\theta}(\mathbf{r}_{i,v}) - E_c^v n_{\mathbf{r}_i,v}^2 - E_c^d n_{\mathbf{r}_i,d}^2}, \tag{180b}$$

where we chose to measure all energies in units of $k_B T$. The summation over vortex and dislocation charges $n_{\mathbf{r}_i}^{v,d}$ can be readily done in the dilute defect limit, corresponding to large core energies E_c. In this limit the summations can be limited to nine lowest-order terms, corresponding to no vortices present, $\vec{N}_{0\text{-}0}$, one vortex of either species and sign at a site, $\vec{N}_{\pm1,0}, \vec{N}_{0,\pm1}$, or two vortices of distinct species existing at a single site, $\vec{N}_{\pm1,\pm1}$. Equivalently, in terms of $\vec{\mathcal{N}}$ vortex-dislocation nomenclature, these respectively correspond to

$$\vec{\mathcal{N}}\text{: } (0,0),\ \pm(\pi,a/2),\ \pm(\pi,-a/2),\ \pm(2\pi,0),\ \pm(0,a). \tag{181}$$

This gives

$$Z \approx \int [d\tilde{\phi}d\tilde{\theta}]e^{-\tilde{H}_0[\tilde{\phi},\tilde{\theta}]}\Big[1 + 2\sum_{\mathbf{r}_1}\left(e^{-\frac{1}{4}E_c^v - \frac{1}{4}E_c^d}\cos[\pi(\tilde{\phi}+\tilde{\theta})] + e^{-\frac{1}{4}E_c^v - \frac{1}{4}E_c^d}\cos[\pi(\tilde{\phi}-\tilde{\theta})] + e^{-E_c^v}\cos(2\pi\tilde{\phi}) + e^{-E_c^d}\cos(2\pi\tilde{\theta})\right)\Big]. \tag{182}$$

All other vortex configurations (for example, two defects of either species existing on *distinct* sites) are not included as they correspond to higher-order

contributions, suppressed at low fugacity. After reexponentiating, this equation leads to a generalized sine-Gordon model for the coupled $\tilde{\phi},\tilde{\theta}$ fields, with the dual Hamiltonian

$$\tilde{H} = \frac{1}{2}\int_{\mathbf{q}} \left[\frac{\Gamma^{XY}_{\mathbf{q}}}{\sqrt{\rho_s^{\perp}\rho_s^{\parallel}}} |\tilde{\phi}_{\mathbf{q}}|^2 + \frac{\Gamma^{\mathrm{Sm}}_{\mathbf{q}} q_0^2}{K q_{\perp}^2} |\tilde{\theta}_{\mathbf{q}}|^2 \right] - \int_{\mathbf{r}} [g_{\pi,a/2}\cos(\pi\tilde{\phi})\cos(\pi\tilde{\theta}) + g_{2\pi,0}\cos(2\pi\tilde{\phi}) + g_{0,a}\cos(2\pi\tilde{\theta})], \tag{183}$$

where the couplings are $g_{\pi,a/2} = \frac{4}{a^2} e^{-\frac{1}{4}E_c^v - \frac{1}{4}E_c^d}$, $g_{2\pi,0} = \frac{2}{a^2} e^{-E_c^v}$, and $g_{0,a} = \frac{2}{a^2} e^{-E_c^d}$, and we converted the sum over $\mathbf{r}_1$ into an integral over $\mathbf{r}$ via a lattice constant a.

In the opposite limit of a small core energy $E_c^{v,d}$, the defect density is high and the summation over the integer charges $n_{\mathbf{r}}^{\pm}$ can be carried out utilizing the Poisson summation formula, which leads to a replacement of the, e.g., $\cos(2\pi\tilde{\phi})$ potentials above by the Villain potential, defined by

$$e^{-\beta V_V[\tilde{\phi}]} = \sum_n e^{i2\pi n\tilde{\phi} - E_c n^2} \tag{184a}$$

$$= \sum_p e^{-\frac{1}{4E_c}(2\pi\tilde{\phi} - 2\pi p)^2}. \tag{184b}$$

The latter can be approximated by a single harmonic with an effective coupling $g_{\mathrm{eff}}^{v,d} = 1/(2E_c^{v,d}a^2)$.

The resulting generalized sine-Gordon model is convenient for analyzing the effects of defects on the LO state, particularly for the computation of their screening on long scales, unbinding, and for the analysis of the resulting disordered state. From the form (183) it is clear that (aside from an inconsequential anisotropy) the dual vortex sector described by $\tilde{\phi}$ has a standard sine-Gordon form. In contrast, the dual dislocation sector described by $\tilde{\theta}$ is qualitatively modified by the highly nonlocal and qualitatively anisotropic smectic kernel $\Gamma^{\mathrm{Sm}}_{\mathbf{q}}$ [169].

We next turn to a detailed discussion of the implication of these defects for possible phases and transitions associated with the LO state.

VII. PHASES AND PHASE TRANSITIONS: LARKIN-OVCHINNIKOV LIQUID CRYSTALS

We now turn to a discussion and characterization of a class of phases emerging from the Larkin-Ovchinnikov state by a partial disordering of it. Because these phases partially break spatial symmetries, we will refer to them collectively as LO liquid crystals. We first discuss general symmetry-based possibilities and then explore their concrete realization in terms of fluctuation-driven proliferation of topological defects.

A. Landau's order parameters and spontaneously broken symmetries

A conventional characterization of phases is through the Landau classification, where phases are distinguished by nonvanishing order parameters and corresponding symmetries that they break. From this prospective a zero-temperature LO (smectic pair-density wave) superfluid ($\mathrm{SF_{Sm}}$) breaks three symmetries: the translations $T_{\mathbf{q}_0}$ along $\mathbf{q}_0$ ($\hat{\mathbf{z}}$), the rotations $R_{\mathbf{q}_0}$ about the axis transverse to $\mathbf{q}_0$ [of the full 3D Euclidean group E(3)], and the U(1) symmetry associated with atom conservation. The corresponding nonvanishing order parameter that transforms nontrivially under this group of symmetries is the LO pair-density wave (64).

By considering all possible basic combinations of spontaneously broken subsets of these symmetries, we uncover five additional atomic liquid-crystal phases, which are descendants of the smectic LO state [170]. To enumerate these systematically we begin with the zero-temperature LO state, where all three of these symmetries are broken and partially restore them by progressively disordering the state. Restoring the translational symmetry $T_{\mathbf{q}_0}$, while keeping U(1) and $R_{\mathbf{q}_0}$, leads to a state with orientational and off-diagonal orders, which is a nematic superfluid, SF_N. By analogy with the conventional (nonsuperfluid) nematics the resulting state can be characterized by a complex traceless symmetric second-rank tensor Q_{ij}.

Subsequently disordering the orientational order and thereby also restoring the rotational symmetry $R_{\mathbf{q}_0}$ leads to an isotropic superfluid, SF_I, that exhibits a finite species imbalance. Symmetrywise, the resulting SF_I state is isomorphic to the polarized superfluid SF_M predicted [4,44] and observed to appear at a nonzero imbalance on the BEC side of the BCS-BEC crossover. In contrast (as a descendant of the LO state expected to be stabilized by Fermi surfaces imbalance) here the SF_I state is realized in an imbalanced superfluid on the BCS side, something that has been searched for dating back to Sarma [75], but has not been possible within mean-field treatments, which instead predict an instability to phase separation [4,40,44].

As summarized by Tables I and II the additional three phases, smectic, nematic, and isotropic Fermi liquids, $\mathrm{FL_{Sm}}$,FL_N,FL_I are the nonsuperfluid counterparts of the three discussed above, obtained by first restoring the U(1) symmetry by disordering the off-diagonal long-range order. The fully disordered FL_I state is simply the normal state of the polarized Fermi gas, albeit strongly interacting. Together these intermediate fluctuation-induced phases (along with a number of other possible ones that we discuss below) naturally interpolate between the fully gapped singlet (homogeneously and isotropic) BCS superconductor at zero imbalance and low temperature, and the normal polarized Fermi liquid at large imbalance and/or high temperature.

TABLE I. Five phases that naturally emerge as disordered descendants of the LO (superfluid smectic, $\mathrm{SF_{Sm}}$) state.

$\mathrm{FL_{Sm}}$	$\longrightarrow$	FL_N	$\longrightarrow$	FL_I
$\uparrow$U(1)		$\uparrow$U(1)		$\uparrow$U(1)
$\mathrm{SF_{Sm}}$	$\longrightarrow$	SF_N	$\longrightarrow$	SF_I

TABLE II. A summary of LO liquid-crystal Fermi liquid (FL) and superfluid (SF) phases, and corresponding order parameters and broken symmetries, indicated by ×'s. Unbroken symmetries are marked by check marks. The subscripts I, N, Sm respectively indicate the isotropic, nematic, and smectic orders.

Phases	U(1)	$T_{\mathbf{q}_0}$	$R_{\mathbf{q}_0}$
FL_I	√	√	√
FL_N	√	√	×
FL_{Sm}	√	×	×
SF_I	×	√	√
SF_N	×	√	×
SF_{Sm}	×	×	×

B. Larkin-Ovchinnikov liquid crystals via topological defect unbinding

A complementary way to characterize phases and phase transitions between them is in terms of topological defects proliferation [141]. For conventional phases and transitions (e.g., 3D *XY* or Ising models) this is simply a complementary description that is sometimes convenient. However, for topological phases, where the Landau order parameter is unavailable or just insufficient to distinguish two phases, this defect-proliferation approach is indispensable and therefore superior to soft-spin description of the order parameter. One prominent and familiar example is the description of the low-temperature quasi-long-range-ordered phase of the 2D *XY* model and its disordering. In this case, both the low- ("ordered") and high-temperature (disordered) phases exhibit a vanishing *XY* order parameter, and are respectively only topologically (not symmetry) distinguished by bound and unbound vortex defects and by the associated behavior of the correlation functions (power law and exponential, respectively) [141].

With this in mind, we characterized the LO and its descendant states in terms of a proliferation of the four types of topological defects $\vec{\mathcal{N}} = (0,a),(2\pi,0),(\pi,\pm a/2)$, introduced and analyzed in Sec. VI.

As discussed above, at $T = 0$ the LO phase is characterized by long-range off-diagonal and translational order and is thereby distinguished by a nonzero LO order parameter Δ_{LO}. In this ground state all of the above topological defects are absent, confined into topologically neutral pairs.

1. 3D phases and transitions

Although, (as we explicitly demonstrated in Sec. V) at nonzero temperature the LO order parameter vanishes in 3D (and in 2D), the 3D LO phase is distinguished from its more disordered descendants by the absence of unbound topological defects, in direct analogy with the quasi-long-range-ordered state of the 2D *XY* model. Thus, in this same sense at nonzero T the 3D LO smectic is a topologically ordered (but phonon, elastically disordered) phase.

Upon increasing temperature or decreasing the stiffnesses (e.g., by tuning the strength of the Feshbach-resonant interactions, or by adjusting the fermionic species imbalance), one or more of the four topological defects will proliferate, thereby leading to a transition of the LO smectic SF_{Sm} (PDW) into one of its descendants. The actual sequence of defect unbinding is determined by the relative energetics, given by Eqs. (159), (171), and (175). Lacking a reliable calculation (throughout the T-P-$1/k_F a$ phase diagram) of the dependences of the stiffnesses on the experimentally tunable parameters (T, imbalance P, interactions $1/k_F a$, and the number of atoms), the phase diagram can only be qualitatively mapped out in terms of the three effective stiffnesses $K, \rho_s^{\parallel,\perp}$. In the thermodynamic limit ($L_{\perp,z} \to \infty$, not necessarily relevant to atomic traps; see below), the relative defect energetics is quite unambiguous:

$$E^{d}_{(0,a)} \sim K L \ll E^{v\text{-}d}_{(\pi,a/2)} \sim \frac{\rho_s}{4} L \ln L + \frac{K}{4} L \ll E^{v}_{(2\pi,0)} \sim \rho_s L \ln L \quad \text{for} \quad L_{\perp,z} \sim L \to \infty, \tag{185}$$

where for simplicity we ignored anisotropies in ρ_s^i. Based on this energetics one may be tempted to conclude that in this limit (unless preempted by a first-order transition) it is the integer dislocation loop defects that proliferate first and the LO smectic preferentially disorders into a nematic superfluid, SF_N. However, in contrast to the 2D Kosterlitz-Thouless (KT) mechanism [141], the 3D disordering transitions take place when the relevant stiffness, renormalized by quantum and thermal fluctuations, is continuously driven to zero at the transition, or takes place at a finite (rather than a vanishing) fugacity. For a thermal transition this roughly corresponds to a transition temperature set by the corresponding stiffnesses, $\overline{\rho}_s = \sqrt{\rho_s^{\parallel}\rho_s^{\perp}}$ and K, B.

Lacking a detailed quantitative theory of such 3D transitions we can only construct a qualitative phase diagram, which we display in Fig. 4. It summarizes all basic phases that naturally appear upon disordering of the LO smectic superfluid by unbinding the four fundamental types of topological defects discussed above. One important physical input is the observation that increasing the Zeeman energy h (or equivalently, the species imbalance $m = n_\uparrow - n_\downarrow$) toward the normal Fermi liquid state, FL_I at h_{c2}, predominantly leads to a suppression of the superfluid stiffness and therefore to a destruction of the SF order. Conversely, a reduction of the Zeeman field (and species imbalance) toward a conventional isotropic and homogeneous superfluid SF_I at h_{c1} primarily leads to a reduction of the elastic moduli of the smectic pair-density wave by increasing its period $1/q_0$ and thereby weakening the interaction between the LO domain walls [see Eq. (97b)]. Thus lowering of h is expected to predominantly suppress, i.e., melt the positional smectic order.

Thus, starting with the LO SF_{Sm} state and *decreasing* h leads to the unbinding of the integer dislocations $(0,a)$, and a transition to an orientationally ordered, i.e., a nematic

charge-4 superfluid, SF_N^4. The latter charge-4 feature of SF_N^4 naturally appears as the remaining secondary order parameter $\Delta_{sc}^{(4)} = \Delta_{LO}^2$ once the LO positional order Δ_{LO} is destroyed by unbinding of integer dislocation loops. General arguments predict a subleading singularity $\sim(h - h_{N\text{-Sm}})^{1-\alpha}$ of $\Delta_{sc}^{(4)}(h)$ at the continuous transition $h_{N\text{-Sm}}$ between SF_N^4 and SF_{sc}. Since in contrast, the "charge"-2 SF nematic order vanishes in the LO state, a direct transition to it from the LO state can generically only proceed through a first-order transition.

Conversely, we expect that *increasing* h starting with the LO SF_{Sm} will lead to a suppression of ρ_s, a proliferation $(2\pi,0)$, and a transition to a $2q$-smectic Fermi liquid, FL_{Sm}^{2q}, a nonsuperfluid periodic state with a wave vector that is twice that of the LO state. Alternatively, as suggested by the energetics in Eq. (185), it may be that the lower-energy half-vortex dislocation defects $(\pi,a/2)$ [or the $(\pi,-a/2)$, but not both] unbind first, in which case a transition to a nematic Fermi liquid, FL_N^{**} [with the restored translational and U(1) charge symmetries] takes place. The resulting state is qualitatively distinct from the more conventional nematic (orientationally ordered) FL_N phase in which both $(\pi,a/2)$ and $(\pi,-a/2)$ are proliferated. Both are also distinct from the nematically ordered FL_N^* state, in which only integer dislocations $(0,a)$ and integer vortices $(2\pi,0)$ are unbound. One can envision a number of other states and phase transitions at low h by further considering the disordering of the nematic superfluid SF_N^4 by unbinding various patterns of disclinations and π-vortices. We leave a more detailed analysis of these to a future study.

2. 2D phases and transitions

The nature of the phase diagram changes qualitatively in two dimensions at nonzero temperature. Based on the work of Ref. [142] (in the context of conventional smectic liquid crystals) and from the analysis in Sec. VI B, which shows a finite energy cost of a 2D smectic dislocation, we conclude that at any nonzero T in 2D, the dislocations proliferate, thereby destroying the LO (SF_{Sm}) phase. It is replaced by a homogeneous, but quasi-orientationally-ordered, charge-4 superfluid nematic, SF_N^4. Upon rotation this superfluid will display 1/4 "charge" vortices ($\oint \nabla\phi \cdot d\mathbf{l} = \pi\hbar/2m$), that, because of its nematic order we expect to form a uniaxially distorted hexagonal lattice. Upon changing T, h, and $k_F a$, the nematic superfluid can then undergo further disordering transitions toward a polarized Fermi liquid and an isotropic (e.g., BCS) superfluid. In particular, we expect two Kosterlitz-Thouless transitions associated with the loss of 2D superfluid and orientational (nematic) quasi-long-range orders. Because Δ_q and therefore $\sqrt{\rho_\perp^s \rho_\parallel^s} \sim \Delta_q^3$ vanishes strongly near h_{c2}, we expect the superfluid KT transition to precede the nematic-isotropic one.

C. Fractionalized phases and topological order

In the discussion above, we argued for the existence of at least three topologically distinct Fermi liquid phases that naturally emerge from disordering of the LO (SF_{Sm}) phase by unbinding different combinations of allowed defects. Because, as demonstrated above, the conventional vortex $(2\pi,0)$ and a conventional dislocation $(0,a)$ are composites of the fundamental defects $(\pi,\pm a/2)$ the nonsuperfluid states FL_N^*,FL_N^{**} and their isotropic cousins FL_I^*,FL_I^{**} (in which disclinations are also unbound) are expected to be "fractionalized' " [171], topologically distinct from their conventional Fermi liquid analogs, where $(\pi,\pm a/2)$ are also unbound.

These phases are analogous to the putative phase-disordered fractionalized states obtained by unbinding double (hc/e) vortices, studied extensively by Sachdev, and by Balents, Senthil, Fisher, and collaborators [171–173] in the context of high-temperature superconductors. The resulting nonsuperfluid phase is distinguished from a conventional Fermi liquid by a gapped vison, a $\mathbb{Z}_2$ defect that is a remnant of the fundamental $hc/2e$ vortex after the composite hc/e (double) vortices proliferate. These states are also characterized by fractionalized charge-neutral spin-1/2 bosonic and charge-e spinless fermionic excitations.

The states FL_N^*,FL_N^{**} also bear a close relation to the collective-mode fractionalization discussed by Sachdev and others [174–176] in the context of quantum paramagnetic phases, emerging from disordering a collinear spin-density wave. As with the $[U(1)\otimes U(1)]/\mathbb{Z}_2$ LO state, where the order parameter is a product of the superfluid and smectic order parameters, Eq. (64), there too the order parameter is of $[S_2 \otimes U(1)]/\mathbb{Z}_2$ product form, encoding spatial modulation of the spin density, and therefore admits half-integer (visonlike) defects.

As we have seen in the previous section, a characterization of both the conventional and the fractionalized (topologically ordered but otherwise disordered) phases can be faithfully formulated directly in terms of distinct patterns of proliferation of the four types of vortex and dislocation defects, listed in Eq. (149). It can also equivalently be done in terms of a dual sine-Gordon [and in 3D U(1) gauge-theory] model $\tilde{H}$, Eq. (183). We now present a complementary effective Ising gauge theory description that can sometimes be convenient. In the absence of an underlying rotational invariance (which otherwise has been our focus throughout) and for simplicity ignoring anisotropy of the striped LO state, all the phases and transitions can be captured by a Euclidean action [in space-time $\vec{x} = (\tau,\mathbf{r})$]

$$S = -t_\phi \sum_{\langle \vec{x},\vec{x}'\rangle} \sigma_{\vec{x},\vec{x}'} \cos(\phi_{\vec{x}} - \phi_{\vec{x}'}) - t_\theta \sum_{\langle \vec{x},\vec{x}'\rangle} \sigma_{\vec{x},\vec{x}'} \cos(\theta_{\vec{x}} - \theta_{\vec{x}'}) - K_\sigma \sum_{\square} \prod \sigma_{\vec{x},\vec{x}'}, \tag{186}$$

where the Ising gauge field $\sigma_{\vec{x},\vec{x}'}$ couples to the $U(1)\otimes U(1)$ bosonic (rotor) matter fields $e^{i\phi_{\vec{x}}}$,$e^{i\theta_{\vec{x}}}$, and its nonzero $\mathbb{Z}_2$ flux through a plaquette encodes the presence of a half-integer $(\pi,a/2)$ defect. The gauge field $\sigma_{\vec{x},\vec{x}'}$ encodes the local Ising redundancy of splitting the LO order parameter (64) into a charge-2 boson, $b_{\mathbf{r}}^\dagger = e^{-i\phi_{\mathbf{r}}}$, that creates a zero-momentum Cooper pair (diatomic molecule) and a neutral boson, $\rho_{q,\mathbf{r}}^\dagger = e^{-i\theta_{\mathbf{r}}}$, that creates a density wave at a LO wave vector q. Formally, the gauge field σ can be introduced as a Hubbard-Stratonovic field that decouples the LO order parameter $\Delta_q = b\rho_q$ into its charge- and density-wave parts. The variety of phases and transitions between them are summarized in the phase diagram Fig. 4 and a flowchart Fig. 12.

In this formulation, the LO superfluid (SF_{Sm}) is a state at large t_ϕ,t_θ and arbitrary K_σ, in which both b and ρ_q are Bose

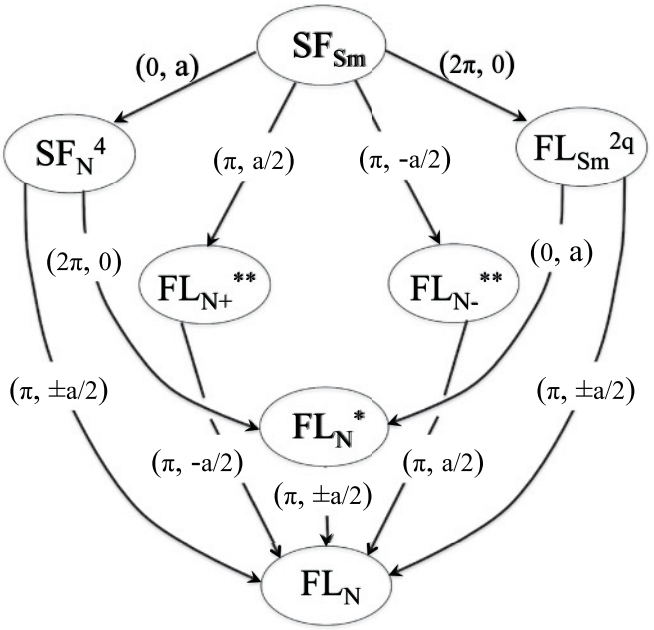

FIG. 12. A flowchart of superfluid (SF) and nonsuperfluid (FL) phases, exhibiting smectic (Sm) and nematic (N) conventional orders as well as topological orders (indicated by $*$ and $**$), induced by a proliferation of various combinations of topological defects $(0,a)$, $(2\pi,0)$, and $(\pi,\pm a/2)$.

condensed, and σ is gapped through a Higg's mechanism. In this state, gapped 2π-vortices in ϕ and θ respectively correspond to the $(2\pi,0)$ superconducting vortex and the $(0,a)$ integer dislocation that we discussed in the previous section.

For small t_ϕ and large t_θ, 2π-vortices in ϕ proliferate, driving b normal and restoring the $\mathrm{U}_\phi(1)$ (atom conservation) symmetry, while keeping ρ_q condensed. A large K_σ forces a vanishing Ising flux with $\sigma = 1$, which corresponds to a gapped vison. The resulting nonsuperfluid state is deconfined in the sense that it exhibits a gapped bosonic b excitation carrying an Ising charge and thereby acquiring a phase π upon encircling a vison. In our earlier notation this is the nonsuperfluid periodic state we dubbed $\mathrm{FL}^{2q}_{\mathrm{Sm}}$, in which $(2\pi,0)$ vortices have proliferated, but dislocations remain bound. Lowering K_σ drives visons gapless, corresponding to a proliferation of the $(\pi,a/2)$ fractional defects that induces a transition to the homogeneous but orientationally ordered (nematic) nonsuperfluid state, FL_N. We note that condensation of $(\pi,a/2)$ in the presence of unbound $(2\pi,0)$ defects automatically also leads to a proliferation of $(\pi,-a/2)$ defects and therefore (aside from the nematic conventional order) the resulting FL_N is fully disordered.

In the opposite regime of large t_ϕ and small t_θ, 2π vortices in θ proliferate, driving ρ_q "normal" (homogeneous state) and restoring the $\mathrm{U}_\theta(1)$ translational symmetry, while keeping b condensed. For large K_σ the vison remains gapped and the resulting superfluid homogeneous state exhibits gapped density excitations ρ_q, carrying an Ising charge and nontrivial statistics with the vison. The resulting state is the charge-4 nematically ordered superfluid SF^4_N. Upon reducing K_σ visons proliferate, driving a transition to FL_N through this alternate route.

In contrast to lowering K_σ, the transitions out of the $\mathrm{FL}^{2q}_{\mathrm{Sm}}$ and SF^4_N states at large K_σ can be driven by respectively lowering t_ϕ and t_θ and thereby unbinding the second set of integer defects, $(0,a)$ and $(2\pi,0)$, respectively. Since visons remain gapped, the resulting nonsuperfluid nematic state is the topologically ordered FL^*_N, qualitatively distinct from FL_N. The deconfinement transition FL^*_N-FL_N is then driven by lowering K_σ through a condensation of visons and is in the inverted Ising universality class.

A naive attempt at a generalization of the above Ising gauge theory action (186) to the rotationally invariant smectic form suggests a replacement of the t_θ operator by a gauge-invariant lattice Laplacian. However, on general grounds, without fine-tuning, such an Ising lattice form appears to preclude a fully rotationally invariant formulation necessary for a fully rotationally invariant LO (superfluid smectic) state.

Finally, we note that the above orientationally ordered state can further disorder into isotropic states by proliferation of disclinations. We leave a more detailed study of these phases and the corresponding transitions to future research.

VIII. FERMIONS

So far all of our discussion following the defining microscopic model in Sec. II has been confined to the bosonic sector of the Larkin-Ovchinnikov state. The resulting low-energy quantum thermodynamics is encoded in the Hamiltonian H_{LO}, Eq. (77c) [and the Lagrangian $\mathcal{L}_{\mathrm{LO}}$, Eq. (88)] for the superfluid phase ϕ and smectic phonon u Goldstone modes. In contrast to the fully gapped superconductors where this is sufficient at low energies, the gapless nature of the LO state also requires the inclusion of gapless fermionic excitations for a complete description of the state. While a detailed analysis of these is beyond the scope of the present paper, below we comment on a few key features of the fermionic sector of the LO state.

A. Gapless fermionic excitations in the Larkin-Ovchinnikov state near h_{c2}

As we have seen in our discussion of the Goldstone modes, there are two complementary descriptions of the FFLO states, respectively valid near h_{c2} and h_{c1}. Just below h_{c2} at the continuous FL-FFLO phase the pairing order parameter $\Delta(\mathbf{r})$ is small with a weak sinusoidal modulation, and the momentum-space description is most appropriate. The corresponding mean-field many-body wave function for, e.g., the FF state is given by Eq. (20). It is of the BCS form with a range of $\mathbf{k}$ over which the energy of the corresponding Bogoliubov quasiparticles is driven negative by the Zeeman field. These therefore form a Fermi sea with all the phenomenology associated with the gapless fermionic excitations at the Fermi surface.

For a more general FFLO state defined by a set of reciprocal lattice vectors $\mathbf{q}_n$, no exact analytical solution of the BdG Hamiltonian is available. The periodic $\Delta(\mathbf{r})$ couples all particle (atoms) and hole states connected by the reciprocal lattice $\mathbf{q}_n$, leading to an anomalous $\Delta(\mathbf{r})$-dependent band structure of Bogoliubov quasiparticles.

However, some progress can be made for a purely sinusoidal LO state with only $\pm\mathbf{q}$ reciprocal lattice vectors.

As discussed earlier a BCS-like mean-field Hamiltonian for such a state is given by

$$H^{\mathrm{LO}} = \sum_{\mathbf{k},\sigma}(\epsilon_k - \mu_\sigma)\hat{c}^\dagger_{\mathbf{k}\sigma}\hat{c}_{\mathbf{k}\sigma} + \sum_{\mathbf{k}}(\Delta^*_{\mathbf{q}}\hat{c}_{-\mathbf{k}\downarrow}\hat{c}_{\mathbf{k}+\mathbf{q}\uparrow} + \Delta^*_{-\mathbf{q}}\hat{c}_{-\mathbf{k}\downarrow}\hat{c}_{\mathbf{k}-\mathbf{q}\uparrow} + \mathrm{H.c.}). \tag{187}$$

The difference from the FF BCS Hamiltonian, analyzed exactly in Sec. II is in the appearance of both $\mathbf{q}$ and $-\mathbf{q}$ Fourier components of $\Delta(\mathbf{r})$, taken to be equal for the simplest cosine LO form. These couple each creation operator $\hat{c}^\dagger_{-\mathbf{k}\downarrow}$ to two fermionic atom annihilation operators $\hat{c}_{\mathbf{k}+\mathbf{q}\uparrow}$ and $\hat{c}_{\mathbf{k}-\mathbf{q}\uparrow}$, with each in turn coupling to another set of two operators at different $\mathbf{k}$'s, thereby generating an infinite-dimensional space that needs to be diagonalized. Focusing on the three-dimensional subspace for each $\mathbf{k}$, the Hamiltonian can be rewritten in the following Bogoliubov–de Gennes form:

$$\begin{aligned} H^{\mathrm{LO}} &= \sum_{\mathbf{k}} \hat{\Psi}^\dagger_{\mathbf{k}} \begin{pmatrix} \xi_{\mathbf{k}+\mathbf{q}\uparrow} & \Delta_{\mathbf{q}} & 0 \\ \Delta^*_{\mathbf{q}} & -\xi_{-\mathbf{k}\downarrow} & \Delta^*_{-\mathbf{q}} \\ 0 & \Delta_{-\mathbf{q}} & \xi_{\mathbf{k}-\mathbf{q}\uparrow} \end{pmatrix} \hat{\Psi}_{\mathbf{k}} + \sum_{\mathbf{k}} \xi_{-\mathbf{k}\downarrow} \\ &= \sum_{\mathbf{k}} \hat{\Psi}^\dagger_{\mathbf{k}} \hat{H}_{\mathrm{BdG}} \hat{\Psi}_{\mathbf{k}} + \sum_{\mathbf{k}} \xi_{-\mathbf{k}\downarrow}, \end{aligned} \tag{188}$$

with the three-component generalization of the Nambu spinor given by

$$\hat{\Psi}_{\mathbf{k}} \equiv \begin{pmatrix} \hat{c}_{\mathbf{k}+\mathbf{q}\uparrow} \\ \hat{c}^\dagger_{-\mathbf{k}\downarrow} \\ \hat{c}_{\mathbf{k}-\mathbf{q}\uparrow} \end{pmatrix}, \tag{189}$$

and $\hat{H}_{\mathrm{BdG}}$ the corresponding Bogoliubov–de Gennes Hamiltonian matrix. The nontrivial eigenstates encode that the excitation in the LO state is a linear combination of a hole $(-\mathbf{k},\downarrow)$, an atom $(\mathbf{k}+\mathbf{q},\uparrow)$, and an atom $(\mathbf{k}-\mathbf{q},\uparrow)$.

Although it appears that the problem reduces to a diagonalization in this three-dimensional subspace, in fact (in contrast to the single-Fourier-component FF state, where $\hat{H}_{\mathrm{BdG}}$ is block diagonal) there is a coupling between the bottom component of a spinor $\hat{\Psi}_{\mathbf{k}}$ and the top component of the spinor $\hat{\Psi}_{\mathbf{k}'=\mathbf{k}-2\mathbf{q}}$,

$$\hat{\Psi}_{\mathbf{k}-2\mathbf{q}} = \begin{pmatrix} \hat{c}_{\mathbf{k}-\mathbf{q}\uparrow} \\ \hat{c}^\dagger_{-\mathbf{k}+2\mathbf{q}\downarrow} \\ \hat{c}_{\mathbf{k}-3\mathbf{q}\uparrow} \end{pmatrix}. \tag{190}$$

This leads to the aforementioned infinite-dimensional space to diagonalize, corresponding to the band structure of the Bogoliubov quasiparticles, analogous to a system with a diagonal periodic potential.

Despite these complications, for a large enough q (such that $q^2/2m \gg \Delta_q$, well satisfied near h_{c2} where $q \approx 1/\xi$) an approximate treatment is possible because the coupling is dominated by the degenerate particle-hole states near the Fermi surface, which reduces the problem to only a *pair* of states for every value of $\mathbf{k}$. For positive (negative) $\mathbf{k}$ the pair is the top (bottom) two components of the spinor $\hat{\Psi}_{\mathbf{k}}$, leading to a Cooper pair with $\mathbf{q}$ $(-\mathbf{q})$ the center-of-mass momentum.

Diagonalizing the BdG Hamiltonian then leads to two sets of the Bogoliubov quasiparticle operators $\hat{\alpha}_{\mathbf{k}\sigma\mathbf{q}}$,$\hat{\alpha}_{\mathbf{k}\sigma-\mathbf{q}}$:

$$\hat{\alpha}_{\mathbf{k}\uparrow\mathbf{q}} \approx u_{\mathbf{k},\mathbf{q}}\hat{c}_{\mathbf{k}+\frac{\mathbf{q}}{2}\uparrow} + v_{\mathbf{k},\mathbf{q}}\hat{c}^\dagger_{-\mathbf{k}+\frac{\mathbf{q}}{2}\downarrow}, \tag{191a}$$

$$\hat{\alpha}^\dagger_{-\mathbf{k}\downarrow\mathbf{q}} \approx -v^*_{\mathbf{k},\mathbf{q}}\hat{c}_{\mathbf{k}+\frac{\mathbf{q}}{2}\uparrow} + u^*_{\mathbf{k},\mathbf{q}}\hat{c}^\dagger_{-\mathbf{k}+\frac{\mathbf{q}}{2}\downarrow}, \tag{191b}$$

$$\hat{\alpha}_{\mathbf{k}\uparrow-\mathbf{q}} \approx u_{\mathbf{k},-\mathbf{q}}\hat{c}_{\mathbf{k}-\frac{\mathbf{q}}{2}\uparrow} + v_{\mathbf{k},-\mathbf{q}}\hat{c}^\dagger_{-\mathbf{k}-\frac{\mathbf{q}}{2}\downarrow}, \tag{191c}$$

$$\hat{\alpha}^\dagger_{-\mathbf{k}\downarrow-\mathbf{q}} \approx -v^*_{\mathbf{k},-\mathbf{q}}\hat{c}_{\mathbf{k}-\frac{\mathbf{q}}{2}\uparrow} + u^*_{\mathbf{k},-\mathbf{q}}\hat{c}^\dagger_{-\mathbf{k}-\frac{\mathbf{q}}{2}\downarrow}, \tag{191d}$$

with the corresponding four branches of the excitation spectrum $E_{\mathbf{k}\sigma\mathbf{q}_i}$:

$$E_{\mathbf{k}\uparrow\mathbf{q}} \approx \left(\varepsilon_k^2 + \Delta_{\mathbf{q}}^2\right)^{1/2} - h + \frac{\mathbf{k}\cdot\mathbf{q}}{2m}, \tag{192a}$$

$$E_{\mathbf{k}\downarrow\mathbf{q}} \approx \left(\varepsilon_k^2 + \Delta_{\mathbf{q}}^2\right)^{1/2} + h - \frac{\mathbf{k}\cdot\mathbf{q}}{2m}, \tag{192b}$$

$$E_{\mathbf{k}\uparrow-\mathbf{q}} \approx \left(\varepsilon_k^2 + \Delta_{\mathbf{q}}^2\right)^{1/2} - h - \frac{\mathbf{k}\cdot\mathbf{q}}{2m}, \tag{192c}$$

$$E_{\mathbf{k}\downarrow-\mathbf{q}} \approx \left(\varepsilon_k^2 + \Delta_{\mathbf{q}}^2\right)^{1/2} + h + \frac{\mathbf{k}\cdot\mathbf{q}}{2m}, \tag{192d}$$

with $\varepsilon_k = \frac{k^2}{2m} - \mu + \frac{q^2}{8m}$ and the coherence factors u_k,v_k, approximately given by the FF expressions in Eq. (15). In the first (second) pair of equations, Eqs. (191a) and (191b) [Eqs. (191c) and (191d)], the particle-hole hybridization is via $\Delta_q e^{i\mathbf{q}\cdot\mathbf{r}}$ $(\Delta_q e^{-i\mathbf{q}\cdot\mathbf{r}})$, as for the FF state.

As demonstrated for the FF state in Sec. II it is clear from the spectra $E_{\mathbf{k}\sigma\pm\mathbf{q}}$, Eq. (192), that the LO state exhibits $\mathbf{k}$ regions of both gapped and gapless fermionic excitations, with closing of the gap driven by a combination of the Zeeman (imbalance) energy h and the Doppler shift $\mathbf{k}\cdot\mathbf{q}$. For pairing driven by $\Delta_q e^{i\mathbf{q}\cdot\mathbf{r}}$ $(\Delta_q e^{-i\mathbf{q}\cdot\mathbf{r}})$, the gapless states appear at the minimum of the $E_{\mathbf{k}\uparrow\mathbf{q}}$ $(E_{\mathbf{k}\uparrow-\mathbf{q}})$ located in a wedge $-\theta_m < \theta < \theta_m$ around $\mathbf{k} \parallel -\mathbf{q}$ $(\mathbf{k} \parallel \mathbf{q})$, where for positive h, $E_{\mathbf{k}\uparrow\mathbf{q}}$ $(E_{\mathbf{k}\uparrow-\mathbf{q}})$ is driven negative. The LO ground state thus takes the form given in Eq. (20), exhibiting Fermi pockets of Bogoliubov quasiparticles, with a Fermi surface of gapless excitations defined by $E_{\tilde{\mathbf{k}}_{\mathrm{F}}\sigma,\pm\mathbf{q}} = 0$, as illustrated in Fig. 13.

In the complementary wedge of $\mathbf{k}$ around $\mathbf{k}\cdot\mathbf{q} = 0$, i.e., running along the LO stripes given by the nodes of the LO order parameter, the superconducting gap remains finite, growing to

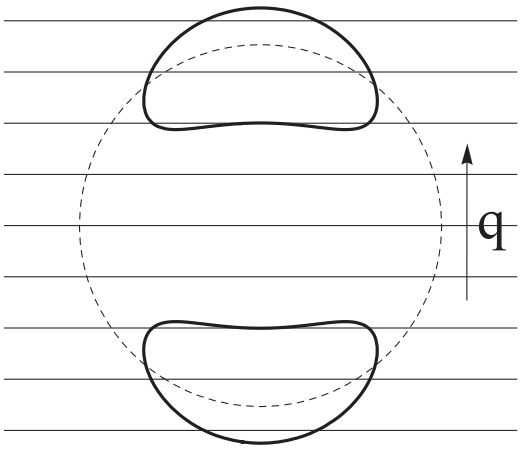

FIG. 13. An illustration of Fermi pockets (full curve) of the gapless Bogoliubov quasiparticles characteristic of the Larkin-Ovchinnikov ground state. The periodic array of domain walls in $\Delta_{\mathrm{LO}}(z)$, the associated wave vector $\mathbf{q}$, and the Fermi surface of the underlying normal state (dashed circle) are also indicated.

its maximum value $\Delta_{\mathbf{q}} - h > 0$ (suppressed by h) as

$$E_{\rm gap} \approx E_{\rm gap}^{\rm max} - \frac{qk_z}{2m} \approx E_{\rm gap}^{\rm max} - \frac{qk_{\rm F}}{2m}\sqrt{1-k_\perp^2/k_{\rm F}^2}. \quad (193)$$

The quadratic $k_\perp$ dispersion along the stripes is characterized by an enhanced effective mass $m_{\rm eff} \approx m\epsilon_{\rm F}/\Delta_{\rm BCS} \gg m$.

While above analysis gives some understanding of the LO states, it is approximate and does not address the detailed nature of more generic LO-like states. These may be understood by self-consistently diagonalizing the BdG equations in real space. An estimate of the mean-field BCS-LO and LO-FL phase boundaries requires a computation of the total energy as was done in Ref. [4] for the FF state. A complete solution for the LO state requires a numerical analysis [95–97].

B. Gapless fermionic excitations in the Larkin-Ovchinnikov state near h_{c1}

The above calculation of the LO quasiparticle spectrum near h_{c2} can be complemented by a treatment valid near h_{c1}. At low h, the LO order parameter $\Delta_{\rm LO}(z)$ is given by a periodic (period $2\pi/q$) array of $\pm\Delta_0 \approx \pm\Delta_{\rm BCS}$ domain walls of width ξ [95–98], rather than a single harmonic.

The form of the quasiparticle excitations is determined by a two-component Nambu wave function $\vec{\psi} = (\psi_\uparrow(\mathbf{x},z), \psi_\downarrow(\mathbf{x},z))$ satisfying the BdG equation

$$\begin{pmatrix} \frac{\hat{p}^2}{2m} - \epsilon_{\rm F} & \Delta(z) \\ \Delta(z) & -\frac{\hat{p}^2}{2m} + \epsilon_{\rm F} \end{pmatrix} \begin{pmatrix} \psi_\uparrow \\ \psi_\downarrow \end{pmatrix}_\alpha = E_\alpha \begin{pmatrix} \psi_\uparrow \\ \psi_\downarrow \end{pmatrix}_\alpha, \quad (194)$$

where $\hat{p} \equiv -i\nabla$ and we took the order parameter to be real (characteristic of the mean-field LO state) stripe domain walls lying in the $\mathbf{x}$ plane, with the normal along $\hat{\mathbf{z}}$, and approximated the chemical potential by a Fermi energy $\epsilon_{\rm F}$, valid deep in the BCS regime. In a matrix form, the BdG equation is given by

$$\left[\left(\frac{\hat{p}^2}{2m} - \epsilon_{\rm F}\right)\sigma_z + \Delta(z)\sigma_x\right]\vec{\psi}(\mathbf{x},z) = E\vec{\psi}(\mathbf{x},z). \quad (195)$$

For a striped LO state we can utilize translational invariance along the stripes $\mathbf{x}$, taking $\vec{\psi}(\mathbf{x},z) = \vec{\psi}_{\mathbf{k}_\perp}(z)e^{i\mathbf{k}_\perp\cdot\mathbf{x}}$, with $\vec{\psi}_{\mathbf{k}_\perp}(z)$ satisfying

$$\left[\left(\frac{\hat{p}_z^2}{2m} - \tilde{\epsilon}_{\rm F}(k_\perp)\right)\sigma_z + \Delta(z)\sigma_x\right]\vec{\psi}_{\mathbf{k}_\perp}(z) = E_{k_\perp}\vec{\psi}_{\mathbf{k}_\perp}(z), \quad (196)$$

with $\tilde{\epsilon}_{\rm F}(k_\perp) = \epsilon_{\rm F} - k_\perp^2/2m$ the effective 1D Fermi energy.

The low-energy spectrum is determined by the excitations near the Fermi energy,

$$\vec{\psi}_{\mathbf{k}_\perp}(z) \approx \vec{\phi}^+_{\mathbf{k}_\perp}(z)e^{i\tilde{k}_{\rm F}z} + \vec{\phi}^-_{\mathbf{k}_\perp}(z)\, e^{-i\tilde{k}_{\rm F}z} \quad (197)$$

with $\tilde{k}_{\rm F}^2/2m \equiv \tilde{\epsilon}_{\rm F}(k_\perp)$ and the envelope wave functions $\vec{\phi}^\pm_{\mathbf{k}_\perp}(z)$ satisfying

$$\left[\left(\pm\tilde{v}_{\rm F}\hat{p}_z + \frac{\hat{p}_z^2}{2m} - \tilde{\epsilon}_{\rm F}\right)\sigma_z + \Delta(z)\sigma_x\right]\vec{\phi}^\pm_{\mathbf{k}_\perp}(z) = E_{k_\perp}\vec{\phi}^\pm_{\mathbf{k}_\perp}(z). \quad (198)$$

For $\tilde{\epsilon}_{\rm F}(k_\perp)$ sufficiently large, so that we can linearize around the Fermi points $\pm\tilde{k}_{\rm F}$ by neglecting the quadratic correction to the dispersion, $H_{p^2} = \frac{\hat{p}_z^2}{2m}\sigma_z$, we obtain

$$[(\mp i\tilde{v}_{\rm F}\partial_z - \tilde{\epsilon}_{\rm F})\sigma_z + \Delta(z)\sigma_x]\vec{\phi}^\pm_{\mathbf{k}_\perp}(z) = E_{k_\perp}\vec{\phi}^\pm_{\mathbf{k}_\perp}(z). \quad (199)$$

For a single "$-$ to $+$" domain wall, the solution can be readily found [177,178] and exhibits two normalizable Andreev zero-energy bound states,

$$\vec{\phi}^\pm_{\mathbf{k}_\perp}(z) = A\begin{pmatrix} 1 \\ \mp i \end{pmatrix} e^{-\frac{1}{\tilde{v}_{\rm F}}\int_0^z \Delta(z')dz'} \quad (200a)$$

$$\approx \frac{1}{\sqrt{2\tilde{\xi}}}\begin{pmatrix} 1 \\ \mp i \end{pmatrix} e^{-|z|/\tilde{\xi}}, \quad (200b)$$

where $\tilde{\xi} \equiv \tilde{v}_{\rm F}/\Delta_0$ is the effective coherence length (setting the width of the bound state) and in the second line we approximated the $-$ to $+$ domain wall by a step function $\Delta(z) = \Delta_0{\rm sgn}(z)$ valid for $z \gg \tilde{\xi}$. For the opposite-sign $-$ to $+$ domain wall, $\Delta(z) = -\Delta_0{\rm sgn}(z)$, the normalizable Andreev zero modes are given by identical expressions, but with the reversed sign in front of the i in the second component of the Nambu spinor.

The minimum excitation gap is determined by the nonlinear correction to the free spectrum, the perturbation $H_{p^2} = \frac{\hat{p}_z^2}{2m}\sigma_z$, which we incorporate through a degenerate perturbation theory in the two-component degenerate subspace of Andreev zero modes, $\vec{\phi}^\pm_{\mathbf{k}_\perp}(z)$. A simple computation gives the off-diagonal matrix elements $H_\pm = \langle\vec{\phi}^+|H_{p^2}|\vec{\phi}^-\rangle \approx \frac{1}{2m\tilde{\xi}^2}$, splitting the Andreev zero modes to $E^\pm_{k_\perp} = \pm E_{k_\perp}$, with

$$E_{k_\perp} \approx \frac{1}{2m\tilde{\xi}^2} = \frac{\Delta_0^2}{4\tilde{\epsilon}_{\rm F}(k_\perp)} \quad \text{for } k_\perp^2/2m \ll \epsilon_{\rm F}, \quad (201a)$$

$$= \frac{\Delta_0^2}{4(\epsilon_{\rm F} - k_\perp^2/2m)} \approx \frac{\Delta_0^2}{4\epsilon_{\rm F}} + \left(\frac{\Delta_0}{2\epsilon_{\rm F}}\right)^2\frac{k_\perp^2}{2m}. \quad (201b)$$

The maximum of the gap can be estimated through a variational solution of Eq. (198) for the nondegenerate case of $\tilde{v}_{\rm F} = \tilde{\epsilon}_{\rm F} = 0$, giving

$$\xi_{\rm min} \approx \xi_0(\Delta_0/\epsilon_{\rm F})^{1/3}, \quad (202a)$$

$$E_{\rm gap}^{\rm max} \approx \Delta_0(\Delta_0/\epsilon_{\rm F})^{1/3} \quad (202b)$$

for the width of the state localized on the domain wall and the maximum of the gap.

For a periodic array of domain walls with period $a = 2\pi/q_0$ (the LO state), the coupling between the Andreev states localized on each domain wall splits their energy into bands separated by gaps and dispersing with $-\pi/a < k_z \leqslant \pi/a$. The eigenstate for the bottom of the band, $k_z = \tilde{k}_{\rm F}$, can be obtained by generalizing the single domain-wall zero-energy state, Eq. (200), to a periodic array $\Delta_{\rm LO}(z)$. The solution for the bottom of the Andreev band is simply a sum of two periodic arrays of states, localized on $-$ to $+$ (at $z = 0$) and on $+$ to $-$ (at $z = a/2$) domain-wall arrays, respectively,

$$\vec{\phi}^\pm_{\mathbf{k}_\perp}(z) = \frac{1}{\sqrt{4N\tilde{\xi}}}\left[\begin{pmatrix} 1 \\ \mp i \end{pmatrix} e^{-\frac{1}{\tilde{v}_{\rm F}}\int_0^z \Delta_{\rm LO}(z')dz'} + \begin{pmatrix} 1 \\ \pm i \end{pmatrix} e^{\frac{1}{\tilde{v}_{\rm F}}\int_{a/2}^z \Delta_{\rm LO}(z')dz'}\right]. \quad (203)$$

FIG. 14. Lowest-order Feynman diagram of a fermionic contribution that corrects the superfluid stiffness.

For a nonzero chemical-potential difference h (Zeeman energy) to impose the spin imbalance, the spin-up excitation spectrum (201b) simply uniformly shifts down by h. When h exceeds the minimum gap $E_{\rm gap}^{\rm min} = \Delta_0^2/4\epsilon_{\rm F}$, Eq. (201), it generically induces Fermi pockets (Fig. 13) of the Bogoliubov quasiparticles centered around $\pm\mathbf{q}$ out to $k_\perp^\pm = \pm\frac{2\epsilon_{\rm F}}{\Delta_0}\sqrt{2m(h-\Delta_0^2/4\epsilon_{\rm F})}$ [179]. As expected (from the fact that these are different regimes of the same LO phase) the spectrum outlined above is in qualitative agreement with that near h_{c2}, found in the previous section.

C. Fermion–Goldstone-mode coupling in the Larkin-Ovchinnikov state

As discussed above, the LO state is characterized by a simultaneous presence of gapless Goldstone modes (particularly soft for the fully rotationally invariant geometry of an isotropic trap) and gapless fermions. Consequently, for a complete description a coupling between these must be included (see Figs. 14–16). These can in principle be derived from the microscopic BCS Hamiltonian evaluated inside the LO state beyond a conventional mean-field treatment. Alternatively, the fermion–Goldstone-mode couplings can be simply deduced based on symmetry considerations. The leading ones include the coupling of the supercurrent and of the LO phonon to the quasiparticle current and number density, and are given by

$$H_{j_s,j} \sim \nabla\phi\cdot\psi^\dagger i\nabla\psi + \text{H.c.}, \tag{204a}$$

$$H_{j_s,n} \sim (\nabla\phi)^2\psi^\dagger\psi, \tag{204b}$$

$$H_{a\text{-}p} \sim \left(\partial_z u + \tfrac{1}{2}(\nabla u)^2\right)\psi^\dagger\psi + (\nabla u\cdot\psi^\dagger i\nabla\psi)^2 + \text{H.c.} \tag{204c}$$

Because atom number conservation is effectively "broken" in the superfluid LO state, these couplings must be supplemented by the anomalous (number-violating) operators, such as, e.g., $(\nabla\phi)^2\psi\psi + \text{H.c.}$ The effects of these interactions on the fermionic and collective bosonic (ϕ,u) spectral functions require a detailed analysis, which parallels studies of gauge fields [180–185], Goldstone modes [117], and critical modes

FIG. 15. Lowest-order Feynman diagram of a fermionic contribution that corrects the smectic compressional modulus.

FIG. 16. Lowest-order subdominant Landau-damping contribution to the superfluid stiffness coming from finite fermion density.

[186,187] coupling to electrons in gapless superconductors and metals. A preliminary analysis suggests that in the LO state these derivative couplings (enforced by the underlying gauge and spatial symmetries) only lead to a finite renormalization of the model's parameters as well as Landau-like damping of the Goldstone modes. In addition to the above symmetry-dictated couplings, the presence of gapless fermions can generate Berry's phase terms [155], which can qualitatively modify the conventional LO phonon dynamics derived in Sec. III D. We leave a detailed study of these interesting questions to future research.

IX. LARKIN-OVCHINNIKOV STATES IN A TRAP

The primary experimental application of our results is to polarized paired superfluidity in trapped degenerate atomic gases. It is thus crucial to extend our bulk analysis to take into account the effect of the trapping potential $V_t(\mathbf{r})$, which in a typical experiment is well approximated by a harmonic-oscillator potential. While a full analysis of the effect of the trap is beyond the scope of this paper, in the present section we study this problem within the well-known local density approximation (LDA). We note that several recent studies (e.g., Refs. [4,44,52,55–58,60,61]) have also addressed polarized superfluidity in a trap.

A. The local density approximation

Much like the WKB approximation, the LDA corresponds to using expressions for the bulk system, but with an effective local chemical potential $\mu(r) = \mu - V_t(r)$ in place of μ. The validity of the LDA relies on the smoothness of the trap potential, with the criterion that $V_t(r)$ varies slowly on the scale of the *longest* physical length λ (the Fermi wavelength, scattering length, effective range, etc.) in the problem, i.e., $[\lambda/V_t(r)]dV_t(r)/dr \ll 1$. Its accuracy can be equivalently controlled by a small parameter that is the ratio of the single-particle trap level spacing δE to the smallest characteristic energy E_c of the studied phenomenon (e.g, the chemical potential, condensation energy, etc.), by requiring $\delta E/E_c \ll 1$. Within the LO state the longest length is clearly the LO period $a = 2\pi/q_0$, which near h_{c2} is bounded by the coherence length (this near unitarity can be as short as the interatomic spacing $\sim R/N^{1/3}$, where R is the trapped condensate radius and N is the total number of atoms), and thus $\ll R$. Thus, in this regime, away from h_{c1} (where for a continuous BCS-LO transition the period a is expected to diverge) the effects of the trap can be safely treated within the LDA.

The generalization of the model of an imbalanced resonant Fermi gas to a trap is straightforward:

$$H = \int d^3r \left(\hat{\psi}_\sigma^\dagger \frac{-\nabla^2}{2m} \hat{\psi}_\sigma + [V_t(\mathbf{r}) - \mu_\sigma(\mathbf{r})] \hat{\psi}_\sigma^\dagger \hat{\psi}_\sigma + g \hat{\psi}_\uparrow^\dagger \hat{\psi}_\downarrow^\dagger \hat{\psi}_\downarrow \hat{\psi}_\uparrow \right), \tag{205}$$

where $\hat{\psi}_\sigma(\mathbf{r})$ is a fermionic field operator with a Fourier transform $\hat{c}_{\mathbf{k}\sigma}$. Henceforth, to be concrete, we shall focus on an isotropic harmonic trap (although this simplification can easily be relaxed) with

$$V_t(\mathbf{r}) = \frac{1}{2} m \omega_t^2 r^2 \tag{206a}$$

$$\equiv \mu \frac{r^2}{R^2}, \tag{206b}$$

the latter expression defining the cloud size R. Within the LDA [valid for a sufficiently smooth trap potential $V_t(r)$; see above], locally the system is taken to be well approximated as *uniform*, but with a local chemical potential given by

$$\mu(r) \equiv \mu - \frac{1}{2} m \omega_t^2 r^2 \tag{207a}$$

$$= \mu \left(1 - \frac{r^2}{R^2} \right), \tag{207b}$$

where the constant μ is the true chemical potential (a Lagrange multiplier) enforcing the total atom number N. The spatially varying spin-up and spin-down local chemical potentials are then

$$\mu_\uparrow(r) = \mu(r) + h, \tag{208a}$$

$$\mu_\downarrow(r) = \mu(r) - h, \tag{208b}$$

with the chemical-potential difference h *uniform*.

Consequently, within the LDA the system's energy density is approximated by that of a uniform system, (17), with the spatial dependence (via the trap) entering only through $\mu(r)$. The ground-state energy is then simply a volume integral of this loacal energy density. Thus, the phase behavior of a uniform system as a function of chemical potential μ translates into a spatial cloud profile through $\mu(r)$, with the critical phase boundaries μ_c corresponding to critical radii defined by $\mu_c = \mu(r_c, h)$ [4,44]. As first predicted in [44], this leads to a shell-like cloud structure that has subsequently been observed experimentally [34–37].

Within the LDA, we can furthermore deduce the effects of the trap on the structure of the LO state. We turn to this analysis next.

B. Trap-induced elastic distortion

As discussed earlier, the Larkin-Ovchinnikov state breaks translational symmetry and like other crystals thereby exhibits a rigidity to stress. Confinement in a trap induces a variation in the chemical potential that (as observed experimentally in the BCS superfluid [34–37]) has the effect of expelling the imbalance (polarization) to the edge of the cloud (see Fig. 17). Since in the LO state the BCS order parameter domain walls "carry" the imbalance (the imbalanced fermions are confined to domain walls in $\Delta_{\mathrm{LO}}(z)$, where their cost is minimum), in the LO state the increased imbalance is accommodated by

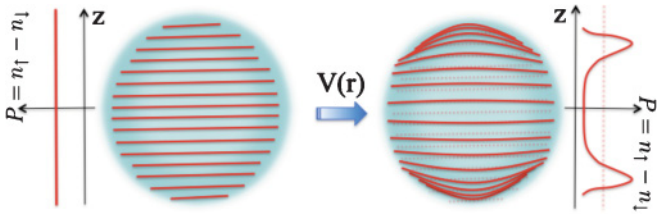

FIG. 17. (Color online) The collinear Larkin-Ovchinnikov state, compressed by an isotropic trap, $V_t(r)$ (on the right), showing the enhanced imbalance ($P \sim -\partial_z u$) confined to the edge of the trap.

the increase in the density of domain walls. Thus, the trap confinement introduces an effective longitudinal stress that acts to compress the LO state [increase its local wave vector $q_0(r)$], where the chemical potential is reduced. This tendency is captured by introducing a local longitudinal stress $\sigma(r)$ into the LO phonon Hamiltonian,

$$H_u^0 = \int dz d^2 r_\perp \left[\frac{B}{2} (\partial_z u)^2 + \frac{K}{2} (\nabla_\perp^2 u)^2 - \sigma(r) \partial_z u \right]. \tag{209}$$

This trap-phonon coupling arises by repeating our derivation in Secs. II and III with the trap potential $V_t(r)$, treating it within the LDA. The effective local chemical potential $\mu(r)$ enters through many contributions, but the leading-order effect comes from a position-dependent wave vector generalization of Eq. (25),

$$q_0(r) = 2\alpha \frac{h}{v_{\mathrm{F}}(r)} \tag{210a}$$

$$= q_0 [1 - V_t(r)/\mu]^{-1/2} \tag{210b}$$

$$\approx q_0 \left(1 + \frac{V_t(r)}{2\mu} \right). \tag{210c}$$

Here, consistent with the LDA applicability, we utilized the $V_t(r)/\mu \ll 1$ limit. Since $\delta q_0/q_0 \approx -\partial_z u \approx -\sigma/B$, we deduce that the local stress is given by

$$\sigma(r) \approx -\frac{1}{2} \frac{B}{n_0 \mu} n(r) V_t(r) \tag{211a}$$

$$\approx -\sigma_0 \frac{r^2}{R^2} \left(1 - \frac{r^2}{R^2} \right), \tag{211b}$$

where $\sigma_0 = B/2$ is the trap-induced stress scale, and we inserted an additional factor of $n(r)/n_0$ to crudely account for the breakdown of LDA-based analysis near the cloud edge, where the atom density $n(r)$ vanishes at R. As expected on physical grounds, $\sigma(r)$ is a function that vanishes at the trap center and is peaked on its outer shell set by R (Fig. 18). With this, the distortion $u_0(\mathbf{r})$ is given by a standard form:

$$u(\mathbf{r}) = \int d^3 r' G_z(\mathbf{r} - \mathbf{r}') \sigma(r'), \tag{212}$$

in terms of a Green's function $G_z(\mathbf{r}) = \partial_z G(\mathbf{r})$ that is a derivative of the smectic Green's function, with

$$G_z(\mathbf{r}) = \int \frac{d^3 q}{(2\pi)^3} \frac{i q_z e^{i \mathbf{q} \cdot \mathbf{r}}}{K q_\perp^4 + B q_z^2} \tag{213a}$$

$$= \frac{-1}{8\pi B \lambda |z|} e^{-\frac{r_\perp^2}{4\lambda |z|}}. \tag{213b}$$

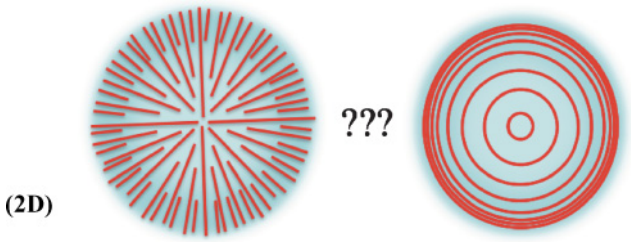

FIG. 18. (Color online) Possible alternative forms of the LO state confined in a *tight* isotropic trap. The form on the right trades off the cost of the curvature energy for the dislocation energy.

From this the trap-induced imbalance distortion, $\delta P(\mathbf{r})$ is straightforwardly computed:

$$\delta P(\mathbf{r}) \approx -P\partial_z u(\mathbf{r}) \tag{214a}$$

$$= P\int_{\mathbf{r}'} \partial_z G_z(\mathbf{r}-\mathbf{r}')\sigma(r') \tag{214b}$$

$$\approx \frac{P}{\mu n_0} n(r)V_t(r) \approx P\frac{r^2}{R^2}\left(1-\frac{r^2}{R^2}\right), \tag{214c}$$

with the final unnecessary crude approximation by construction of $\sigma(r)$ and its coupling to u recovering the expected result.

C. Trap-induced LO 3D-2D dimensional crossover

A microscopically accurate account of the trap inside the LO state, and in particular its coupling to the Goldstone modes with appropriate boundary conditions (beyond the crude treatment above) is not currently available. Perhaps a numerical analysis (e.g., numerical solution of the BdG equations or full quantum Monte Carlo simulation) [52,56,70] can provide the desired description.

However, lacking such first-principles analysis, we are constrained to proceed phenomenologically, working directly with the effective Goldstone-mode theory of u. Expanding the LO state about the trap-distorted state $u_0(\mathbf{r})$ discussed above, the distortion $\delta u(\mathbf{r})$ is again governed by the smectic Hamiltonian (142b). Although some of the effects of the trap will enter through the position-dependent elastic moduli $B(r), K(r)$, we expect that the leading effects of the trap are incorporated through the physically motivated boundary conditions on $u(r)$. Because atom density vanishes at the edge of the cloud, the LO inner shell is expected to be surrounded by an outer shell of a fully polarized normal cloud lacking any positional order. Thus, we expect the Neumann boundary condition,

$$\hat{n}_t \cdot \nabla u = 0 \tag{215}$$

($\hat{n}_t$ is the unit normal to the cloud's boundary), to be the most appropriate to supplement the Euler-Lagrange equation for $u(\mathbf{r})$. However, the appearance of a fourth derivative along $\mathbf{r}_\perp$, Eq. (142b), requires that this boundary condition be supplemented by additional ones on the domain-wall normal $\nabla_\perp u$.

Given the cylindrical form of smectic elasticity, Eq. (142b), analytical implementation of such spherically symmetric boundary conditions is quite challenging. However, because our goal here is more modest, a qualitative understanding of the trap-induced dimensional crossover can be obtained by simply using the cloud size scale R to cut off long scales appearing in a bulk analysis. Technically, our analysis amounts to instead working with periodic boundary conditions and a cylindrical trap. The calculational convenience of such boundary conditions is that they do not modify the form of the eigenmodes (still Fourier modes), and enter only through a restriction on the allowed eigenvalues $q_z = 2\pi n_z/L_z, q_\perp = 2\pi n_\perp/L_\perp$, with $n_{z,\perp} \in \mathbb{Z}$. Thus, length scales associated with the trap and finite cloud size, $L_z, L_\perp$, crudely enter through the minimum allowed momentum eigenvalues (roughly set by the cloud size $R_{z,\perp}$) and thereby capture the spatial extent of the lowest phonon eigenmode even for correct boundary conditions.

A key observation that emerges from such treatment is that because of the "infinite" anisotropy of the bulk smectic modes in Eq. (142b), with $z \sim r_\perp^2/\lambda$ (or equivalently $q_z \sim \lambda q_\perp^2$), the dimensional crossover is *qualitatively* different from that in systems with more conventional, scalingwise isotropic elasticity. That is, examining the smectic bulk propagator $G_q = 1/(Bq_z^2 + Kq_\perp^4)$, it is clear that unless $L_z \approx L_\perp^2/\lambda \gg L_\perp$, the phonon fluctuations will not be controlled by bulk modes. That is, as illustrated in Fig. 19, for any reasonably shaped trap (even a quite anisotropic one, other than an extremely anisotropic trap with $L_z \approx L_\perp^2/\lambda$), fluctuations will be controlled by the $(d-1)$-dimensional "zero" modes $u_0(\mathbf{r}_\perp)$, which are uniform along the z axis, representing compression-free LO undulations. Indeed this is allowed because of the expected Neumann boundary condition on $u(z,\mathbf{r}_\perp)$, which allows a zero-energy-cost rigid displacement along z of the LO domain walls.

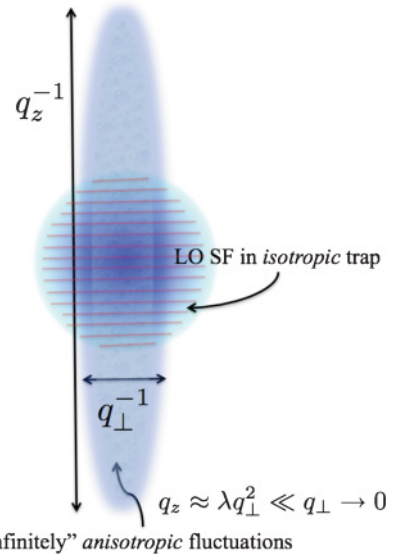

FIG. 19. (Color online) Illustration of the $q_z = 0$ (z-independent) phonon modes, even in an isotropic trap (indicated by a blue circle) dominating over the (scalingwise) anisotropic $q_z \sim \lambda q_\perp^2$ bulk smectic modes (indicated by an ellipse).

To demonstrate this expectation, we account for these zero modes by using a generalized mode expansion of $u(\mathbf{r})$ that explicitly includes the z-independent modes:

$$u(\mathbf{r}) = \frac{1}{L_z L_\perp^2}\left[\sum_{q_z,\mathbf{q}_\perp} u(q_z,\mathbf{q}_\perp)e^{i\mathbf{q}\cdot\mathbf{r}} + \sum_{\mathbf{q}_\perp} u^0(\mathbf{q}_\perp)e^{i\mathbf{q}_\perp\cdot\mathbf{r}_\perp}\right]. \tag{216}$$

In terms of these the Hamiltonian becomes

$$H_u^0 = \frac{1}{2L_z L_\perp^2}\sum_{q_z,\mathbf{q}_\perp}\left[\left(Bq_z^2 + Kq_\perp^4\right)|u_{\mathbf{q}}|^2 + K\delta_{q_z,0}q_\perp^4\left|u^0_{\mathbf{q}_\perp}\right|^2\right], \tag{217}$$

and can be used to calculate smectic phonon fluctuations. For example, using H_u^0 and equipartition, local root-mean-squared (rms) fluctuations are given by

$$\langle u^2(\mathbf{r})\rangle = \frac{1}{L_z L_\perp^2}\sum_{q_z,\mathbf{q}_\perp}\frac{T}{Bq_z^2 + Kq_\perp^4} + \frac{1}{L_z L_\perp^2}\sum_{\mathbf{q}_\perp}\frac{T}{Kq_\perp^4} \tag{218a}$$

$$= \int_{q_z,\mathbf{q}_\perp}\frac{T}{Bq_z^2 + Kq_\perp^4} + \frac{1}{L_z}\int_{\mathbf{q}_\perp}\frac{T}{Kq_\perp^4} \tag{218b}$$

$$\approx \frac{T}{4\pi\sqrt{BK}}\ln(\sqrt{L_z\lambda}/a) + \frac{T}{8\pi^3 K}\frac{L_\perp^2}{L_z} \tag{218c}$$

$$\approx \frac{T}{8\pi^3 K}\frac{L_\perp^2}{L_z} \quad \text{for } L_z < L_\perp^2/\lambda, \tag{218d}$$

where in the second line we approximated mode sums by integrals in a standard way. Indeed as summarized by (218d), by comparing the two (bulk and zero-mode) contributions to $u^2_{\rm rms}$, as anticipated on general grounds above it is clear that for isotropic (and even highly anisotropic) traps, the zero-mode second contribution dominates as long as $L_z < L_\perp^2/\lambda$.

Applying this to a spherically symmetric trap with $L_z \sim L_\perp \approx R \ll R^2/\lambda$, we conclude that indeed fluctuations are controlled by the zero-mode LO phonons. We thus conclude that all the *correlation-function* properties of the LO state will be even more anomalous, characterized by a $(d-1)$-dimensional zero-mode action that at a harmonic level is given by

$$S_u^0 = \int_0^\beta d\tau d^{d-1}r_\perp\left[\frac{\kappa}{2}(\partial_\tau u_0)^2 + \frac{K}{2}(\nabla_\perp^2 u_0)^2\right]. \tag{219}$$

More detailed implication of these observations, particularly in contexts of specific experimental geometries, remain to be explored. We hasten to add, however, that by equipartition, the finite-temperature LO *thermodynamics* will nevertheless be dominated by bulk modes, simply due to their bulk-to-surface dominance.

X. EXPERIMENTAL IMPLICATIONS

There are a large number of experimentally observable effects that emerge from our study. A comprehensive treatment of these requires further extensive studies, which lie outside the scope of the present paper. Here we simply sketch out a few of the most important experimental signatures of our predictions.

A. Larkin-Ovchinnikov order parameter

As discussed in the Introduction and in Sec. V, at finite temperature in the thermodynamic limit (see below for the discussion in the trap) the *isotropically* trapped Larkin-Ovchinnikov phase is characterized by a *vanishing* average LO order parameter, i.e., $\langle\Delta_{\rm LO}\rangle = 0$. Reminiscent of 2D superfluids and crystals [130,141], this is a reflection of its enhanced thermal fluctuations. As with these well-known examples and other topological phases, this does not however imply that the state is unstable (at least not in 3D), but that it requires a finer characterization (e.g., correlation functions, topological defects, etc.) beyond a simple Landau order parameter. One of the experimental implications is that, consequently, the leading nonzero Landau order parameter characterizing the LO state is the translationally invariant charge-4 (four-atom pairing) superconducting order parameter $\Delta_{\rm sc}$, introduced in Eq. (70a). Thus, in the presence of thermal fluctuations the LO phase corresponds to an exotic state in which the off-diagonal order is exhibited by pairs of Cooper pairs, i.e., a bound quartet of atoms, rather than by the conventional two-atom Cooper pairs [119]. In 2D and 3D this higher-order pairing is driven by arbitrary low-T fluctuation, rather than by a fine-tuned attractive interaction between Cooper pairs, and therefore akin to 2D superfluids and crystals has no mean-field description. While a direct experimental probe of $\Delta_{\rm sc}$ may be challenging, enhanced fluctuations in the LO state can be directly observed through correlation functions, to which we turn next.

B. Momentum distribution function

Probably the most striking signature of the LO state is the interesting form of the Cooper-pair momentum distribution function $n_{\mathbf{k}} = \langle\Delta_{\mathbf{k}}^\dagger\Delta_{\mathbf{k}}\rangle$. As for a conventional resonantly paired superfluid, $n_{\mathbf{k}}$ should be accessible by a detuning sweep (controlled by a magnetic field) that projects the finite-momentum LO Cooper pairs $\Delta_{\mathbf{k}}$ on the BCS side onto tightly bound molecules on the BEC side of the Feshbach resonance [7], and then observed through a standard time-of flight imaging of the resulting molecular condensate. In contrast to conventional bosonic and BCS condensates (that in a trap display a single peak, associated with a condensation into a lowest trap state, or its interaction-swelled equivalent), the LO condensate is expected to display a *spontaneous* reciprocal lattice of condensate peaks associated with its periodic structure, Fig. 20.

While in mean-field approximation $n_{\mathbf{k}}$ is predicted [4,44,53,112] to resemble a superfluid in an optical periodic potential [1,188], the spontaneous nature of its translational and orientational symmetry breaking, in the presence of thermal fluctuations, leads to important qualitative distinctions. Although the full anisotropic form is quite complex and best evaluated numerically, the asymptotic form of $n_{\mathbf{k}}^{\rm LO}$ can be readily obtained analytically. As calculated in Sec. V, $n_{\mathbf{k}}^{\rm LO}$ exhibit power-law (algebraic) peaks around harmonics $\mathbf{q}_n$ of the ordering wave vector $\mathbf{q}_0$, replacing the mean-field δ-function Bragg peaks of bosons in a periodic potential [1,188]:

$$n_{\mathbf{k}}^{\rm LO} \approx \sum_{q_n\neq 0}\frac{n_{q_n}}{|k_z - nq_0|^{2-n^2\eta}} \quad \text{for } d = 3, \tag{220}$$

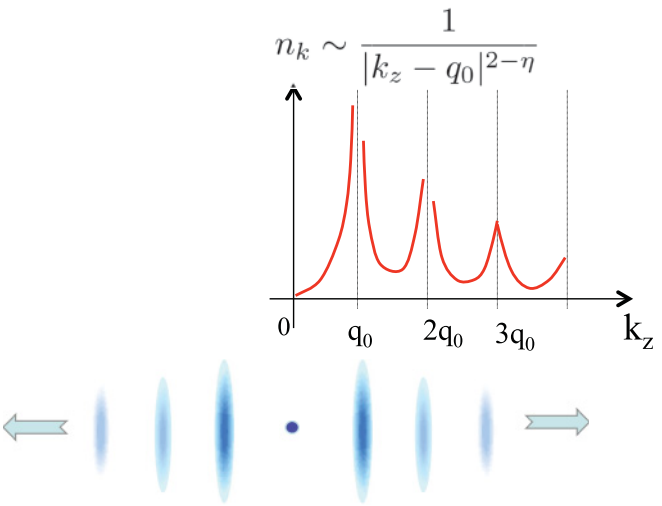

FIG. 20. (Color online) The finite momentum pairing at q_0 and divergent 3D smectic phonon fluctuations in the LO state are predicted to be reflected in the Cooper-pair center-of-mass momentum distribution function $n_{\mathbf{k}}$, displaying power-law Bragg peaks, characteristic of the spatial quasi-long-range order. We expect these to be observable through time-of-flight measurements.

where for simplicity we specialized to $\mathbf{k} = k_z\hat{\mathbf{z}}$, the form factor n_{q_n} is given after Eq. (124), and $\eta = q_0^2 T/(8\pi\sqrt{BK})$. This form is reminiscent of (1 + 1)D Luttinger liquids and two-dimensional crystals [136–138,141], and is a reflection of the quasi-long-range order of the nonzero-temperature 3D LO state. While physically quite distinct, $n_{\mathbf{k}}^{\mathrm{LO}}$ is mathematically closely related to the structure function of a conventional smectic [129,134]. Another feature of $n_{\mathbf{k}}^{\mathrm{LO}}$ is the absence of the $k = 0$ condensate peak, which qualitatively distinguishes the LO state from a supersolid [87–90], where crystalline and superfluid orders merely independently coexist. We expect these features to be the smoking gun for the LO state, in principle observable in time-of-flight imaging.

C. Structure function

The density-density correlations, conventionally measured in the reciprocal space using x-ray or neutron scattering, are other important quantities that can be experimentally probed. The simplest is the static structure function, which, using $\rho(\mathbf{r}) \approx |\Delta_{\mathrm{LO}}(\mathbf{r})|^2$, is straightforwardly computed (see Sec. V):

$$S^{\mathrm{LO}}(\mathbf{q}) = \langle \rho_{-\mathbf{q}}\rho_{\mathbf{q}}\rangle \tag{221a}$$

$$\approx \sum_{q_n} \frac{A_{2q_n}}{|q_z - 2nq_0|^{2-4n^2\eta}}, \tag{221b}$$

where for simplicity we evaluated it at $\mathbf{q} = q_z\hat{\mathbf{z}}$, and A_{2q_n} is a form factor. $S^{\mathrm{LO}}(\mathbf{q})$ contrasts with $n_{\mathbf{k}}^{\mathrm{LO}}$ by its insensitivity to the off-diagonal (i.e., superfluid) order. In three dimensions it also displays quasi-Bragg peaks, but at twice the reciprocal lattice vectors, $2nq_0$, with the $4n^2\eta$ fluctuation exponent, and just like conventional smectics [129,130,135] (unlike $n_{\mathbf{k}}^{\mathrm{LO}}$) does exhibit the $q_{n=0} = 0$ peak (see Fig. 21).

After a projection onto the molecular BEC state, a density profile $\rho(\mathbf{r})$ for a large atomic cloud should be measurable *in situ*. Computing a Fourier transform of its correlations

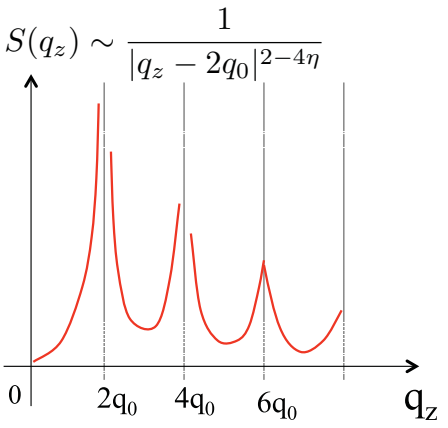

FIG. 21. (Color online) The structure function $S(\mathbf{q})$ for the 3D LO state, displaying power-law (as opposed to δ-function) Bragg peaks, characteristic of the LO superfluid's spatial quasi-long-range order.

then allows one to test $S_{\mathbf{q}}^{\mathrm{LO}}$, above. In this way, in principle the dynamic structure function $S_{\mathbf{q},\omega}$ (a Fourier transform of the two-time density correlation function) should also be accessible.

Alternatively, the dynamic structure function can be directly measured using Bragg spectroscopy [157–159], with its static limit obtained by integrating over frequencies. Based on successful measurements of the Bogoliubov mode in bosonic condensates [158,159], we expect that the peaks in $S_{\mathbf{q},\omega}^{\mathrm{LO}}$ (associated with its poles) can be used to give the dispersion of the collective modes, the superfluid phase ϕ, and LO phonon u,

$$\omega_\phi(\mathbf{k}) = \sqrt{\left(\rho_s^\perp k_\perp^2 + \rho_s^\parallel k_z^2\right)/\chi_0}, \tag{222a}$$

$$\omega_u(\mathbf{k}) = \sqrt{\left(Kk_\perp^4 + Bk_z^2\right)/\chi_0}, \tag{222b}$$

with the corresponding lifetimes remaining to be determined.

Related to the dynamic structure function is the generalized density and polarization (spin-imbalance) response function to a periodic potential. The periodic nature of the LO state makes it possible to use a perturbation at half the wavelength of the LO state to resonantly excite long-scale collective modes, such as the polarization-dipole mode, which can be readily detected in a trapped gas. This was proposed and carefully investigated for a 1D LO state in Ref. [189] and should also apply in the two- and three-dimensional cases considered here. We leave the analysis of these and related experiments to a future more detailed study.

D. Trap effects

As is clear from the discussion in Sec. IX a detailed study of the effects of the trap is essential for an explicit contact with experiments. By introducing system boundaries, a trap modifies the structure of and fluctuations in the LO state, which, away from h_{c1} (where the LO period can potentially diverge [96,102]), can be treated within the LDA.

1. Fluctuations

The detailed phenomenology of the LO state in a trap depends on the nature of the boundary conditions, which still remain to be understood. However, for large atomic clouds with small surface-to-volume ratio, the boundary effects are expected to be a weak perturbation to the bulk. As discussed in Sec. IX, in this case its effects can be taken into account phenomenologically in the spirit of the finite-size scaling of critical phenomena [130,164] by introducing a long-scale cutoff (set by the cloud size R) into our bulk quantities. For observables related to the soft LO phonon u, which is strongly affected by fluctuations, this introduces an experimentally observable sensitivity to the cloud size R and by extension to the atom number N, trapping frequency ω_t, and explicit trap anisotropy $\omega_t^{\perp}/\omega_t^{\parallel}$.

Referring to the analysis of Secs. V and IX, which give phonon rms fluctuations for a gas in a "box" of size $L_\perp \times L_z$, we conclude that in an isotropic trap with cloud size $R \sim L_\perp = L_z$, the phonon fluctuations are large but finite, in 3D given by

$$u_{\rm rms}^2 \approx \frac{T}{8\pi^3 K} R + \frac{T}{4\pi\sqrt{BK}} \ln R/a, \qquad (223)$$

where we approximated the phonons by Gaussian fluctuations, neglecting the weak nonlinear elastic effects of Sec. V B 2 [that can become important on scales $R > \xi_{\perp,z}^{\rm NL}$, (128)], and assumed Neumann boundary conditions that allow for the $q_z = 0$ zero modes. The crossover from the bulk to the zero-mode-dominated regimes takes place for a cloud size $R \gtrsim R_* = \sqrt{K/B} \ln \sqrt{K/Ba^2}$.

One consequence of this result is that in a trap the thermally averaged LO order parameter $\langle \Delta_{\rm LO}(\mathbf{r})\rangle^T = 2\tilde{\Delta}_{q_0}(R)\cos\left(\mathbf{q}_0\cdot\mathbf{r}\right)$ no longer vanishes (as it does in an infinite bulk system), but strongly depends on the cloud size. For Neumann boundary conditions, its thermally suppressed amplitude in 3D is given by

$$\tilde{\Delta}_{q_0}(R) \approx \Delta_{q_0} e^{-\frac{1}{2}T/(\xi_0\sqrt{\rho_s^{\perp}\rho_s^{\parallel}})} e^{-R/R_0} \left(\frac{a}{R}\right)^{\eta/2}, \qquad (224)$$

with $R_0 \approx q_0^2 T/K$ the scale beyond which the zero modes become particularly important. Thus through $R(N,\omega_t)$ the order-parameter amplitude is also exponentially sensitive to the atom number N and trap frequency ω_t. We note that the exponential dependence on R is a consequence of the dominance of the $q_z = 0$ zero modes (under Neumann boundary conditions on u) over the anisotropic smectic bulk modes in an isotropic trap. In contrast, under Dirichlet boundary conditions that exclude these zero modes, the exponential factor is suppressed, and the LO amplitude is a weaker power-law function of the cloud size, reminiscent of 2D XY systems, such as a superfluid confined to two dimensions. We note that Kosterlitz-Thouless phase fluctuation physics has been reported in 2D trapped atomic superfluids [190,191], despite the finite trap size. We therefore expect our predictions for strong fluctuation effects in the LO phase to also be experimentally accessible.

Finally we note that given our prediction that generically the LO state is sandwiched by its descendants' phases (SF_N, FL_{Sm}, FL_N, FL^*, etc, rather than a simple vacuum) the analysis and implementation of boundary conditions for a trap are further significantly complicated, particularly near h_{c1}.

2. Phase diagram through shell structure

As discussed and analyzed in Sec. IX, an even stronger effect of the trap is that it leads to an effective locally varying chemical potential $\mu(r) = \mu(1 - r^2/R^2)$, and therefore gives slices through the chemical-potential phase diagram as a function of radius r. We thus expect that the phase diagram in Fig. 4 can be "imaged" in the spatial cloud profile, with critical phase boundaries $\mu_c^{(i)}$ (to phase i) translating to critical radii of shells defined by $\mu_c^{(i)} = \mu(r_c^{(i)},h)$. Given the past success of such phase detection with bosons in optical potentials (exhibiting "wedding cake" profiles) [1], and the uniformly paired superfluids and Fermi liquids of an imbalanced Fermi gas [2,34,35,37], we expect that similar identification will be possible for some of the LO liquid-crystal phases.

E. Response to rotation

Consistent with its neutral superfluid order, above a critical rate of rotation Ω_{c1} a FFLO state responds to an imposed rotation by nucleating quantized vortices. Because of its crystalline superfluid form, even within a mean-field description its vortices are predicted to form a rich variety of vortex lattices [192–194], which depend on the nature of the "host" FFLO state.

We predict a number of additional interesting vortex features that are special to strongly fluctuating LO states. One distinguishing feature of the smectic LO state studied here is its uniaxial anisotropy, which is strongly tunable with species imbalance. It manifests itself in the (quantitative) anisotropy of the superfluid densities (stiffnesses) $\rho_s^{\perp} \ll \rho_s^{\parallel}$, Eq. (82), and the *qualitatively* anisotropic dispersion of the LO phonon, Eq. (89). The former leads to vortices with spontaneously elliptical vortex cores, (158), which we expect to form a centered rectangular lattice for vortices (rotation axis) oriented transversely to $\mathbf{q}_0$. This striking feature should be easily identifiable in rotation experiments of the type previously used to identify phase separation in imbalanced Fermi gases [2,34]. In this transverse geometry we also expect vortices to be pinned to LO phase fronts, localized in zeros of domain walls in $\Delta_{\rm LO}(\mathbf{r})$, akin to vortices in layered superconductors, e.g., BISCCO [195]. In contrast, for rotation about an axis along $\mathbf{q}_0$, a conventional hexagonal vortex lattice is expected.

Another striking feature of the LO state found in Sec. VI is the π-vortex bound to a half-$a/2$ dislocation, with $1/4$ the energy cost (in the thermodynamic limit) of a conventional 2π-vortex. We therefore predict that it is this fractional vortex that will be preferentially induced by the rotation. One experimental consequence of this is the reduction in the lower critical frequency Ω_{c1} down to $1/2$ of the conventional value $\frac{\hbar}{2mR^2}\ln R/\xi$ in a large cloud of radius R. Concomitantly, in addition to its imbalance-tunable anisotropy (which diverges near the upper, h_{c2}, phase boundary), the vortex lattice is characterized by a vortex density $n_v = \frac{4m\Omega}{\pi\hbar}$, which is increased by a factor of 2 from the conventional value of a rotated paired superfluid. Perhaps the most striking feature that we predict is that a rotation-induced lattice of half dislocations must accompany and be locked to this π-vortex lattice. We

expect these features to be most pronounced for a rotation axis transverse to $\mathbf{q}_0$, with a more conventional rotational response for $\Omega \parallel \mathbf{q}_0$. Finally, the LO state may exhibit more than one critical rotational velocity Ω_{ci} corresponding to distinct onsets of the penetration of half-integer and integer vortices.

F. Fermionic excitations

As we have seen above, in addition to the low-energy Goldstone modes ϕ, u, the LO state is characterized by gapless fermionic excitations associated with the imbalanced atom, which are localized on zeros of domain walls in $\Delta_{\mathrm{LO}}(\mathbf{r})$. The most direct probe of these midgap fermionic states is through the Feshbach resonance [196] and rf spectroscopies [149,197–200], with the momentum-resolved extension [201, 202], allowing one to measure the dispersion and Fermi surface pockets of the Andreev states calculated in Sec. VIII. An observation of coexisting gapped and (Andreev) gapless features in these spectroscopies, along with the superfluid phase coherence in $n_{\mathbf{k}}$, would provide strong evidence for realization of a FFLO state.

Such measurements can be complemented with shot-noise correlation spectroscopy [203], which has been successfully used to probe bosonic Mott insulators [1] and fermionic paired condensates [204]. In the LO state, we expect pairing shot-noise correlations to be peaked for $-\mathbf{k}_{\mathrm{F}} + \mathbf{q}_0/2,\downarrow \longleftrightarrow \mathbf{k}_{\mathrm{F}} + \mathbf{q}_0/2,\uparrow$ and $\mathbf{k}_{\mathrm{F}} - \mathbf{q}_0/2,\downarrow \longleftrightarrow -\mathbf{k}_{\mathrm{F}} - \mathbf{q}_0/2,\uparrow$ atom pairs. In contrast to a conventionally paired BCS state, shot-noise correlations are furthermore anisotropically distributed in the center-of-mass pair momentum, with peaks around $\pm\mathbf{q}_0$, reflecting the spontaneous nematic anisotropy of the LO state.

The low-energy excitations in the LO state can also be probed less directly through thermodynamics, modifying the power-law-in-T behavior of, for example, the heat capacity. They will also manifest themselves in thermal transport, although its experimental implementation in the context of trapped atomic gases remains an open problem.

Probably the most direct way to detect the existence of the LO state is to simply image the population species imbalance. Because imbalanced fermions are confined to Andreev states localized on the LO domain walls, the polarization density is periodic, with its phase locked to that of $\Delta_{\mathrm{LO}}(\mathbf{r})$. As illustrated for the thermally averaged LO order parameter, in a trap the amplitude of this periodic component of polarization will be nonzero and strongly R dependent.

Quite clearly, significant detailed theoretical analysis is necessary beyond this qualitative discussion, but is left for future research.

G. Phase transitions and unusual phases

In addition to our findings of the rich fluctuation-driven phenomenology of the LO (superfluid smectic) state, in Sec. VII we predicted a variety of putative descendant phases, that emerge when the LO state is disordered through a set of continuous phase transitions. If indeed realized as stable phases (something that our phenomenological approach is unable to determine) organized into the phase diagram in Fig. 4, then many of the predicted features should be readily detectable in experiments on imbalanced resonant Fermi gases. Each of these states (SF_N, FL_N, $\mathrm{FL}_{\mathrm{Sm}}$, etc.) exhibits its own qualitatively distinct phenomenology, discussed in Sec. VII, where they were defined. For example, Bragg peaks in the time-of-flight images can distinguish the periodic $\mathrm{SF}_{\mathrm{Sm}}$ (LO superfluid smectic) state from the homogeneous SF_N^4 (superfluid nematic), which are in turn distinguished from the $\mathrm{FL}_{\mathrm{Sm}}^{2q}$ and FL_N states (normal smectic and nematic) by their superfluid properties, broken spatial symmetries (periodicity and anisotropy), collective modes, quantized vortices, and condensate peaks. Standard thermodynamic signatures (e.g., heat capacity) will identify the corresponding phase transitions, though some of strongly non-mean-field topological type between two gapped (disordered) phases (e.g., FL^* and FL) may be more difficult to detect. In a trap (see above), the most vivid manifestation of these states is the appearance of a shell structure, corresponding to slices through the chemical grand-canonical phase diagram of an imbalanced resonant Fermi gas, Fig. 4. Again, we leave the detailed analyses of all these features to extended future studies.

XI. OPEN QUESTIONS

While this paper addresses a broad range of phenomena associated with the Larkin-Ovchinnikov state, it leaves many interesting questions open. Certainly the most important of these is the long-standing question of the range of energetic stability of the crystalline superconductor discussed in the Introduction. If the state is indeed stable over a sufficiently broad range of detuning and imbalance to be experimentally accessible, is its lowest-energy form indeed the striped collinear LO type, assumed throughout this paper? While for large atomic clouds and shallow traps (such that the LDA remains valid), we expect only a small deformation of the LO state near the boundaries of the phase, for tighter traps a more detailed treatment of the trap is necessary, and may lead to a distinct global form of the LO state, such as the "onion" and "radial" structures illustrated in Fig. 18. To address such questions undoubtedly requires numerical solutions in experiment-specific geometries.

Furthermore, the nature of the (2D and 3D) transition into the LO state at the lower critical Zeeman field h_{c1} [96], and the extent to which it resembles a commensurate-incommensurate transition (as in 1D [95,108]) remains an open question. More broadly, in Sec. VII we predicted a number of different LO descendant phases adjacent to the LO smectic superfluid state, but have left open the detailed nature of their phenomenology and stability to quantum and thermal fluctuations, as well the nature of the associated phase transitions. Similarly to the LO state, these phases are expected to exhibit gapless fermionic excitations coupled to their Goldstone modes. The understanding of the effects of these fermionic modes on the properties of the phases and the associated transitions remains wide open and extremely interesting problems.

Finally, as is clear from the discussion of the previous section, much detailed theoretical analysis remains to be done to make contact of our general predictions with specific experiments. We leave these and many other interesting questions to future studies.

XII. SUMMARY AND CONCLUSIONS

To summarize, we studied a wide range of fluctuation phenomena in a LO state, expected to be realizable in an imbalanced resonant Fermi gas. Starting with a microscopic description of a resonant Fermi gas, supported by robust model-independent and very general symmetry arguments, we have demonstrated that in an isotropic trap the LO state is a gapless superfluid smectic liquid crystal, whose elastic moduli and superfluid stiffness we derived near h_{c2}. Consequently, the state is extremely sensitive to thermal fluctuations that destroy its long-range positional order even in three dimensions, replacing it by a quasi-longer-range order of the resulting algebraic quantum smectic state, characterized by power-law correlations, akin to a system tuned to a critical point or two-dimensional XY-model systems. We showed that this exotic state also exhibits vortex fractionalization, where the basic superfluid vortex is half the strength of a vortex in a regular paired condensate, and is accompanied by half dislocations in the LO smectic (layered) structure.

Studying the fluctuation-driven disordering of the LO smectic, we predicted a rich variety of descendant phases such as the superfluid (SF_N) and Fermi liquid nematics (FL_N) and the fractionalized nonsuperfluid states (FL^*), which generically intervene between the LO state and the conventional BCS superfluid (at low population imbalance) and a conventional Fermi liquid (at high population imbalance). We outlined a large variety of experimental implications of our findings, but leave their detailed analysis to future studies.

ACKNOWLEDGMENTS

I thank A. Vishwanath for stimulating discussions and a collaboration on the early stages of this work [112], as well as for his and the Berkeley Physics Department's hospitality during a sabbatical stay. I acknowledge fruitful discussions with V. Gurarie, M. Hermele, D. Huse, and M. Levin, and thank S. Choi for careful reading of the manuscript. This work was supported by the National Science Foundation through Grant No. DMR-1001240, and through the MRSEC DMR-0213918.

APPENDIX A : GINZBURG-LANDAU EXPANSION

In this appendix we provide some of the technical details necessary to derive the quartic interaction in $\Delta_{\mathbf{q}}$ of the Ginzburg-Landau expansion appearing in Eqs. (30) and (50) and in particular the current-current contribution (49), which determines the transverse superfluid stiffness $\rho_s^{\perp}$. As outlined in the main text, we use the coherent-state imaginary-time path-integral formulation of the BCS partition function. We decouple the quartic fermion interaction g by introducing the Cooper-pair Hubbard-Stratonovich field $\Delta(\mathbf{x})$, and formally integrate out the fermionic atoms, obtaining

$$Z = \int [d\Delta^* d\Delta] e^{-S_{\rm eff}[\Delta^*,\Delta]}, \tag{A1}$$

where the effective Ginzburg-Landau action is given by

$$S_{\rm eff}[\Delta^*,\Delta] = -\ln\left[\int [d\psi_\sigma^* d\psi_\sigma] e^{-S_\tau[\psi_\sigma^*,\psi_\sigma,\Delta^*,\Delta]}\right], \tag{A2}$$

where S_τ is the microscopic action defined in Eq. (33).

Taylor-expanding S_τ in powers of $S_{\rm int}$, Eq. (35b), we obtain

$$S_{\rm eff}[\bar\Delta,\Delta] = -\ln Z_0 - \ln\left[1 - \langle S_{\rm int}\rangle_0 + \frac{1}{2!}\langle S_{\rm int}^2\rangle_0 - \frac{1}{3!}\langle S_{\rm int}^3\rangle_0 + \frac{1}{4!}\langle S_{\rm int}^4\rangle_0 + \cdots\right] \tag{A3a}$$

$$= -\ln Z_0 - \frac{1}{2!}\langle S_{\rm int}^2\rangle_0 - \frac{1}{4!}\langle S_{\rm int}^4\rangle_0 + \frac{1}{8}\langle S_{\rm int}^2\rangle_0^2 + \cdots, \tag{A3b}$$

where $Z_0 = \int [d\psi_\sigma^* d\psi_\sigma] e^{-S_0}$, $\langle\cdots\rangle_0 = \int [d\psi_\sigma^* d\psi_\sigma] \cdots e^{-S_0}/Z_0$. Above, all odd-power-in-Δ terms clearly vanish, and the quadratic $\Delta^*\hat\varepsilon\Delta$ term has already been analyzed in the main text [4,44,77].

Thus, we focus on the contribution quartic in Δ, which is a connected fourth cumulant. Using the definition of $S_{\rm int}$, Eq. (35b), we find

$$S_4 = -\frac{1}{4!}\left[\langle S_{\rm int}^4\rangle_0 - 3\langle S_{\rm int}^2\rangle_0^2\right] = -\frac{1}{4!}\langle S_{\rm int}^4\rangle_0^c \tag{A4a}$$

$$= \frac{12}{4!}\int_{\mathbf{x}_1\mathbf{x}_2\mathbf{x}_3\mathbf{x}_4} V(\mathbf{x}_1,\mathbf{x}_2,\mathbf{x}_3,\mathbf{x}_4)\Delta_{\mathbf{x}_1}^*\Delta_{\mathbf{x}_2}\Delta_{\mathbf{x}_3}^*\Delta_{\mathbf{x}_4}, \tag{A4b}$$

where

$$V(\mathbf{x}_1,\mathbf{x}_2,\mathbf{x}_3,\mathbf{x}_4) = G_\uparrow^0(\mathbf{x}_2-\mathbf{x}_1)G_\downarrow^0(\mathbf{x}_2-\mathbf{x}_3) \times G_\uparrow^0(\mathbf{x}_4-\mathbf{x}_3)G_\downarrow^0(\mathbf{x}_4-\mathbf{x}_1), \tag{A5}$$

with the noninteracting fermionic Green's function (in Fourier space) as usual given by

$$G_\sigma^0(\omega_n,q) = -\langle\psi_\sigma\psi_\sigma^*\rangle_0 \tag{A6a}$$

$$= \frac{1}{i\omega_n - \varepsilon_{q\sigma}}. \tag{A6b}$$

Because we are interested in τ-independent $\Delta(\mathbf{r})$, the τ integrals can be taken, giving $S_4 = \int d\tau H_4$, with

$$H_4 = \frac{1}{2}\int_{\tilde{\mathbf{q}}_i}(2\pi)^d\delta^d(\tilde{\mathbf{q}}_1-\tilde{\mathbf{q}}_2+\tilde{\mathbf{q}}_3-\tilde{\mathbf{q}}_4)\Bigg[\sum_{\mathbf{q}_1=\pm\mathbf{q}}\tilde V(\mathbf{q}_1+\tilde{\mathbf{q}}_1,\mathbf{q}_1+\tilde{\mathbf{q}}_2,\mathbf{q}_1+\tilde{\mathbf{q}}_3,\mathbf{q}_1+\tilde{\mathbf{q}}_4)\Delta_{\mathbf{q}_1}^*(\tilde{\mathbf{q}}_1)\Delta_{\mathbf{q}_1}(\tilde{\mathbf{q}}_2)\Delta_{\mathbf{q}_1}^*(\tilde{\mathbf{q}}_3)\Delta_{\mathbf{q}_1}(\tilde{\mathbf{q}}_4)$$
$$+4\tilde V(\mathbf{q}+\tilde{\mathbf{q}}_1,\mathbf{q}+\tilde{\mathbf{q}}_2,-\mathbf{q}+\tilde{\mathbf{q}}_3,-\mathbf{q}+\tilde{\mathbf{q}}_4)\Delta_{\mathbf{q}}^*(\tilde{\mathbf{q}}_1)\Delta_{\mathbf{q}}(\tilde{\mathbf{q}}_2)\Delta_{-\mathbf{q}}^*(\tilde{\mathbf{q}}_3)\Delta_{-\mathbf{q}}(\tilde{\mathbf{q}}_4)\Bigg]. \tag{A7}$$

A Taylor expansion of $\tilde V(\mathbf{q}_{n_1}+\tilde{\mathbf{q}}_1,\mathbf{q}_{n_2}+\tilde{\mathbf{q}}_2,\mathbf{q}_{n_3}+\tilde{\mathbf{q}}_3,\mathbf{q}_{n_4}+\tilde{\mathbf{q}}_4)$ in $\tilde{\mathbf{q}}_i$ gives $H_4 = H_4^{(0)} + H_4^{(2)}$, where $H_4^{(0)}$ has already been computed by LO in their mean-field approximation [77] and in Ref. [4] from the expansion of the BdG ground-state energy of the FF state discussed in Sec. II B.

We focus on the second $H_4^{(2)}$ term and Taylor-expand it to second order in $\tilde{\mathbf{q}}_i$,

$$\begin{aligned}\tilde{V}(\mathbf{q}+\tilde{\mathbf{q}}_1,\mathbf{q}+\tilde{\mathbf{q}}_2,-\mathbf{q}+\tilde{\mathbf{q}}_3,-\mathbf{q}+\tilde{\mathbf{q}}_4)\\ \approx v_{+-}^{(0)}+\frac{v_{ij}^{(2)}(\mathbf{q})}{4m^2}(\tilde{q}_{1i}\tilde{q}_{4j}+\tilde{q}_{1i}\tilde{q}_{3j}+\tilde{q}_{2i}\tilde{q}_{4j}+\tilde{q}_{2i}\tilde{q}_{3j}),\end{aligned} \tag{A8}$$

which gives the key current-current interaction vertex $v_{ij}^{(2)} j_i j_j$, with

$$v_{ij}^{(2)} = m^2\int\frac{d\omega d^dk}{(2\pi)^{d+1}}\tilde{G}^0_\uparrow(\mathbf{k},\omega)^2\partial_i\tilde{G}^0_\downarrow(\mathbf{q}-\mathbf{k},-\omega)\partial_j\tilde{G}^0_\downarrow(-\mathbf{q}-\mathbf{k},-\omega) \tag{A9a}$$

$$= \int_{\omega,\mathbf{k}}\frac{(\mathbf{q}-\mathbf{k})_i\big(\mathbf{q}+\mathbf{k}\big)_j}{\big(i\omega-\frac{k^2}{2m}+\mu+h\big)^2\big(-i\omega-\frac{(\mathbf{k}-\mathbf{q})^2}{2m}+\mu-h\big)^2\big(-i\omega-\frac{(\mathbf{k}+\mathbf{q})^2}{2m}+\mu-h\big)} \tag{A9b}$$

$$\approx \int_{\omega,\varepsilon,\hat{\mathbf{k}}}\frac{(\mathbf{q}-k_F\hat{\mathbf{k}})_i(\mathbf{q}+k_F\hat{\mathbf{k}})_j}{(i\omega-\varepsilon+h)^2\big(i\omega+\varepsilon-v_F\hat{\mathbf{k}}\cdot\mathbf{q}+\frac{q^2}{2m}+h\big)^2\big(i\omega+\varepsilon+v_F\hat{\mathbf{k}}\cdot\mathbf{q}+\frac{q^2}{2m}+h\big)^2}. \tag{A9c}$$

We first carry out the ω integral using simple identity,

$$\begin{aligned}I_\omega &= \int\frac{d\omega}{2\pi}\frac{1}{(i\omega-a)^2(i\omega-b)^2(i\omega-c)^2}\\ &= \frac{\partial^3}{\partial a\partial b\partial c}\int\frac{d\omega}{2\pi}\frac{1}{(i\omega-a)(i\omega-b)(i\omega-c)}\\ &= \frac{\partial^3}{\partial a\partial b\partial c}\left[\frac{\Theta(-a)}{(a-b)(a-c)}+\frac{\Theta(-b)}{(b-c)(b-a)}+\frac{\Theta(-c)}{(c-a)(c-b)}\right]\\ &= -\frac{\delta(a)}{b^2c^2}-\frac{\delta(b)}{c^2a^2}-\frac{\delta(c)}{a^2b^2}-2\Theta(-a)\frac{2a-b-c}{(a-b)^3(a-c)^3}-2\Theta(-b)\frac{2b-c-a}{(b-c)^3(b-a)^3}-2\Theta(-c)\frac{2c-a-b}{(c-a)^3(c-b)^3},\end{aligned} \tag{A10}$$

which, when used in the expression above, gives

$$\begin{aligned}v_{ij}^{(2)} \approx \int_{\varepsilon,\hat{\mathbf{k}}}(k_F\hat{\mathbf{k}}-\mathbf{q})_i(k_F\hat{\mathbf{k}}+\mathbf{q})_j\Bigg[&\frac{4\big(2\varepsilon+\frac{q^2}{2m}\big)\Theta(h-\varepsilon)}{\big[\big(2\varepsilon+\frac{q^2}{2m}\big)^2-(v_F\hat{\mathbf{k}}\cdot\mathbf{q})^2\big]^3}-\frac{\big(2\varepsilon+\frac{q^2}{2m}+3v_F\hat{\mathbf{k}}\cdot\mathbf{q}\big)\Theta\big(\varepsilon+\frac{q^2}{2m}+h+v_F\hat{\mathbf{k}}\cdot\mathbf{q}\big)}{4(v_F\hat{\mathbf{k}}\cdot\mathbf{q})^3\big(2\varepsilon+\frac{q^2}{2m}+v_F\hat{\mathbf{k}}\cdot\mathbf{q}\big)^3}\\ &+\frac{\big(2\varepsilon+\frac{q^2}{2m}-3v_F\hat{\mathbf{k}}\cdot\mathbf{q}\big)\Theta\big(\varepsilon+\frac{q^2}{2m}+h-v_F\hat{\mathbf{k}}\cdot\mathbf{q}\big)}{4(v_F\hat{\mathbf{k}}\cdot\mathbf{q})^3\big(2\varepsilon+\frac{q^2}{2m}-v_F\hat{\mathbf{k}}\cdot\mathbf{q}\big)^3}+\frac{\delta(\varepsilon-h)}{\big[\big(2h+\frac{q^2}{2m}\big)^2-(v_F\hat{\mathbf{k}}\cdot\mathbf{q})^2\big]^2}\\ &+\frac{\delta\big(\varepsilon+\frac{q^2}{2m}+h+v_F\hat{\mathbf{k}}\cdot\mathbf{q}\big)}{4(v_F\hat{\mathbf{k}}\cdot\mathbf{q})^2\big(2h+\frac{q^2}{2m}+v_F\hat{\mathbf{k}}\cdot\mathbf{q}\big)^2}+\frac{\delta\big(\varepsilon+\frac{q^2}{2m}+h-v_F\hat{\mathbf{k}}\cdot\mathbf{q}\big)}{4(v_F\hat{\mathbf{k}}\cdot\mathbf{q})^2\big(2h+\frac{q^2}{2m}-v_F\hat{\mathbf{k}}\cdot\mathbf{q}\big)^2}\Bigg]\\ \approx N(\epsilon_F)\frac{1}{4\pi}\int d\Omega_{\hat{\mathbf{k}}}&\frac{(k_F\hat{\mathbf{k}}-\mathbf{q})_i(k_F\hat{\mathbf{k}}+\mathbf{q})_j}{\big[\big(2h+\frac{q^2}{2m}\big)^2-(v_F\hat{\mathbf{k}}\cdot\mathbf{q})^2\big]^2}.\end{aligned} \tag{A11}$$

Here we split the $\mathbf{k}$ integration into an integration over its orientations $\hat{\mathbf{k}}$ and magnitude k, and approximated the latter using a nearly constant density of states at the Fermi energy, equivalently ignoring small quadratic contributions in $\delta k \equiv k - k_F$, valid in the BCS limit. However, in contrast to a standard isotropic calculation, here the integral over $\hat{\mathbf{k}}$ is

nontrivial because of the anisotropy introduced by $\mathbf{q}$. That is, we used

$$\int \frac{d^3k}{(2\pi)^3}\cdots = \int_0^\infty dk k^2 \frac{1}{(2\pi)^3}\int d\Omega_{\hat{\mathbf{k}}}\cdots$$
$$= \int_0^\infty d\epsilon N(\epsilon)\frac{1}{4\pi}\int d\Omega_{\hat{\mathbf{k}}}\cdots$$
$$\approx N(\epsilon_F)\int_{-\infty}^{\infty} d\varepsilon \frac{1}{4\pi}\int d\Omega_{\hat{\mathbf{k}}}\cdots, \quad \text{(A12)}$$

where the density of states per spin is

$$N(\epsilon) = \frac{m^{3/2}}{2^{1/2}\pi^2\hbar^3}\epsilon^{1/2} \equiv c\epsilon^{1/2} \quad \text{(A13a)}$$
$$= N(\varepsilon+\epsilon_F)$$
$$\approx N(\epsilon_F) = \frac{3}{4}\frac{n}{\epsilon_F}. \quad \text{(A13b)}$$

By symmetry $v_{ij}^{(2)}$ is clearly uniaxial along $\mathbf{q}$. Thus it can be written as

$$v_{ij}^{(2)} = g_1\delta_{ij} + g_2\hat{\mathbf{q}}_i\hat{\mathbf{q}}_j, \quad \text{(A14)}$$

where

$$g_1 = \tfrac{1}{2}v_{ii}^{(2)} - \tfrac{1}{2}v_{ij}^{(2)}\hat{\mathbf{q}}_i\hat{\mathbf{q}}_j, \quad \text{(A15a)}$$
$$g_2 = -\tfrac{1}{2}v_{ii}^{(2)} + \tfrac{3}{2}v_{ij}^{(2)}\hat{\mathbf{q}}_i\hat{\mathbf{q}}_j, \quad \text{(A15b)}$$

with the sums over repeated indices implied. Using this inside Eq. (A14) we find

$$g_1 = \frac{1}{2}N(\epsilon_F)k_F^2\frac{1}{4\pi}\int d\Omega_{\hat{\mathbf{k}}}\frac{1-(\hat{\mathbf{k}}\cdot\hat{\mathbf{q}})^2}{\left[\left(2h+\frac{q_0^2}{2m}\right)^2-(v_F\hat{\mathbf{k}}\cdot\mathbf{q})^2\right]^2}$$
$$\approx \frac{N(\epsilon_F)k_F^2}{2v_F^4q_0^4}\int_0^1 d\sigma\frac{1-\sigma^2}{\left[\sigma^2-\frac{4h^2}{v_F^2q_0^2}\right]^2}$$
$$\equiv \frac{N(\epsilon_F)k_F^2}{2v_F^4q_0^4}\alpha_1\left(\frac{2h}{v_Fq_0}\right), \quad \text{(A16a)}$$
$$g_2 = \frac{1}{2}N(\epsilon_F)k_F^2\frac{1}{4\pi}\int d\Omega_{\hat{\mathbf{k}}}\frac{3(\hat{\mathbf{k}}\cdot\hat{\mathbf{q}})^2-1-q_0^2/k_F^2}{\left[\left(2h+\frac{q_0^2}{2m}\right)^2-(v_F\hat{\mathbf{k}}\cdot\mathbf{q})^2\right]^2}$$
$$\approx \frac{N(\epsilon_F)k_F^2}{2v_F^4q_0^4}\int_0^1 d\sigma\frac{3\sigma^2-1}{\left[\sigma^2-\frac{4h^2}{v_F^2q_0^2}\right]^2}$$
$$\equiv \frac{N(\epsilon_F)k_F^2}{2v_F^4q_0^4}\alpha_2\left(\frac{2h}{v_Fq_0}\right), \quad \text{(A16b)}$$

where we evaluated q at the dominant dispersion minimum value of q_0 and ignored subdominant q_0^2/k_F^2 terms.

The dimensionless functions $\alpha_1(x)$ and $\alpha_2(x)$ defined by the above polar-angle (σ) integrals are given by

$$\alpha_1(x) = \int_0^1 d\sigma\frac{1-\sigma^2}{[\sigma^2-x^2]^2}$$
$$= -\frac{1}{2x^2}+\frac{1+x^2}{4x^3}\ln\frac{1+x}{1-x}$$
$$\approx 2.07 \text{ at } h_{c2}\ (x_{c2}=1/\alpha_{c2}=5/6) \text{ transition}, \quad \text{(A17a)}$$

$$\alpha_2(x) = \int_0^1 d\sigma\frac{3\sigma^2-1}{[\sigma^2-x^2]^2}$$
$$= \frac{x-3x^3+\frac{1}{2}(3x^4-2x^2-1)\ln\frac{1+x}{1-x}}{2x^3(1-x^2)}$$
$$\approx -5.75 \text{ at } h_{c2}\ (x_{c2}=1/\alpha_{c2}=5/6) \text{ transition}, \quad \text{(A17b)}$$

with the final values obtained by their evaluation at the upper critical field h_{c2}. Although naively the expressions appear to be linearly divergent, a careful analysis of the integrals regularized with an infinitesimal imaginary part (associated with the analytic continuation to real frequencies, $i\omega \to \omega + i0^+$) gives well-defined values given above.

APPENDIX B : FLUCTUATION IN A FINITE BOX

In the main body of the paper, Sec. IX C, we demonstrated that due to the smectic phonon dispersion anisotropy, for Neumann boundary conditions the zero $q_z = 0$ mode dominates fluctuations over the bulk $q_z \approx \lambda q_\perp^2$ modes and must be explicitly taken into account. This leads to an effective dimensional reduction for a system confined in any reasonably isotropic trap. Here, we rederive this result within a complementary, fully continuum description and contrast the behavior in the smectic state with that of the more familiar isotropic *XY* model.

1. Isotropic models

For an *XY* model (or really any model with isotropic spatial dispersion) described by

$$H = \frac{1}{2}\int d^dx(\nabla u)^2, \quad \text{(B1)}$$

the fluctuations inside a box of aspect ratio $L_z \times L_\perp$, with $L_z < L_\perp$ for free (Neumann) boundary conditions, are given by

$$\langle u^2(\mathbf{x})\rangle = \int \frac{dq_z d^{d-1}q_\perp}{(2\pi)^d}\frac{1}{q_z^2+q_\perp^2}$$
$$\sim \frac{1}{L_z}L_\perp^{3-d} + L_z^{2-d} \quad \text{(B2a)}$$
$$\sim \frac{1}{L_z}L_\perp^{3-d} \gg L_z^{2-d} \quad \text{for } d<2,\ L_z<L_\perp, \quad \text{(B2b)}$$

where the first term is due to the $q_z = 0$ zero mode and is larger than the second bulk mode contribution when $L_z < L_\perp$. It accounts for fluctuations in the reduced dimensionality of a $(d-1)$-dimensional film of thickness L_z. We note that for an isotropic dispersion the crossover to a lower-dimensional scaling takes place only when the actual geometrical aspect ratio of the system is filmlike, i.e., anisotropic.

2. Smectic models

We contrast the above standard finite-size scaling with that of a model with smectic dispersion, described by

$$H = \frac{1}{2}\int d^dx[(\partial_z u)^2 + (\nabla_\perp^2 u)^2]. \quad \text{(B3)}$$

In a finite box, its fluctuations are instead given by

$$\langle u^2(\mathbf{x})\rangle = \int \frac{dq_z d^{d-1}}{(2\pi)^d}\frac{1}{q_z^2+q_\perp^4}$$

$$\sim \frac{1}{L_z}L_\perp^{5-d} + L_z^{(3-d)/2} \tag{B4a}$$

$$\sim \frac{1}{L_z}L_\perp^{5-d} \gg L_z^{(3-d)/2} \quad \text{for } d<3, \quad L_z < L_\perp^2. \tag{B4b}$$

Now, clearly the first zero mode ($q_z = 0$) term dominates over the bulk contribution (second term) for $L_z < L_\perp^2 \gg L_\perp$, and does so even in an isotropic box with all dimensions L. Thus, a smectic confined in a geometrically isotropic environment is effectively deep in the lower, $(d-1)$-dimensional film regime with phonon fluctuations scaling as $u_{\text{rms}}^2 \sim L^{4-d} \gg L^{(3-d)/2}$.

[1] I. Bloch, J. Dalibard, and W. Zwerger, Rev. Mod. Phys. **80**, 885 (2008).

[2] W. Ketterle and M. Zwierlein, in *Ultracold Fermi Gases*, *Proceedings of the International School of Physics "Enrico Fermi," Course CLXIV, Varenna,* 2006, edited by M. Inguscio, W. Ketterle, and C. Salomon (IOS Press, Amsterdam, 2008), pp. 95-287.

[3] V. Gurarie and L. Radzihovsky, Ann. Phys. **322**, 2 (2007).

[4] D. E. Sheehy and L. Radzihovsky, Ann. Phys. **322**, 1790 (2007).

[5] S. Giorgini, L. P. Pitaevskii, and S. Stringari, Rev. Mod. Phys. **80**, 1215 (2008).

[6] L. Radzihovsky and D. E. Sheehy, Rep. Prog. Phys. **73**, 076501 (2010).

[7] C. A. Regal, M. Greiner, and D. S. Jin, Phys. Rev. Lett. **92**, 040403 (2004).

[8] M. W. Zwierlein, C. A. Stan, C. H. Schunck, S. M. F. Raupach, A. J. Kerman, and W. Ketterle, Phys. Rev. Lett. **92**, 120403 (2004).

[9] J. Kinast, S. L. Hemmer, M. E. Gehm, A. Turlapov, and J. E. Thomas, Phys. Rev. Lett. **92**, 150402 (2004).

[10] M. Bartenstein, A. Altmeyer, S. Riedl, S. Jochim, C. Chin, J. H. Denschlag, and R. Grimm, Phys. Rev. Lett. **92**, 120401 (2004).

[11] T. Bourdel, L. Khaykovich, J. Cubizolles, J. Zhang, F. Chevy, M. Teichmann, L. Tarruell, S. J. J. M. F. Kokkelmans, and C. Salomon, Phys. Rev. Lett. **93**, 050401 (2004).

[12] J. Zhang, E. G. M. vanKempen, T. Bourdel, L. Khaykovich, J. Cubizolles, F. Chevy, M. Teichmann, L. Tarruell, S. J. J. M. F. Kokkelmans, and C. Salomon, Phys. Rev. A **70**, 030702(R) (2004).

[13] J. P. Gaebler, J. T. Stewart, J. L. Bohn, and D. S. Jin, Phys. Rev. Lett. **98**, 200403 (2007).

[14] S. S. Botelho and C. A. R. S. de Melo, J. Low Temp. Phys. **140**, 409 (2005).

[15] V. Gurarie, L. Radzihovsky, and A. V. Andreev, Phys. Rev. Lett. **94**, 230403 (2005).

[16] C.-H. Cheng and S.-K. Yip, Phys. Rev. Lett. **95**, 070404 (2005).

[17] D. M. Eagles, Phys. Rev. **186**, 456 (1969).

[18] A. J. Leggett, in *Modern Trends in the Theory of Condensed Matter*, edited by A. Pekalski and R. Przystawa (Springer-Verlag, Berlin, 1980).

[19] P. Nozières and S. Schmitt-Rink, J. Low Temp. Phys. **59**, 195 (1985).

[20] C. A. R. Sá de Melo, M. Randeria, and J. R. Engelbrecht, Phys. Rev. Lett. **71**, 3202 (1993).

[21] E. Timmermans, K. Furuya, P. W. Milonni, and A. K. Kerman, Phys. Lett. A **285**, 228 (2001).

[22] M. Holland, S. J. J. M. F. Kokkelmans, M. L. Chiofalo, and R. Walser, Phys. Rev. Lett. **87**, 120406 (2001).

[23] Y. Ohashi and A. Griffin, Phys. Rev. Lett. **89**, 130402 (2002); Phys. Rev. A **67**, 033603 (2003).

[24] A. V. Andreev, V. Gurarie, and L. Radzihovsky, Phys. Rev. Lett. **93**, 130402 (2004).

[25] J. Stajic, J. N. Milstein, Q. Chen, M. L. Chiofalo, M. J. Holland, and K. Levin, Phys. Rev. A **69**, 063610 (2004).

[26] M. L. Olsen, J. D. Perreault, T. D. Cumby, and D. S. Jin, Phys. Rev. A **80**, 030701(R) (2009).

[27] S. L. Cornish, N. R. Claussen, J. L. Roberts, E. A. Cornell, and C. E. Wieman, Phys. Rev. Lett. **85**, 1795 (2000).

[28] L. Radzihovsky, J. Park, and P. B. Weichman, Phys. Rev. Lett. **92**, 160402 (2004).

[29] M. W. J. Romans, R. A. Duine, S. Sachdev, and H. T. C. Stoof, Phys. Rev. Lett. **93**, 020405 (2004).

[30] L. Radzihovsky, P. Weichman, and J. Park, Ann. Phys. **323**, 2376 (2008).

[31] See e.g., Refs. [1–6] and references therein.

[32] R. A. Barankov, L. S. Levitov, and B. Z. Spivak, Phys. Rev. Lett. **93**, 160401 (2004).

[33] E. Altman and A. Vishwanath, Phys. Rev. Lett. **95**, 110404 (2005).

[34] M. W. Zwierlein, A. Schirotzek, C. H. Schunck, and W. Ketterle, Science **311**, 492 (2006).

[35] G. B. Partridge, W. Li, R. I. Kamar, Y. Liao, and R. G. Hulet, Science **311**, 503 (2006).

[36] Y. Shin, M. W. Zwierlein, C. H. Schunck, A. Schirotzek, and W. Ketterle, Phys. Rev. Lett. **97**, 030401 (2006).

[37] S. Nascimb'ene, N. Navon, K. J. Jiang, L. Tarruell, M. Teichmann, J. McKeever, F. Chevy, and C. Salomon, Phys. Rev. Lett. **103**, 170402 (2009).

[38] R. Combescot, Europhys. Lett. **55**, 150 (2001).

[39] W. V. Liu and F. Wilczek, Phys. Rev. Lett. **90**, 047002 (2003).

[40] P. F. Bedaque, H. Caldas, and G. Rupak, Phys. Rev. Lett. **91**, 247002 (2003).

[41] H. Caldas, Phys. Rev. A **69**, 063602 (2004).

[42] J. Carlson and S. Reddy, Phys. Rev. Lett. **95**, 060401 (2005).

[43] T. D. Cohen, Phys. Rev. Lett. **95**, 120403 (2005).

[44] D. E. Sheehy and L. Radzihovsky, Phys. Rev. Lett. **96**, 060401 (2006).

[45] C.-H. Pao, S.-T. Wu, and S.-K. Yip, Phys. Rev. B **73**, 132506 (2006).

[46] D. T. Son and M. A. Stephanov, Phys. Rev. A **74**, 013614 (2006).

[47] D. E. Sheehy and L. Radzihovsky, Phys. Rev. B **75**, 136501 (2007).

[48] P. Castorina, M. Grasso, M. Oertel, M. Urban, and D. Zappalà, Phys. Rev. A **72**, 025601 (2005).

[49] A. Sedrakian, J. Mur-Petit, A. Polls, and H. Müther, Phys. Rev. A **72**, 013613 (2005).

[50] A. Bulgac, M. M. Forbes, and A. Schwenk, Phys. Rev. Lett. **97**, 020402 (2006).

[51] J. Dukelsky, G. Ortiz, S. M. A. Rombouts, and K. Van Houcke, Phys. Rev. Lett. **96**, 180404 (2006).

[52] T. Mizushima, K. Machida, and M. Ichioka, Phys. Rev. Lett. **94**, 060404 (2005).

[53] K. Yang, Phys. Rev. Lett. **95**, 218903 (2005).

[54] K. Yang and S. Sachdev, Phys. Rev. Lett. **96**, 187001 (2006).

[55] P. Pieri and G. C. Strinati, Phys. Rev. Lett. **96**, 150404 (2006).

[56] J. Kinnunen, L. M. Jensen, and P. Törmä, Phys. Rev. Lett. **96**, 110403 (2006).

[57] W. Yi and L.-M. Duan, Phys. Rev. A **73**, 031604 (2006).

[58] F. Chevy, Phys. Rev. Lett. **96**, 130401 (2006).

[59] L. He, M. Jin, and P. Zhuang, Phys. Rev. B **73**, 214527 (2006).

[60] T. N. De Silva and E. J. Mueller, Phys. Rev. A **73**, 051602 (2006).

[61] M. Haque and H. T. C. Stoof, Phys. Rev. A **74**, 011602 (2006).

[62] S. Sachdev and K. Yang, Phys. Rev. B **73**, 174504 (2006).

[63] X.-J. Liu and H. Hu, Europhys. Lett. **75**, 364 (2006).

[64] C. C. Chien, Q. Chen, Y. He, and K. Levin, Phys. Rev. Lett. **97**, 090402 (2006).

[65] K. B. Gubbels, M. W. J. Romans, and H. T. C. Stoof, Phys. Rev. Lett. **97**, 210402 (2006).

[66] W. Yi and L.-M. Duan, Phys. Rev. A **74**, 013610 (2006).

[67] C.-H. Pao and S.-K. Yip, J. Phys.: Condens. Matter **18**, 5567 (2006).

[68] J.-P. Martikainen, Phys. Rev. A **74**, 013602 (2006).

[69] M. M. Parish, F. M. Marchetti, A. Lamacraft, and B. D. Simons, Nature Phys. **3**, 124 (2007).

[70] A. Bulgac and M. M. Forbes, Phys. Rev. Lett. **101**, 215301, 2008.

[71] Meera M. Parish, Stefan K. Baur, Erich J. Mueller, and David A. Huse, Phys. Rev. Lett. **99**, 250403 (2007).

[72] D. E. Sheehy, Phys. Rev. A **79**, 033606 (2009).

[73] A. M. Clogston, Phys. Rev. Lett. **9**, 266 (1962).

[74] B. S. Chandrasekhar, Appl. Phys. Lett. **1**, 7 (1962).

[75] G. Sarma, J. Phys. Chem. Solids **24**, 1029 (1963).

[76] P. Fulde and R. A. Ferrell, Phys. Rev. **135**, A550 (1964).

[77] A. I. Larkin and Yu. N. Ovchinnikov, Zh. Eksp. Teor. Fiz. **47**, 1136 (1964) [Sov. Phys. JETP **20**, 762 (1965)].

[78] M. Alford, J. A. Bowers, and K. Rajagopal, Phys. Rev. D **63**, 074016 (2001).

[79] J. A. Bowers and K. Rajagopal, Phys. Rev. D **66**, 065002 (2002).

[80] R. Casalbuoni and G. Nardulli, Rev. Mod. Phys. **76**, 263 (2004).

[81] R. Combescot and C. Mora, Europhys. Lett. **68**, 79 (2004).

[82] See footnotes [100,101] in Ref. [4].

[83] Y.-P. Shim, R. A. Duine, and A. H. MacDonald, Phys. Rev. A **74**, 053602 (2006).

[84] Recent experiments have found evidence of a FFLO state in the heavy-fermion compound $CeCoIn_5$ [A. Bianchi, R. Movshovich, C. Capan, P. G. Pagliuso, and J. L. Sarrao, Phys. Rev. Lett. **91**, 187004 (2003); H. A. Radovan, N. A. Fortune, T. P. Murphy, S. T. Hannahs, E. C. Palm, S. W. Tozer, and D. Hall, Nature (London) **425**, 51 (2003)] and in organic κ-$(BEDT\text{-}TTF)_2Cu(NCS)_2$ [R. Lortz, Y. Wang, A. Demuer, P. H. M. Bottger, B. Bergk, G. Zwicknagl, Y. Nakazawa, and J. Wosnitza, Phys. Rev. Lett. **99**, 187002 (2007)] superconductors.

[85] Y. Liao, A. S. C. Rittner, T. Paprotta, W. Li, G. B. Partridge, R. G. Hulet, S. K. Baur, and E. J. Mueller, Nature (London) **467**, 567 (2010).

[86] Throughout we will use FFLO to denote a generic class of fermionic superfluid states paired at a finite center-of-mass momentum.

[87] A. F. Andreev and I. M. Lifshitz, Zh. Eksp. Teor. Fiz. **56**, 2057 (1969) [Sov. Phys. JETP **29**, 1107 (1969)].

[88] G. V. Chester, Phys. Rev. A **2**, 256 (1970).

[89] A. J. Leggett, Phys. Rev. Lett. **25**, 1543 (1970).

[90] E. Kim and M. H. W. Chan, Nature (London) **427**, 225 (2004); Science **305**, 1941 (2004).

[91] We emphasize that while it shows some resemblance to a conventional supersolid, a LO state is qualitatively distinguished from it by the absence of a zero-momentum condensate. More explicitly, while a conventional supersolid also breaks translational and gauge symmetry, this symmetry breaking is controlled by two independent order parameters. In contrast, a LO state is characterized by a single-product order parameter, thereby putting it in a distinct universality class, that is more appropriately referred to as a "pair-density wave" (PDW) [92].

[92] H.-D. Chen, O. Vafek, A. Yazdani, and S.-C. Zhang, Phys. Rev. Lett. **93**, 187002 (2004).

[93] S.-T. Wu, C.-H. Pao, and S.-K. Yip, Phys. Rev. B **74**, 224504 (2006).

[94] Y. He, Chih-Chun Chien, Q. Chen, and K. Levin, Phys. Rev. A **75**, 021602(R) (2007).

[95] K. Machida and H. Nakanishi, Phys. Rev. B **30**, 122 (1984).

[96] H. Burkhardt and D. Rainer, Ann. Phys. **3**, 181 (1994).

[97] S. Matsuo, S. Higashitani, Y. Nagato, and K. Nagai, J. Phys. Soc. Jpn. **67**, 280 (1998).

[98] N. Yoshida, and S.-K. Yip, Phys. Rev. A **75**, 063601 (2007).

[99] P.-G. de Gennes, *Superconductivity of Metals and Alloys* (Benjamin, New York, 1966).

[100] M. Tinkham, *Introduction to Superconductivity* (McGraw-Hill, New York, 1996).

[101] J. R. Schrieffer, *Theory of Superconductivity* (Perseus Books, Reading, MA, 1999).

[102] For a review, see e.g., V. L. Pokrovsky, A. L. Talapov, and P. Bak, in *Solitons*, edited by S. E. Trullinger, V. E. Zakharov, and V. L. Pokrovsky (North-Holland, Amsterdam, 1986), Chap. 3, pp. 71–127.

[103] As we find in Sec. VII, once fluctuations are included, even this direct continuous CI transition is either driven first order (as in Brazovskii's observation in Ref. [104]), or is split into a number of transitions through intermediate phases illustrated in Fig. 4. This observation is quite generic and is due to the fact that the LO state spontaneously breaks *both* translational and rotational symmetries, while the conventional paired SF state breaks neither. Consequently, at least two continuous transitions are required.

[104] S. A. Brazovskii, Zh. Eksp. Teor. Fiz. **68**, 175 (1975) [Sov. Phys. JETP **41**, 85 (1975)].
[105] W. P. Su, J. R. Schrieffer, and A. J. Heeger, Phys. Rev. Lett. **42**, 1698 (1979); Phys. Rev. B **22**, 2099 (1980).
[106] G. Orso, Phys. Rev. Lett. **98**, 070402 (2007).
[107] H. Hu, X.-J. Liu, and P. D. Drummond, Phys. Rev. Lett. **98**, 070403 (2007).
[108] K. Yang, Phys. Rev. B **63**, 140511 (2001).
[109] E. Zhao and W. V. Liu, Phys. Rev. A **78**, 063605 (2008).
[110] Recently, we became aware of an earlier work by H. Shimahara, J. Phys. Soc. Jpn **67**, 1872 (1998), where harmonic fluctuations in the FF state were first studied and found to destroy the order in 2D, in agreement with our findings.
[111] K. V. Samokhin, Phys. Rev. B **81**, 224507 (2010).
[112] L. Radzihovsky and A. Vishwanath, Phys. Rev. Lett. **103**, 010404 (2009).
[113] D. F. Agterberg and H. Tsunetsugu, Nature Phys. **4**, 639 (2008).
[114] D. F. Agterberg, S. Mukherjee, and Z. Zheng, Phys. Rev. Lett. **100**, 017001 (2008).
[115] S. A. Kivelson, E. Fradkin, and V. J. Emery, Nature (London) **393**, 550 (1998).
[116] E. Fradkin and S. A. Kivelson, Phys. Rev. B **59**, 8065 (1999).
[117] V. Oganesyan, S. E. Kivelson, and E. Fradkin, Phys. Rev. B **64**, 195109 (2001).
[118] E. Berg, E. Fradkin, and S. A. Kivelson, Phys. Rev. B **79**, 064515 (2009).
[119] E. Berg, E. Fradkin, and S. A. Kivelson, Nature Phys. **5**, 830 (2009).
[120] S. Sachdev, Ann. Phys. **303**, 226 (2003).
[121] P. Bak and M. H. Jensen, J. Phys. C **13**, L88 (1980).
[122] D. Belitz, T. R. Kirkpatrick, and A. Rosch, Phys. Rev. B **73**, 054431 (2006).
[123] A. M. Berridge, A. G. Green, S. A. Grigera, and B. D. Simons, Phys. Rev. Lett. **102**, 136404 (2009).
[124] A. A. Koulakov, M. M. Fogler, and B. I. Shklovskii, Phys. Rev. Lett. **76**, 499 (1996); M. M. Fogler, A. A. Koulakov, and B. I. Shklovskii, Phys. Rev. B **54**, 1853 (1996).
[125] A. H. MacDonald and M. P. A. Fisher, Phys. Rev. B **61**, 5724 (2000).
[126] L. Radzihovsky and A. T. Dorsey, Phys. Rev. Lett. **88**, 216802 (2002).
[127] G. Gruner, Rev. Mod. Phys. **60**, 1129 (1988).
[128] All our results are quoted for FF and LO states that form in an otherwise isotropic environment, i.e., in the absence of a crystal lattice, as appropriate for a resonant Fermi gas confined in an isotropic trap. The case of an anisotropic background (e.g., a lattice) can be easily incorporated through an explicit orientational symmetry breaking.
[129] P. deGennes and J. Prost, *The Physics of Liquid Crystals* (Clarendon Press, Oxford, 1993).
[130] P. Chaikin and T. C. Lubensky, *Principles of Condensed Matter Physics* (Cambridge University Press, Cambridge, 1995).
[131] G. Grinstein and R. A. Pelcovits, Phys. Rev. Lett. **47**, 856 (1981).
[132] L. Golubovic and Z. G. Wang, Phys. Rev. Lett. **69**, 2535 (1992).
[133] At the longest scales (smaller q) this result, based on Gaussian fluctuations is modified by 3D logarithmic corrections (power law in 2D) associated with nonlinear elastic effects of the smectic phonon u [131,132]. However, it is unlikely that lengths at which this is manifest can be accessible in the trapped atomic gases.
[134] A. Caillé, C. R. Acad. Sci., Ser. B **274**, 891 (1972).
[135] J. Als-Nielsen, J. D. Litster, R. J. Birgeneau, M. Kaplan, C. R. Safinya, A. Lindegaard-Andersen, and S. Mathiesen, Phys. Rev. B **22**, 312 (1980).
[136] L. D. Landau, in *Collected Papers of L. D. Landau*, edited by D. ter Haar (Gordon and Breach, New York, 1965), p. 209; L. D. Landau and E. M. Lifshitz, *Statistical Physics* (Pergamon, London, 1969), p. 403.
[137] R. E. Peierls, Helv. Phys. Acta Suppl. **7**, 81 (1934).
[138] N. D. Mermin and H. Wagner, Phys. Rev. Lett. **17**, 1133 (1966).
[139] P. C. Hohenberg, Phys. Rev. **158**, 383 (1967).
[140] S. Coleman, Commun. Math. Phys. **31**, 259 (1973).
[141] J. M. Kosterlitz and D. J. Thouless, J. Phys. C **6**, 1181 (1973); see also, V. L. Berezinskii, Zh. Eksp. Teor. Fiz. **59**, 907 (1970) [Sov. Phys. JETP **32**, 493 (1971)]; **34**, 610 (1972).
[142] J. Toner and D. R. Nelson, Phys. Rev. B **23**, 316 (1981).
[143] We use the term "charge" in the generalized sense of a conserved quantum number. Here it is associated with the number of fermionic atoms, which are in fact electromagnetically neutral for the case of an atomic gas that is the focus of our work.
[144] P. Nikolić and S. Sachdev, Phys. Rev. A **75**, 033608 (2007).
[145] M. Y. Veillette, D. E. Sheehy, and L. Radzihovsky, Phys. Rev. A **75**, 043614 (2007).
[146] Y. Nishida and D. T. Son, Phys. Rev. Lett. **97**, 050403 (2006).
[147] L. D. Landau and E. M. Lifshitz, *Quantum Mechanics* (Butterworth-Heinemann, Oxford, 1981).
[148] See e.g., Ref. [3] and references therein.
[149] C. A. Regal and D. S. Jin, Phys. Rev. Lett. **90**, 230404 (2003).
[150] The FFLO$\rightarrow N$ transition is only continuous within mean-field theory, and can be argued to be either generically driven first order by fluctuations [104,136] or split into intermediate phases.
[151] L. Radzihovsky (unpublished).
[152] Actually in principle for an arbitrarily oriented $\mathbf{q}$ there is no need to introduce both Δ_+ and Δ_-. However, in practice, because calculations are done perturbatively about a particular spontaneously chosen $\mathbf{q}$, both $\Delta_\pm$ are needed.
[153] Because near h_{c2} the $\rho_s^\perp$ vanishes faster than $\rho_s^\parallel$, these may need to be included to account for an expected long crossover before these irrelevant terms actually vanish.
[154] As we discuss in Secs. VI and VIII, FFLO thermodynamics receives contributions from topological defects (vortices and dislocations) as well as the gapless fermionic (atom) excitations, in addition to these bosonic Goldstone modes.
[155] Additional Berry phase effects may arise and qualitatively modify the dynamics, as argued in, e.g., Ref. [156].
[156] S. Fujimoto, Phys. Rev. B **82**, 060516(R) (2010).
[157] J. Stenger, S. Inouye, A. P. Chikkatur, D. M. Stamper-Kurn, D. E. Pritchard, and W. Ketterle, Phys. Rev. Lett. **82**, 4569 (1999); D. M. Stamper-Kurn, A. P. Chikkatur, A. Gorlitz, S. Inouye, S. Gupta, D. E. Pritchard, and W. Ketterle, *ibid.* **83**, 2876 (1999).
[158] J. Steinhauer, R. Ozeri, N. Katz, and N. Davidson, Phys. Rev. Lett. **88**, 120407 (2002).
[159] S. B. Papp, J. M. Pino, R. J. Wild, S. Ronen, C. E. Wieman, D. S. Jin, and E. A. Cornell, Phys. Rev. Lett. **101**, 135301 (2008).

[160] Quantum fluctuations have a negligible effect on the domain-proliferation (SF-LO) transition at h_{c1}, as they lead to a correction to domain-wall interaction that is Gaussian in z and is therefore even shorter range than the microscopic (exponential) interaction.
[161] W. Helfrich and Ber. Bunsengesell. Phys. Chem. **82**, 927 (1978).
[162] This $d > 1$ long-range-ordered ground state contrasts sharply with the well-explored $d = 1$ system that exhibits quasi-long-range order even at $T = 0$, consistent with the expected Luttinger liquid phenomenology [108] in both charge and spin sectors, and with the exact Bethe-ansatz solution [106,107].
[163] F. Lindemann, Z. Phys. **11**, 609 (1910).
[164] K. G. Wilson and J. Kogut, Phys. Rep. C **12**, 77 (1977).
[165] The rotational invariance guarantees that the form of the nonlinear strain tensor is preserved by graphical corrections, thereby imposing the relation between η_B and η_K, (138a). This relation can also be obtained from the fixed-point condition $dg/d\ell = 0 = (3 - d - \frac{1}{2}\eta_B - \frac{3}{2}\eta_K)g$ at the nontrivial fixed point g_*.
[166] In terms of the "rotated" Goldstone modes $\phi = \frac{1}{2}(\phi_+ + \phi_-)$ and $\theta = \frac{1}{2}(\phi_+ - \phi_-)$, the low-energy LO manifold is described as a half-twisted torus, $[\mathrm{U}(1) \otimes \mathrm{U}(1)]/\mathbb{Z}_2$. Because of the structure of the Hamiltonian (142b) the energetics is best analyzed in terms of ϕ,θ, while topological constraints on defects are most transparently implemented in terms of $\phi_\pm$.
[167] D. Podolsky, S. Chandrasekharan, and A. Vishwanath, Phys. Rev. B **80**, 214513 (2009).
[168] E. Babaev, Phys. Rev. Lett. **89**, 067001 (2002).
[169] An analogous dual sine-Gordon model for an *XY* PDW model (nonrotationally invariant) was recently reported in Ref. [119], and analyzed in C. Lin, X. Li, and W. Vincent Liu, Phys. Rev. B **83**, 092501 (2011).
[170] In addition to the conventional phases classifiable by a Landau order parameter and symmetry breaking, we also find states that are symmetrywise identical, but are distinguished by a more subtle topological order (see Figs. 4 and 12 and below).
[171] T. Senthil and M. P. A. Fisher, Phys. Rev. B. **62**, 7850 (2000); **63**, 134521 (2001).
[172] S. Sachdev, Phys. Rev. B **45**, 389 (1992).
[173] L. Balents, M. P. A. Fisher, and C. Nayak, Phys. Rev. B **60**, 1654 (1999).
[174] S. Sachdev, *Quantum Phase Transitions* (Cambridge University Press, Cambridge, 1999).
[175] S. Sachdev, Ann. Phys. **303**, 226 (2003).
[176] Z. Nussinov and J. Zaanen, J. Phys. IV **12**, 245 (2002); Phys. Status Solidi B **236**, 332 (2003).
[177] A. M. Zagoskin, *Quantum Theory of Many-Body Systems: Techniques and Applications* (Springer, New York, 1998).
[178] A. Vishwanath, Ph.D. thesis, Princeton University Press, 2001.
[179] In contrast, in 1D the effective chemical potential generically lies in the gap between Andreev bands [111]. Thus, a 1D LO state exhibits only collective low-energy excitations ϕ,θ, consistent with its Luttinger-liquid description [108,109].
[180] T. Holstein, R. E. Norton, and P. Pincus, Phys. Rev. B **8**, 2649 (1973).
[181] M. Yu. Reizer, Phys. Rev. B **40**, 7461 (1989).
[182] B. I. Halperin, P. A. Lee, and N. Read, Phys. Rev. B **47**, 7312 (1993).
[183] J. Polchinski, Nucl. Phys. B **422**, 617 (1994).
[184] B. L. Altshuler, L. B. Ioffe, and A. J. Millis, Phys. Rev. B **50**, 14048 (1994).
[185] Sung-Sik Lee, Phys. Rev. B **80**, 165102 (2009).
[186] E.-A. Kim, M. J. Lawler, P. Oreto, S. Sachdev, E. Fradkin, and S. A. Kivelson, Phys. Rev. B **77**, 184514 (2008).
[187] M. A. Metlitski and S. Sachdev, Phys. Rev. B **82**, 075127 (2010).
[188] M. Greiner, O. Mandel, T. Esslinger, T. W. Hänsch, and I. Bloch, Nature (London) **415**, 39 (2002).
[189] J. M. Edge and N. R. Cooper, Phys. Rev. Lett. **103**, 065301 (2009); Phys. Rev. A **81**, 063606 (2010).
[190] Z. Hadzibabic, P. Krüger, M. Cheneau, B. Battelier, and J. Dalibard, Nature (London) **441**, 1118 (2006).
[191] C.-L. Hung, X. Zhang, N. Gemelke, and C. Chin, Nature (London) **470**, 236 (2011).
[192] H. Shimahara and D. Rainer, J. Phys. Soc. Jpn. **66**, 3591 (1997).
[193] U. Klein, Phys. Rev. B **69**, 134518 (2004).
[194] K. Yang and A. H. MacDonald, Phys. Rev. B **70**, 094512 (2004).
[195] G. Blatter, M. V. Feigel'man, V. B. Geshkenbein, A. I. Larkin, and V. M. Vinokur, Rev. Mod. Phys. **66**, 1125 (1994).
[196] M. Greiner, C. A. Regal, and D. S. Jin, Phys. Rev. Lett. **94**, 070403 (2005).
[197] C. Chin, M. Bartenstein A. Altmeyer, S. Riedl, S. Jochim, J. H. Denschlag, and R. Grimm, Science **305**, 1128 (2004).
[198] A. Schirotzek, Y. I. Shin, C. H. Schunck, and W. Ketterle, Phys. Rev. Lett. **101**, 140403 (2008).
[199] P. Törmä and P. Zoller, Phys. Rev. Lett. **85**, 487 (2000).
[200] M. Veillette, E. G. Moon, A. Lamacraft, L. Radzihovsky, S. Sachdev, and D. E. Sheehy, Phys. Rev. A **78**, 033614 (2008).
[201] J. T. Stewart, J. P. Gaebler, and D. S. Jin, Nature (London) **454**, 744 (2008).
[202] J. P. Gaebler, J. T. Stewart, T. E. Drake, D. S. Jin, A. Perali, P. Pieri, and G. C. Strinati, Nature Phys. **6**, 569 (2010).
[203] E. Altman, E. Demler, and M. D. Lukin, Phys. Rev. A **70**, 013603 (2004).
[204] M. Greiner, C. A. Regal, J. T. Stewart, and D. S. Jin, Phys. Rev. Lett. **94**, 110401 (2005).